UNIVERSITY OF MANITOBA

Interaction Design from Wearable to Implantable

by

Teng Han

A THESIS

SUBMITTED TO THE FACULTY OF GRADUATE STUDIES

IN PARTIAL FULFILLMENT OF THE REQUIREMENTS FOR THE

DEGREE OF DOCTOR OF PHILOSOPHY

GRADUATE PROGRAM IN COMPUTER SCIENCE

WINNIPEG, MANITOBA

JAN, 2019

This thesis was reviewed and approved by the following committee members:

Pourang Irani

Professor of Computer Science, University of Manitoba

Thesis Advisor

Yang Wang

Associate Professor of Computer Science, University of Manitoba

Ekram Hossain

Professor of Electrical and Computer Engineering, University of Manitoba

Bing-Yu Chen

Professor of Computer Science and Information Engineering, National Taiwan University

Abstract

We envision the future of wearable devices to be implantable, where devices are no longer attached to the body, but rather, they are embedded as part of the body and provide more ambient experiences. This revolution will not only change the wearable devices in functionality, but also dramatically alter the way we access information and interact with the world. From wearable to implantable, screen based interface is on the verge of disappearing. Touchscreen will become less prominent, to provide more flexibility in terms of the size and structure of the devices. Looking forward, we expect the future implantable devices to be invisible, bringing closer the interactions to the body. Future interactions will be weighted towards human language of symbols, languages and gestures, which are ultra-subtle and intuitive. However, this revolutionary technology will not be maturely developed or widely applied anytime soon. It will take a long period of refinement to bring the implantable devices into the main digital markets.

To help users get accustomed to the changing interfaces, we have to foresee what are the new types of control mechanisms and interaction metaphors that we are collectively going to have. This thesis looks into a interface design space of such transition. Specifically, touchscreen on wearable devices faces input efficiency challenge. Designing touch input on the screen requires improving expressiveness of simple touch gestures. An alternative solution is designing intuitive hand gestures that are performed around the device. Approaches include not only adding new sensing capabilities to the devices, but also leveraging the devices themselves as on-body sensors. In spite of this, devices that are worn or embedded can be used as on-body actuators, providing haptic feedback as an alternative output channel. Finally, skin becomes more important as interface that can be turned into visual or haptic display. Upon summarizing key features, scenarios and challenges, the thesis undertakes a broad exploration of design, implementation and evaluation for the interfaces.

This thesis contributes an interface design space that outlines the possible transitions in the input and output metaphors from wearable to implantable, as well as technical solutions and design innovations that efficiently overcome the challenges raised from the interface paradigms. These include (i) the thesis proposes page-flipping gestures on touchscreen to improve the touch input efficiency; (ii) the thesis proposes an input method that leverages vibration signals produced from hand gestures for in-air and on-body interactions; (iii) the thesis proposes an output method that merges passive force feedback to extend the wearable haptic display's bandwidth; (iv) the thesis proposes a skin-like haptic interface via hydraulic actuation and demonstrates the benefits of using skin as display in a set of applications. Putting together, this thesis work contributes to the challenging and long-term exploration of the forthcoming changing waves in the era of wearable and implantable computing.

Preface

This thesis is an original work by the author. Contents presented in Chapter 3-7 of this thesis have already been published in premier venues in Human-Computer Interaction.

1. Teng Han, David Ahlström, Xing-Dong Yang, Ahmad Byagowi, and Pourang Irani. 2016. Exploring Design Factors for Transforming Passive Vibration Signals into Smartwear Interactions. In *Proceedings of the 9th Nordic Conference on Human-Computer Interaction* (NordiCHI '16). ACM, New York, NY, USA, Article 35, 10 pages.

2. Teng Han, Khalad Hasan, Keisuke Nakamura, Randy Gomez, and Pourang Irani. 2017. SoundCraft: Enabling Spatial Interactions on Smartwatches using Hand Generated Acoustics. In *Proceedings of the 30th Annual ACM Symposium on User Interface Software and Technology* (UIST '17). ACM, New York, NY, USA, 579-591.

3. Teng Han, Qian Han, Michelle Annett, Fraser Anderson, Da-Yuan Huang, and Xing-Dong Yang. 2017. Frictio: Passive Kinesthetic Force Feedback for Smart Ring Output. In *Proceedings of the 30th Annual ACM Symposium on User Interface Software and Technology* (UIST '17). ACM, New York, NY, USA, 131-142.

4. Teng Han, Jiannan Li, Khalad Hasan, Keisuke Nakamura, Randy Gomez, Ravin Balakrishnan, and Pourang Irani. 2018. PageFlip: Leveraging Page-Flipping Gestures for Efficient Command and Value Selection on Smartwatches. In *Proceedings of the 2018 CHI Conference on Human Factors in Computing Systems* (CHI '18). ACM, New York, NY, USA, Paper 529.

5. Teng Han, Fraser Anderson, Pourang Irani, and Tovi Grossman. 2018. HydroRing: Supporting Mixed Reality Haptics Using Liquid Flow. In *Proceedings of the 31st Annual ACM Symposium on User Interface Software and Technology* (UIST '18). ACM, New York, NY, USA, 913-925.

Acknowledgements

I owe a lot of thanks to my supervisor, Pourang Irani, who has always been supportive, and encouraging me to strive for the best work in my research and other endeavours. His patience, motivation, enthusiasm, and immense knowledge has always inspired me. I also feel grateful to have a committee with world experts in their respective fields as well as in HCI. I thank its members, Yang Wang, Ekram Hossain, and Robin Bing-Yu Chen, for providing their excellent reviews in a timely manner, and also, for their insightful discussions that lead me to contemplate during the thorough revisions of my final work.

I am grateful for the friendship and mentorship from the people that I have been collaborating with at the University of Manitoba and beyond. I feel fortunate to have the chances that allow me to work with Xing-Dong Yang, Fraser Anderson, Tovi Grossman, David Ahlström, Keisuke Nakamura, Randy Gomez, Jiannan Li and Khalad Hasan, who helped me tremendously and contributed to the work underlying this thesis. I learned from them, not only their professional skills, but also their interpersonal qualities.

Many thanks are also due to Sriram Subramanian, Xiang Cao, and Jingtao Wang, who used to be my supervisors and provided help and guidance at various stages of my journey to pursue a Ph.D. degree. They have enlightened my interest in continuing onto a research career.

I have had the great fortune of working at different research labs. I express my sincere thanks to the bright colleagues at the University of Bristol, Microsoft Research Asia, University of Pittsburgh, Lenovo Research, Dartmouth College, Honda Research Institute, Autodesk Research, National Taiwan University, and of course, University of Manitoba.

Last, I thank my wife, Huan Zhang, my parents and other members of my family for always loving me, believing in me, and supporting me throughout my journey. They have made countless sacrifices to help me get to this point. I owe them a lot of apologies for being away for so many years, and I hope to return to their sides soon. Their happiness is my lifelong pursuit.

Table of Contents

List of Figures

List of Tables

Chapter 1

Introduction

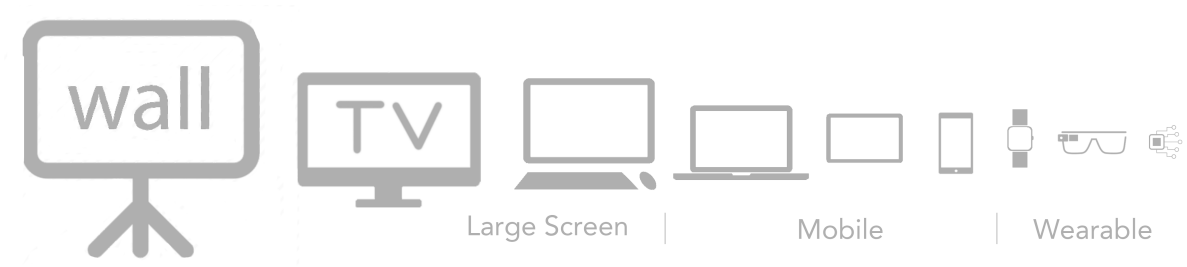

Figure 1.1: Mainstream computing devices in history.

Mainstream computing devices have been decreasing in size (Figure 1.1) while increasing in computational power. Wearable technology continues to increase in popularity with devices like smartwatches, smart glasses, fitness trackers, and smart clothing gaining market share. With increased power and reduced size come new possibilities for processing, exchanging, and displaying information. These new possibilities unlock novel interaction techniques and potential application designs. A richer set of applications stands to reformulate users' creative, analytic, and learning activities, allowing them to become more effective and efficient in their daily lives.

The decreasing size of wearable devices draws attention to the implantable technologies space. Unlike wearables, implantable devices are no longer attached to the body, but rather, they are embedded under the skin. Generic applications of the implantable include birth control, heart monitoring, defibrillation, and inclusion in device such as tiny healing chips and smart tattoos. These applications stand to be further expanded to nearly any domain that we can think of (e.g., communication, entertainment, and even self-actuation). According to [22], the implantable device market was valued at $72,265 Million (2016) and is now expected to reach $116,300 Million by 2022. We envision this implantable revolution to be the next big

wave in technology, which will not only affect the wearable devices in their functionality, but dramatically alter the way we perceive and interact with the world, both physiologically and cognitively [26].

Wearable Device: Smart electronic devices (electronic device with micro-controllers) that can be incorporated into clothing or worn on the body as accessories [128]. Wearable technology achieved mainstream popularity with the Bluetooth headset in 2002. Between 2006 and 2013, iconic wearable technology devices Nike+, Fitbit, and Google Glass were released. In 2014, dubbed "The Year of Wearable Technology" by several media outlets, activity trackers grew in popularity and the Apple Watch was introduced (Figure 1.2).

Figure 1.2: Popular wearable devices in the market: (from left to right) Nike+ Fuelband [91]; Fitbit [25]; Google glass [37]; Apple watch [2].

Implantable Device: Tiny computing devices that are implanted inside body parts or under the skin, and become part of the body [22]. Recent developments in the implantable-device space have been focused on the health industry. Implantable devices of the future are expected to experience mainstream adoption. This is supported by the technology that is being developed now, including examples such as tattoo-like printed circuits, micro-fluids, and micro-needles as shown in Figure 1.3.

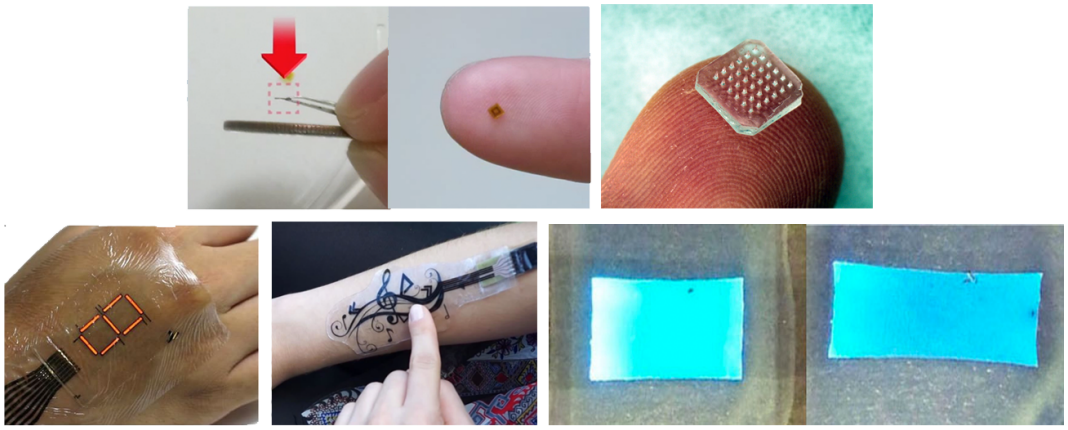

Figure 1.3: Implantable techniques that are currently available: (from left to right, top to bottom) Tiny implantable sensor to detect blood and intracranial pressures [14]; Micro-needles [101]; LED on skin [135]; Tattoo like skin [120]; Strechable OLED screen [81].

As devices shift from wearable to implantable, the conventional screen-based interface that we are familiar

with on mobile and wearable devices will likely fall out of favour. Instead of a touch-screen display, current popular sports and fitness trackers (e.g., Nike+ FuelBand, Fitbit Flex) incorporate a small LED or OLED display, which shows only selected information that is considered critical to the experience. As implantable device research explores methods of exchanging information it is likely that screen size will reduce drastically, or that screens will disappear entirely. On one hand, this transformation brings more design flexibility in terms of the wearable size and structure. Devices are getting smaller, more capable, and more portable, enabling improved integration and interaction with the human body. Implanting devices within the human body will certainly cause profound changes in the way information is presented and the way users interact with their device. A device which is implanted in its user's body presents a unique opportunity for the user to interact with this device anywhere and at any time, allowing for always-available interaction. Implantable devices bring interactions closer to the body, where more subtle and intuitive input and output methodologies are expected to be developed. Interaction approaches that are considered promising for this emerging implantable era are weighted towards human languages of symbols, words, and gestures [26], e.g., voice input, micro-gestures, and subtle expressions. In a scenario where a user touches a table, an implanted device might assist the user to not only feel the texture of the table, but also acquire knowledge of the fibrous structure of the wood that the table was made of. The intriguing thing about implantable devices is that interfaces will virtually disappear and the input devices will be dispersed around the body.

Nonetheless, this transformative technology will not be maturely developed or widely applied in the mainstream digital market anytime soon. The reasons are two fold. First, technology barriers restrict the speed at which these devices can evolve and improve. These barriers require multidisciplinary research in fields such as micro electronics, bio engineering, smart materials and miniature sensors, actuators, and power supply. Second, interaction barriers also exist. New interaction paradigms have to be defined to better adopt the evolving technology and surmount the design challenges faced when vieiwng the human body as an input and output canvas. The right balances between unobtrusiveness and practicality have be to found to surmount these challenges. Whatever interfaces are invented, the potential for social embarrassment should be avoided. The awkward feeling that users get when talking to a device, or waving hands around a device, especially in a public environment, must be considered. Perhaps these interactions will become more socially acceptable in the future, but these interaction modalities still require a long period of refinement before the majority of users get accustomed to them.

It is important for researchers and designers to develop appropriate design spaces, design languages, and interface metaphors as the adoption of implantable devices increases. Insights can be gained and similarities identified by studying the history of computers and mobile phones. Decades and waves of change were required to define and refine the devices used today. Each changing wave refined the formfactors of these

devices, as well as the interface metaphors that were best suited to each type of device. What is the timeline for the implantable revolution? How will the interfaces change from wearable to implantable? And what are the new types of control mechanisms and interaction metaphors that must be considered by researchers, designers, and developers alike for these transformations to take place?

To answer these questions, this thesis devises a design space of interfaces from wearable to implantable. Besides defining their key features, scenarios and challenges, the thesis undertakes a broad exploration of design, implementation, and evaluation for the interfaces. Instead of focusing on technology proceedings, The proposed design space stems from a focus on device formfactors that re-define the input and output metaphors in this transition. Specifically, the input and output spaces will be dramatically changed as the conventional touchscreen becomes less prominent, and even disappears. Implantable devices will be increasingly merged into the body, as will the input and output spaces. Five key interface phases are sketched in the design space, as shown in Figure 1.4.

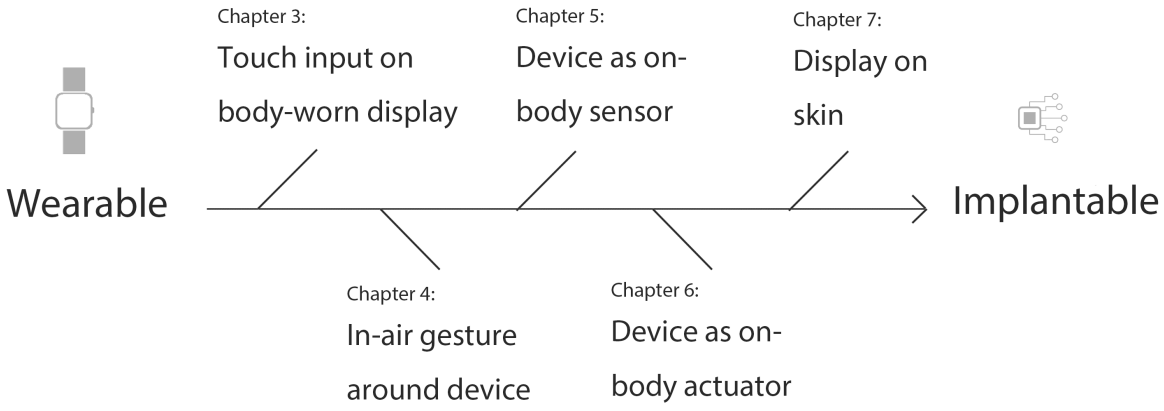

Figure 1.4: Transformation of interface from wearable to implantable.

1.1 Wearable to Implantable Interface Design Space

The interface design space sketched in this thesis is based on the input and output metaphors associated with the evolving wearable and implantable technology. In summary, the transition starts from the conventional touchscreen, which revolutionized and defined mobile phones and now on wearable devices. Being limited in size, the implementation of touchscreens on wearable devices has not as successful as on mobile phones. Gestural input is better suited to the formfactor of wearable devices, expanding the input space around the device and onto the body. As devices get smaller and eventually become embedded into the body, the methods used to acquire information (i.e., the output channel) becomes more important. Instead of visual feedback, haptic feedback can be deployed on the skin and used as information display.

- Touch input on body-worn display

Exploration begins with the touchscreen interface as it continues to play a central role in wearable devices like the smartwatch. As the smartwatch gained market popularity (with the Pebble watch in 2013 [22]), it defined a new paradigm of wrist-worn interface, i.e., wearing touchscreen on the wrist. Similar to hand-held touchscreens on a smartphone, smartwatch touchscreens support interaction with touch input and on-screen information display (Figure 1.5). However, the smartwatch exposes many usability challenges, mainly due to its small sizes. For example, fat finger problems (e.g., occlusion, imprecision) with touch input become more critical on wearable devices. Users usually find tasks that are common on smartphones, like text entry, become frustrating and inefficient on smartwatches. Smartwatch use scenarios are not identical to those common to traditional desktops or mobile phones, requiring designers to explore interfaces better suited for quick and short interactions. The primary challenge for interface design on touchscreen is the improvement of input efficiency.

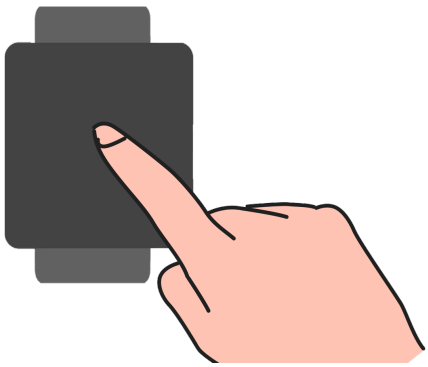

Figure 1.5: Touchscreen as body-worn display for both input and output.

- Body-worn display with in-air gestures

A way to mitigate the on-screen input challenge is by using in-air gestures. The body-worn display is used primarily as an output channel, but no longer for input purpose (Figure 1.6). On wearable devices, gestural input shows great potential including (i) gestural input permits a wide range of operating space around the devices; (ii) gestural input requires no precise pixel-level locating; and (iii) gestural input is expressive and can adapt to various usage contexts, such as hand swiping to flip pages, and subtle fingertip operations to adjust music volume. Supporting hand gesture detection in the air is non-trivial. It often requires sophisticated sensing solutions that are compact in size, power efficient, and robust enough for mobile usage. As a result, designers tend to adapt users to system limits and increase comfort by setting arbitrary conventions and procedures [86]. With these concerns, the primary challenge for the develop of in-air gestures becomes designing a sensing system for wearable devices which supports gestures that are

intuitive and natural, from the user's perspective.

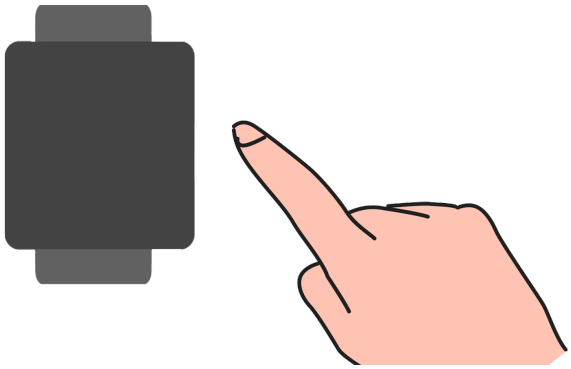

Figure 1.6: Using in-air gestures to interact with body-worn display.

- Device as on-body sensors

Excluding the smartwatch, the touchscreen is becoming less and less prominent on wearable devices as there is less need to have a full, interactive display to provide the desired experiences and services to the user. This brings more design flexibility in terms of wearable size and formfactor. Some devices only provide displays for minimal output, such as LED-based displays, to show information that is critical to user experiences. These types of wearable devices are acting primarily as on-body sensors (Figure 1.7), which augment people in some way and enable tracking and collecting data about user activity or physiological conditions such as fitness, health, and activity type. An LED-based interface setup triggers the exploration of methods to leverage the embedded sensors for gesture input. The benefits of gesture input can be achieved with no need to add extra sensors, while the drawback is two-fold: (i) gestures are often carried out on the wearing hand as it is close to the sensor, and are usually limited to coarse hand movements; and for the same reason, (ii) normal hand activities may accidentally trigger gestures. The challenges for leveraging on-body sensors to design gestural input are thus amplified by expressiveness and false triggering concerns.

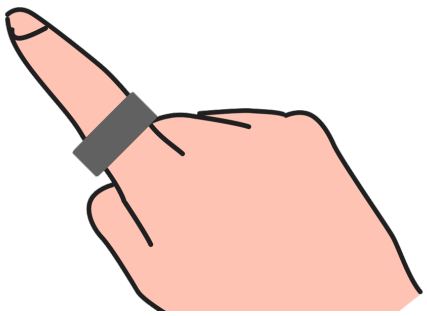

Figure 1.7: Devices are used as on-body sensors.

- Device as on-body actuators

Beyond the ability to provide sensing capabilities, devices that are worn on the body can be composed of electromechanical structures, enabling user augmentation with various forms of mechanical actuation (Figure 1.8). These abilities can be leveraged to render haptic sensations such as vibration and pressure on the skin, in replacement of a visual display. Providing haptic feedback as an alternative output channel becomes an important design consideration, especially as devices get smaller and physically closer to the user's skin (e.g., devices are often in direct contact with skin). The use of haptic feedback as an output modality provides a design space rich with possibilities for the composition of various haptic sensations. Most common haptic feedback provided with wearable devices is vibrations. It is easy to implement and well perceived by users on both mobile and wearable devices. However, the bandwidth of information delivered from haptic or vibrotactile feedback is often limited. The primary challenges of designing an appropriate haptic-based interface are extending the bandwidth of information that can be perceived by the user.

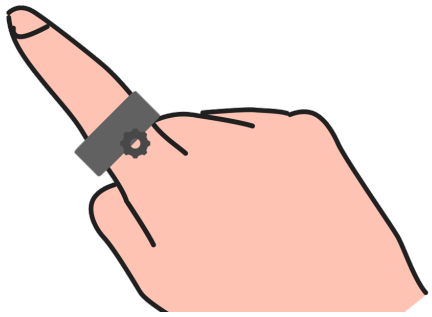

Figure 1.8: Devices are used as on-body actuators.

- Skin as display

Implantable devices are expected to have the capability to change the way we perceive the world, both physiologically and cognitively. As devices move from wearable to implantable, displays, both visual and haptic, move closer to the skin and even into the skin (Figure 1.9). The idea of turning skin into a display is not new and has been shown to be feasible with technologies such as ultra-thin and stretchable screens that are attached onto the skin like a tattoo [120]. Moving screens onto the skin defines an interface where interactions are less device-centric and more body-centric. As these technologies improve, the possible use-case scenarios and interactions required must be defined. For example, besides of visual display, augmented skin can be used for haptic displays. It is both essential and interesting to explore how a haptic display on augmented skin might differ from mechanical haptic approaches, along with the the unique applications such a device might unlock.

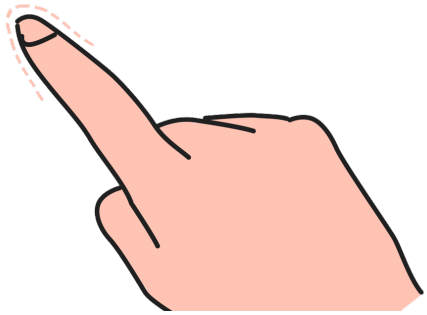

Figure 1.9: Skin is turned into display.

1.2 Challenges and Solutions

The previous section described five interface paradigms in the design space, as well as their associated interaction challenges. Here we summarize the challenges:

1. How to improve the touch input efficiency on small wearable touchscreen?
2. How to enable and detect gestures around wearable platform?
3. How to leverage on-body sensors for expressive gestural input?
4. How to leverage on-body actuators for expressive haptic output?
5. How to turn skin into haptic display?

As mentioned, the design space is based on the input and output metaphors derived from the evolving interfaces of devices from wearable to implantable. This exposes the aforementioned input and output challenges. This thesis explores the challenges faced when developing an appropriate design space and proposes novel solutions to help better design the interfaces.

Challenge 1. requires considering the efficiency lost to the decrease in screen size on the modern smartwach. Current smartwatch interfaces require users to conduct a series of touch and swipe actions to select an app or command. Switching UIs is inefficient as users need to navigate back and forth between the home screen and applications. To mitigate this challenge, Chapter three proposes PageFlip, an interface design that leverages page-flipping gestures on touchscreen. PageFlip enables a user to drag a finger from a corner towards a certain direction and for a certain distance. Such an action is commonly seen in page navigation for e-books. Chapter three demonstrates that this action provides an efficient touch input for menu and value selections on a smartwatch.

Challenges 2. and 3. require the design of novel sensing approaches to provide alternative input channels when touchscreen is no longer used or embedded in the device. In Chapter four and Chapter five, the use

of vibrational signals for gesture-input sensing is studied. Specifically, Chapter four proposes the detection of audible sounds produced with the hands and the classification of these sounds as certain gestures. Hand-generated sounds are rich and familiar to us. Examples include finger snap, finger rub, finger flip, hand clap, hand rub, on body/surface scratch. To demonstrate the use of such hand-generated sounds for wearable interaction, a system called SoundCraft is developed. SoundCraft leverages microphone array acoustic processing techniques to localize and classify sound sources, which are then used to detect the acoustic signatures made by hands.

As displays disappear and devices become smaller, embedded sensors will eventually get closer to body and even become part of the body. This on-body sensor setup adds sensing capabilities to hands and arms and thus allow always-available input. Chapter five describes an approach that leverages motion sensors embedded in the hand to capture the vibrational signals emitted when swiping a finger over an object or surface, then convert this energy into an interaction. To increase the expressiveness of the gesture, various design factors regarding use patterns and bumpy surfaces are explored.

While devices such as on-body sensors enable many possibilities for the design of always-available input, Challenge 4. requires the design of appropriate output channels. Traditional vibration feedback is often used for notification and is limited to the information bandwidth of a device. Chapter six proposes a method to design passive kinesthetic force feedback on devices as an output modality. To test the feasibility and benefits of using the passive kinesthetic force feedback, a smartring prototype, Frictio, is developed, which leverages a ring's form factor and provides friction force feedback in response to users' rotating input. More importantly, this feedback can be enriched using different force profiles based on rotating angle, time, or both. Chapter six demonstrates that users can perceive the force profiles accurately, while also being engaged in additional physical and mental activities.

When devices are embedded into the body, skin will act as an important interface and output channel. Going beyond visual feedback, skin can be turned into a haptic display, thus removing the requirement for visual attention from the user. Challenge 5. identifies that conventional mechanical structures and actuation will no longer be suitable to design such skin-like haptic interfaces as they are often rigid and bulky. Chapter seven presents a solution that leverages fluid as an actuation medium, where fluid such as water can be transported and controlled to end-effector; a very thin latex tube is slightly stretched over the skin (i.e., to simulate a skin-like display) and provides haptic senstations such as pressure, vibration, and temperature. A benefit of such a skin-like haptic display, is an active manner of operation, which can provide haptic sensations when needed, and a passive manner of operation, as to not interfere with user's interactions in the physical world.

1.3 Contributions

This thesis' work makes several contributions. The thesis sketches the transition of interfaces from wearable to implantable, based on the deriving input and output design spaces. The design space derived could help us better foresee the implantable revolution, with the understanding that wearable interfaces will undergo a long period of refinement while technologies evolve. Meanwhile, the design space could also help us identify design challenges, especially when composing input and output metaphors which are well suited to the interfaces. In addition, the thesis undertakes a broad exploration of design, implementation, and evaluation of the interfaces identified in Figure 1.4.

General contributions that are made in this thesis include:

1. An input and output design space that sketches the transitions of interfaces from wearable to implantable, and the identification of the design challenges for the interfaces.

2. The design of an input method that leverages vibration signals produced from hand gestures. These signals can be captured and recognized to infer the hand gestures that are commonly used in real life.

3. The design of an output method which merges passive force feedback experiences with wearable devices. This passive force feedback leverages a haptic perception which is common in daily life to design valid output modalities for wearable interactions.

4. The design of a skin-like haptic interface with hydraulic actuation. Such an interface presents the benefits of supporting mix-reality scenarios.

5. An touchscreen interface design which takes advantages of page-flipping gestures to improve touch-input efficiency.

Along with the design solutions, this thesis also contributes:

6. A set of studies focused on to understanding design factors that affect the recognition of finger swiping gestures using embedded motion sensors.

7. A series of signal processing steps to classify and localize acoustic signals using a smartwatch sized, 4-microphone array, and systematic evaluations of its performance.

8. A study to evaluate users' perceptions of force feedback on fingers under mobile-use conditions, including physical mobility and mental workload.

9. A study to evaluate design factors when using page-flipping gestures on a miniature-sized touchscreen.

Chapter 2

Background

Designing interactions on wearable devices has a long history, dating back to 1500s when small watches were invented and worn as necklaces. In 1900s, watch becomes wrist-worn device, bringing the benefit that the device would not occupy hands for their dominate tasks. The modern development of wearable devices is led by the visions of "Natural User Interface (NUI)", "Ubiquitous Computing", and "Internet of Things". Interactions are focused on the design and development of gestures and feedback, aiming to improve the expressiveness, as well as the natural feelings of the input and output methods on wearable devices.

With the development of modern technologies in nano-technology, smart material and wireless communication etc., the increase of implantable technology has been noticed over years. There exist some early stage exploration to design the possible implantable interfaces. Implantable devices bring closer the interactions to the body and skin, and weight towards interface paradigms with human language of symbols, words, and gestures.

This chapter first goes through the history of wearable devices and its prominent development in recent years. It then looks into the development and applications of implantable devices, as well as work on exploring and designing implantable interfaces. Lastly, the chapter reviews recent work on wearable interactions with novel input and output techniques.

2.1 Wearable Computing Devices

Portable clocks (i.e., watches) were invented in 1500s, and after centuries, they became wrist worn devices for convenient usage without interrupting hands' ongoing tasks [128]. According to [34], the first wearable computing devices was invented by Edward Throp in 1960s, who built a computer small enough to fit into a shoe in order to cheat at roulette. Over the next couple of decades, several devices popularized and

modernized wearable technology. The first calculator wristwatch was released to the public in 1975, and the Sony Walkman arrived four years later. In the 1980s, digital hearing aids were first released.

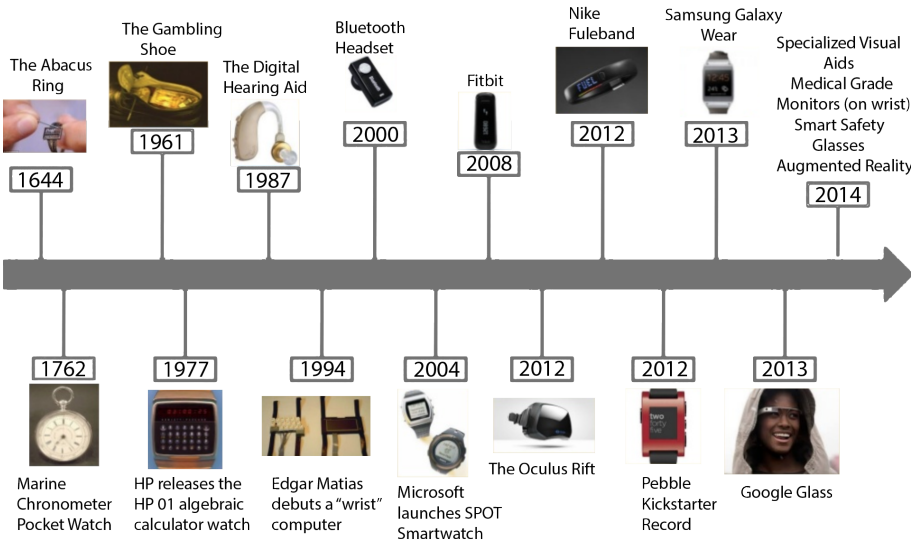

Figure 2.1: Wearable devices in history.

Wearable technology achieved mainstream popularity with the Bluetooth headset in 2002. Between 2006 and 2013, iconic wearable technology devices Nike+, Fitbit and Google Glass were released. In 2014, dubbed "The Year of Wearable Technology" by several media outlets, activity trackers grew in popularity and the Apple Watch was introduced. Other wearable technology devices, such as those that track seizures or sunlight exposure, continued expanding the industry (Figure 2.1)[1].

Wearable devices are applied in many different areas nowadays, including fitness, healthcare, entertainment, retail etc. Besides, wearable devices have been explored and shown promising in creative [71], analytic [55] and learning [32] activities. Majority wearable devices support either touchscreen input, or physical button input, or both. Some of them also support gross hand/arm gestures using embedded motion sensors (e.g., IMU) [122]. For output, devices are usually embedded with LCD displays at various sizes. Displays of smartwatch are about $1.2''$ - $1.4''$ in size, with about 300ppi resolution. Other wearable devices such as fitness trackers have much smaller sized displays, that are used to show brief information and simple icons. Some devices may even have no display, or just micro LEDs to indicate status. These types of devices reply more on using paired smartphones to support users for browsing information (e.g., heart rate). The current input and output methods are limited due to the size of the wearable devices. Designing alternative input and output channels are thus desired on wearable devices, to support their better use in different applications.

[1] www.media.mit.edu/wearables/lizzy/timeline.html

2.2 Implantable Devices

With the decreasing size of wearable devices, the increase of implantable technology has been noticed over the years. The focus of its recent development is in health industry. The generic applications of the implantable include birth control, hear monitoring, defibrillators, tiny healing chips and smart tattoos [22]. Due to its tiny size and the special attribute of being embedded into the body, researchers expect to use the implantable to track health condition and even heal special diseases. The Smart tattoos can monitor their heart rhythms. Using the smart tattoos can also help people get treated from sleeping disorders. The defibrillators are used to deliver electrical power to the heart, to manage the unusually fast heart rhythms.

Looking forward, the implantable can be applied in many other domains as we can think of. Researchers envision the future with the implantable where the devices can be embedded inside our digestive tracts, sensing organs, blood vessels, and even our cells. This will cause profound changes on the way we perceive and recognize the world. We, as human beings, can be enhanced in perceptions, both physiologically and cognitively, with the power of implantable devices [26]. For example, the small devices inside our body could keep tracking the data and feed them into a system, turning our surrounding objects to be super responsive and predictive.

This upcoming technology wave will bring profound challenges to design interfaces with the implantable. The screen based interface is on the verge of disappearing, being replaced by the small devices embedded inside the body. Researchers have been exploring what the implantable interface will like, what new experiences they will bring to the users, how much we need to interact with them and how shall we interact with them, etc. For instance, skin is considered to be the next generation of interface, with enhanced sensing and displaying capabilities empowered by the ultra-thin and stretchable electronics. iSkin [120] proposed the idea of adding a very thin sensor overlay on various locations of the body such as the finger, forearm, or ear, turning them into input canvas. Later on, the same team developed a skin overlay with high resolution of touch sensing and supports multi-touch input on the skin [121]. Researchers also developed ultra-thin flexible LED display that can be attached onto the body, turning the skin into visual displays [135]. Recently, Withana et al. [125] worked on adding haptic tactiles to the skin overlay that made the smart tatttos into haptic display attached on skin. These work define new interface paradigms that could be envisioned with implantable devices. To help better understanding how users would interact with the new interfaces, Weigel et al. [121] explored a design space of gestures working with skin as interface. More comprehensively, Holz et al. [54] looked into the design possibilities of input and output channels for underskin gadgets.

2.3 Touchscreen Input on Wearable Devices

Best known and widely applied touchscreen gestures include touch, swipe, flip, and pinch. On small screen touch displays, direct touchscreen gestures expose usability challenges. Researchers are interested in investigating new paradigms to improve input efficiency on small screens.

Kin et al. [65] designed a multi-stroke two-handed marking menu for simultaneous menu and sub-menu selections tasks. Benko et al. [6] used two fingers to select small targets. Lepinski et al. [75] designed a marking menu based on simultaneous finger touches. MarkPad [31] used visual and tactile marks to create gestural shortcuts on a touchpad. Similarly, Blaskó et al. [9] proposed to use device corners and edges as tactile landmarks on wearables to support value selections without visual attention. TapSense [47] detects which finger part is used to increase the expressiveness of tapping gestures. ForceDrag [52] used pressure sensing for the same purpose. Pin-and-Cross [79] requires users to uses one finger to pin an object and another finger to select a target from a pre-activated menu. FastTap [43], built on users' spatial memory, is another touch-based interface for rapid access to menu items. A thumb-press on a button displays available items on the screen and an item of interest can be invoked via the index finger while keeping the thumb pressed on the button. A smartwatch version of FastTap was designed in Faster Command [72], where the technique was shown to be faster than standard touch input for command invocation. Their results revealed that multi-touch solutions are promising, but not applicable in many cases due to the miniature sized touch input space.

Other approaches use common finger gestures such as single tap, double tap and dwell. ZoomBoard [97] leveraged a sequence of tap actions that zooms the keyboard with the first tap and selects a key with the second tap. Besides tapping, crossing gestures to select have been shown to be efficient on touch screens [78], but have not been explored for target acquisition on smartwatches. Swipeboard [17] used a sequence of directional swipes to enter text. Both ZoomBoard and Swipeboard work efficiently with a keyboard layout, but have not been applied to general menu selections. Additionally, gestural control usually suffers from lack of established guidelines and feedbacks [94]. Furthermore, previous research mainly focused on discrete target selection and did not explore the feasibility of continuous input on smartwatches.

2.4 Novel Input Techniques on Wearable Devices

Composing gestures is directly constrained by sensing approaches. Well studied sensing techniques include those based on infrared (IR) light, motion sensors, electric/magnetic fields, ultrasound, cameras and biometric sensors.

Wrist-worn devices provide sensing instruments near to hands and fingers. Early approach like GestureWrist [105] leveraged capacitively measuring wrist-shape changes caused by hand postures. More sophisticated approaches use bio signals such as Electromyography (EMG) [107] and Tomography [139]. Serendipity [122] explored sensing fine-grained in-air finger gestures such as pinching, tapping with the hand wearing a smart watch via embedded motion sensor (i.e., IMU). Infrared (IR) is usually used to monitor beam breaks or reflections caused by finger interruptions. Its application on continuous pose estimation was demonstrated by Kim et al.'s Digits [62]. SideSight [11] and HoverFlow [66] used embedded IR proximity sensors to detect objects appear in the adjacent region of mobile devices, including fingers. zSense [127] evaluated three efficient IR emitter and receiver setups for detecting mid-air gestures. Besides, electric field (EF) sensing for floating finger gestures and pre-touch interaction is also explored in [35] [53]. Project Soli [104] [119] used radar signal to track single hand micro gestures which has been shown promising for smartwatches. Abracadabra [46] leveraged magnetic field changes to detect gestural events such as rotation and clicking with a finger wearing a magnet. This solution supports input from a sufficient large area in radical 2D and estimated spatial 2D. However, it could not support high resolution gestures, especially when the finger is far from the device.

On mobile devices, camera-based sensing systems are often used. For instance, PointPose [67] used a short-range depth camera on a tablet for gesture and periphery detection. Low-cost RGB cameras are also often used [13] [42] [131]. Watchme [117] used embedded camera on watch and image processing techniques to detect raw gestures like user stroking.

Piezoelectric acoustic sensors show the potential for contacting gestures. Scratch Input [45] and Acoustic Barcodes [48] used contact piezo microphone to monitor finger scratching over textured surfaces. Ono et.al [98] made everyday objects interactive by detecting vibration response with hand touch. Skinput [49] recognized touches on arm via bone conducted sound with a modified piezo microphone. Recently, Zhang et.al [140] investigated using body transmitting AC signal for continuous skin touch input.

2.5 Novel Output Techniques on Wearable Devices

The miniature sized device also restricts its output capabilities. Providing rich haptic feedback becomes more prominent in HCI research. Vibrotactile is the most common haptic feedback on nowadays' wearable devices, but is often limited to notification purpose. For example, Marti, et al. [80] used vibrotactile feedback as a mechanism to inform users of an incoming call. Pingu [61] vibrated to alert the users about important messages from a coupled smart device. Pradana et al. [103] and Werner et al. [123] used vibrotactile feedback to create a sense of presence for remote couples. Freeman et al. [28] and Yeom et al. [133] used vibrotactile

feedback for mid-air hand gestures. Roumen et al. [106] examined light, sound, vibration, poking, and temperature manipulation on a ring. They found that the haptic modalities (vibration, and poking) were among the most noticeable for notifications.

Other haptic methods are investigated to enrich output vocabulary on smartwears. Skin drag device can be used on smartwatch [57] to provide more expressive and memorable messages such as characters or simple icons. TactoRing [58] demonstrated the benefits of using skin drag haptics to encode messages on fingers. Pin arrays move multiple tactors and create spatially distributed indentations into the skin. Retroshape [56] leveraged pin arrays to provide co-located haptic feedback from the back side of smartwatch to respond on-screen contents. A recent work RokeRing [59] investigated the pin-array's adaptation into ring formfactor and showed that it is useful on providing encoded information. Another popular approach is providing pressure onto skin with pneumatic systems. Pohl et al. [100] developed a wristband that provides pressure on arm by inflating air into the embedded bladder. Lee et al. [74] applied non-contact pressure on skin with air-blow devices embedded on the back of smartwatches. HaptiClench [41] applied pressure on wrist by squeezing a memory alloy. Other than this, Jetto [36] explored how lateral force could enrich smartwatch applications.

The previous ones are leveraging tactile feedback through stimulating skin on finger or wrist, while another group of research focus on kinesthetic feedbacks. Kinesthetic haptics are resulted from the use of muscle, tendons, and joints, and are thus often involved with locomotion of body parts. Xiao et al. [130] developed a watch that supports users to carry out mechanical operations such as pan, tilt, twist and click. The operating hand feels kinesthetic feedback as a result of the motions. Similar approaches were introduced in [4] where users used the edge of round-screen smartwatch to perform gestures, and in [132] where users tilt and pan the watch without touching the screen. COMPASS [134] introduced a rotatory keyboard for text entry on smartwatch by rotating the bezel of the device. Although the projects were more on discussing input methods for smartwatches, they introduced the kinesthetic feedbacks on the operating hand. This fits to our life experiences that kinesthetic feedback are often produced as a result of hand input. For instance, haptic knob [44] [112] [113] produces haptic feeling when users rotate the knob, to simulate the real-life situations like rotating a door knob, or volume knob on radio.

2.6 Finger Worn Haptic Devices

Finger-based wearable haptic devices have been well studied in recent years, as they have been shown to be effective in providing localized cutaneous stimuli [8] to, for example, fingertips that are most often used for grasping, manipulating and probing the environment. Pacchierotti et al. presented a comprehensive

taxonomy of wearable haptic systems, including finger-worn devices [99]. Such devices are typically comprised of two structures - one structure that houses actuators on the back of the finger and another structure that is in contact with the volar surface of the fingertip. These devices can be categorized based on the cutaneous sensations they produce, including but not limited to, indentation, lateral force, and vibration.

Indentation: Frisoli et al. [30] presented a fingertip wearable device to improve the curvature discrimination of virtual objects by placing a plate in contact with users' fingerpads at different orientations. Using this concept, many indentation haptic displays [18] have been developed which have various degrees of freedom (DOF) and levels of contact force to improve the haptic exploration of virtual objects. Such indentation displays have been successfully employed to convey pressure [63], and curvature [29].

Lateral force: Gleeson et al. [38] designed a fingertip-mounted tactile device that laterally stretches the skin of the fingerpad along any path in the plane to provide navigational cues. In Gravity Grabber [84], lateral force was applied to the fingertips to render gravity without proprioceptive sensations. It consisted of two motors and a belt that were in contact with the fingertip and provided vertical or shearing stress based on the rotational direction of the motors. Bianchi et al. [10] adopted the same two-motor approach to control the tension of fabric, with the resulting stiffness being used to convey the softness of a surface. LinkTouch [115] replaced the belt with a five-bar linkage mechanism to support contact and directional force perception.

Vibration: Another common cutaneous feedback actuator built into wearable devices are vibrotactile motors. As vibrotactile motors are very small, they can be embedded within wearable devices such as gloves [19]. Vibrotactile feedback applied to the fingertips can be used to simulate contact events [76], texture [7], etc. However, the rigidity of the vibrotactile actuators dampens the user's sensations of the real world.

In recent years, there has been a growing need to develop wearable haptic devices that are capable of conveying compelling interaction feedback with virtual objects, such as grasping, squeezing, pressing, lifting and stroking. This normally requires combining multiple cutaneous stimuli into one compact device. For instance, Schorr and Okamura [110] designed a fingertip wearable device that renders forces in multiple directions to investigate users' perceptions of mass, friction, and stiffness while manipulating virtual objects. Altered Touch [87] was a fingertip haptic device with a dual motor design and a Peltier module that provided shear and vertical force as well as thermal feedback. Grabity [20] demonstrated kinesthetic feedback with a handheld device to support grasping in VR, including virtual weight, inertia forces, and stiffness.

2.7 Organization of The Thesis

The rest of the thesis is organized as follows. Chapter 3 starts the exploration of the design space by proposing page-flipping gestures on touchscreen to improve the touch input efficiency on wearable devices. Compared to touch input, in-air gestures are considered promising as devices are getting smaller but challenging. Chapter 4 explores the use of audible acoustic signals produced by hand gestures for around device interactions that expand the input space. In-air gestures can be efficient and expressive, but may face barriers for social acceptance. On the other hand, as devices are getting smaller and closer to users' body, interactions become more body centric. Chapter 5 explores the use of devices as on-body sensors, which enables more opportunities for users to interact with the devices via surrounding daily objects. Besides the input, the transition of the device raises the challenge of designing output channels. Haptic feedback is gaining more attention but faces the limited bandwidth problem. Chapter 6 explores the merge of passive force feedback into wearable devices to extend the expressive of using the devices as haptic display. Beyond that, skin is envisioned to be the future interface when devices are implantable. Turning skin into haptic display would be valuable but undoubtedly challenging. Chapter 7 explores a hydraulic actuation method which helps designing a skin-like haptic display, and demonstrates the unique benefits of the skin interface. In the end, Chapter 8 summarizes the thesis content and discusses the future work.

Chapter 3

Touch Input on Body-Worn Display

Touchscreen revolutionarily altered the way that mobile phone was designed and the way we interact with the phones. Smartwatch is designed with touchscreen and supports touch input as a matter of course. However, in many instances, interactions on these small devices are tedious and time-consuming, requiring minute touch operations such as swiping and tapping while browsing alternatives and selecting an item of interest. For instance, popular apps such as activity tracking, scheduling, and messaging employ sequential operations such as feature invocation followed by value selection. Additionally, fine-grained control like continuous input is not well supported on smartwatches.

Prior work on smartwatch interface design suggests using simple gestures such as a side tap [4], or multiple taps [95] to support rapid command invocation. However, tapping on the small screen is known to be error-prone due to small item sizes [72]. Swiping gestures are shown to be faster than tapping in many instances such as in command invocation [68] and text-entry [17]. However, swiping requires multiple actions and becomes time-consuming as the number of items grow. Additionally, complex gestures such as drawing strokes are limited as they lack established guidelines and feedback [90]. Besides, these work primarily focused on invoking discrete items instead of continuous input, and are therefore only applicable in limited contexts.

This chapter looks into a touchscreen interaction approach that leverages a page-flipping gesture to combine command invocation and value selection into a single action.

3.1 Page-Flipping Gestures on Touchscreen

The gesture of page-flipping has been digitalized in many applications. Pagination with curled edges and translucent text rendered on the opposite page has a strong visual similarity to e-book readers. The tran-

sition, compared with traditional page scrolling, is designed to blend the tactility of real-world pages [126]. On mobile devices, the page-flipping gesture was introduced by the iBook [1], and has been modified in many other commercial apps such as FlipBoard [24]. Bezel-Flipper [64] demonstrated how multi-touch could enhance the design of flipping interfaces for e-books. Beaudouin [70] designed the stacked windows metaphor supporting page rotating and peeling. The page-flipping interface was also used in tangible interactions such as in [114] and a recent work Flippin' [137].

Interestingly, page-flipping gestures embody rich information, such as flipping directions, flipping distances, and number of pages to flip. These variables can be considered the attributes of the gesture. This formalizes the idea of a touchscreen interaction approach that leverages a page-drag gesture to combine command invocation and value selection into a single action. Page-flipping gestures are executed via dragging a corner on the screen to different directions and distances. Each corner is mapped to a certain command and can be curled/peeled to browse values available under the command (Figure 3.1). Such target selection and value adjustment with a single action has been demonstrated on desktop platforms (e.g., marking menu [69]), but never been explored on smartwatches.

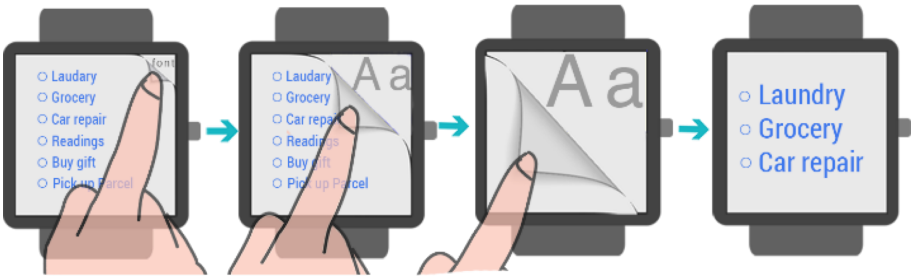

Figure 3.1: With Page-flipping gesture, a user selects a command (e.g. font size) by dragging the top-right corner, and adjusts its values (e.g., text size) by 'peeling' the corner of the page.

The gesture's novel features offer several advantages. First, it exploits users' spatial memory for corner-command mappings and reduces frequent swiping and tapping actions. Second, it provides real-time and intuitive visual feedback (i.e., curled page effect that maps naturally to users' dragging action) which indicates the current dragging direction and distance from a corner. Third, it supports accessing items in advanced menu layouts where hierarchal or sub-menu items can be accessed via directions and distances. Finally, it allows users to interact with stacked page layouts to make the applications scalable.

3.2 Designing Page-Flipping Interface

The first study explored how to design Page-Flipping gesture as a command invocation mechanism. More specifically, the interface aimed to support simultaneous command invocation and value selection with Page-

Flipping gesture via hierarchically structured menus and sub-menus. This led to an evaluation of the interface's design parameters such as how best to use corners, drag directions and distances from corners for invoking items hierarchically.

Corner. Though all edges and corners could be adopted on the design, only using the corners is considered as this can be easily distinguished from existing swiping gestures on smartwatches. Accordingly, the interface allows a page-drag gesture only from the top-left, top-right, bottom-left and bottom-right corners of the screen.

Angular Segments. Intuitively, a page corner can be dragged to different angular directions to invoke different commands. For instance, a page can be dragged from the top-left corner towards the bottom-left to access a command feature (e.g., font size) whereas moving the curled corner towards the bottom-right corner could be used to invoke another feature (e.g., font face). Each corner is divided into 3, 5, and 7 angular segments to identify a suitable number of discrete angular directions i.e., Angular Segments that interface can support without affecting users' performance (Figure 3.2).

Distance Segments. Likewise, the corner can be dragged to different distances and be used to browse discrete or continuous values such as font faces or font sizes. Ideally, a corner tip could at most be moved towards the opposite corner of the touchscreen, revealing half of the second page. Therefore, this space is included to place items. This distance is further divided into 3, 5 and 7 segments where performance differences were expected. This creates a 90° semi-circular layout to place items as shown in Figure 3.2. The region close to the tip of a corner is extremely small and not ideal for placing more than one menu items. Therefore, this space is excluded in the study. It can be used for higher level commands and previews.

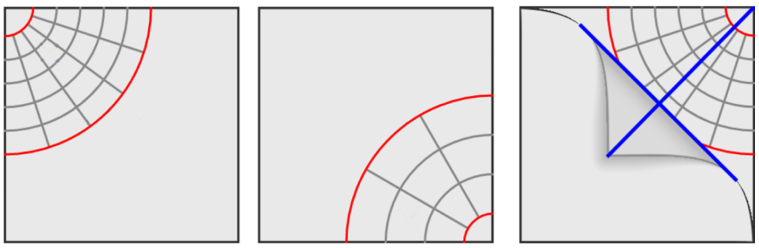

Figure 3.2: Visualization used to show (a, b) 5 (3) angular segments and 5 (3) distance segments at the top-left (bottom-right) corner. (c) the intersection point between the line from the corner to the flipped tip and the curled edge induces the currently highlighted item.

Selection and visual feedback. The page-flipping interface activates when a user starts dragging a corner of the top page. This action creates a folded page and reveals the visible area on the second page. To show the currently highlighted item, the interface calculates an intersection point of two lines: an imaginary line from the origin corner to the flipped tip and the line created with the curled edge (Figure 3.1c). Due to

indirect input, this visualization reduces finger occlusion and allows precise selection on the small-sized menu items.

Participants and Apparatus

12 participants (3 females, average age 23.2) from a local community took part in the study. Most participants were in their 20's with a few between 30 and 40 years of age. All of them were right-handed and had no prior experiences of using a smartwatch. An Asus ZenWatch-2 (1.63-inch screen, 320 x 320 pixels) was used. The page-flipping interface was implemented using the OpenGL ES framework in an Android Wear application.

Task and Experimental Design

During the experiment, participants were asked to sit in a chair and wear the smartwatch on their non-dominant hand (Figure 3.3). The watch band was adjusted to align with their natural viewing angle and to fit on their wrists. They were only allowed to use the index finger of the dominant hand to operate on the watch.

Figure 3.3: A participant in the study.

The study used a target selection task as shown in Figure 3.4. A trial starts with a visualization of the next target position on the 90° semi-circular layout (Figure 3.4a). A participant then starts dragging a corner to flip the top page. This action starts the trial time and unveils the visualization used to display Angular Segments and Distance Segments (Figure 3.4b). A blue 'x' symbol was used to indicate the target item that the user needs to select. A green '+' was used as a cursor to represent the currently highlighted item. When the cursor enters the target, the target turns into a green '$*$' symbol (Figure 3.4c). With the cursor inside the target region, the participant releases the finger to confirm the selection. A successful selection ends the timer and shows the next trial on the screen. A selection attempt outside the target item is ignored, and the trial continues until the participant selects the target successfully.

A 4 × 3 × 3 within-subject design was used for factors Corner (top-left, top-right, bottom-left, bottom-right), Angular Segments (3, 5, 7) and Distance Segments (3, 5, 7). Participants performed 15 repetitions

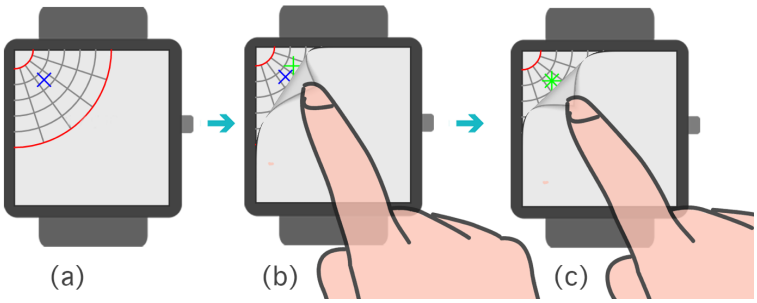

Figure 3.4: Study design: (a) a target is shown when a trial starts; (b) a user drags the target corner to start selection; (c) the target is successfully selected.

for each condition, yielding a total 540 trials per participant. Participants had practice trials until they felt comfortable with the technique.

All conditions were presented to participants in a random order. The targets were placed randomly in an Angular Segment and then in a Distance Segment. The participants were instructed to select the target as quickly and accurately as possible. After completing all the trials, they were asked to fill a NASA-TLX form to rate the workload the factors from 1 to 7. The study lasted about 50 mins for each participant.

Trial time was recorded from when a participant starts dragging a corner to the time she successfully selected it. Error rate was calculated by first marking an erroneous trial when the participant failed to select the target. The total number of erroneous trials was then divided by the total number of trials for each condition to get the error rate.

Results

The trial time was analyzed using repeated measures ANOVA with Bonferroni corrected pair-wise comparison. The error rate was examined using Friedman tests and Wilcoxon tests for pairwise comparison.

Trial Time. The average task completion time (Figure 3.5) across all conditions was 1.40s. The repeated measure yielded a significant effect of Corner ($F_{3,33} = 14.75, p < .001$), Angular Segment ($F_{2,22} = 74.46, p < .001$) and Distance Segment ($F_{2,22} = 109.06, p < .001$) on trial time, but no significant interaction effect. Post-hoc pairwise comparisons between corners showed that accessing item with the bottom-right corner (M = 1.50s) was significantly slower than with the top-left (M = 1.26s), top-right (M = 1.25s) and bottom-left (M = 1.31s) corners (all $p < .05$). There was no difference between the other corners. Post-hoc pairwise comparisons between Angular Segments showed significant difference between each pair (3-segment: M = 1.19s, 5-segment: M = 1.34s, and 7-segment: M = 1.46s) (all $p < .001$). Similar results were found on Distance Segments where there were significant differences for each pair (3-segments: M = 1.15s, 5-segments: M = 1.33s, 7-segments: M = 1.51s).

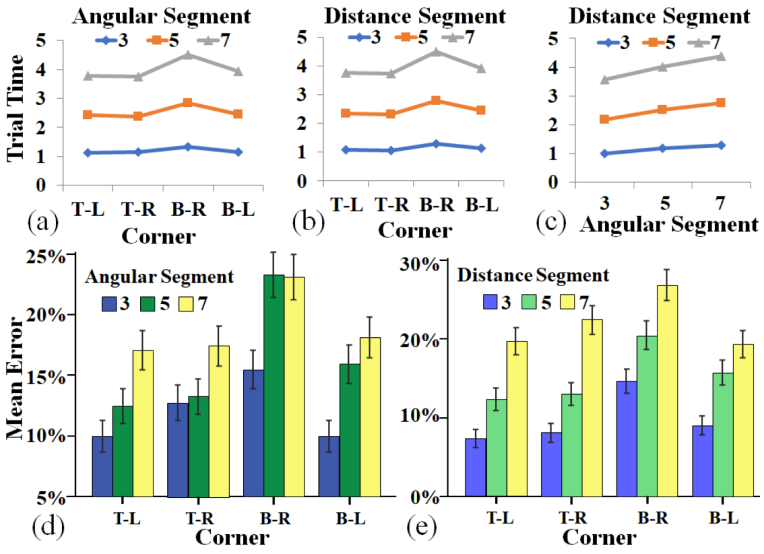

Figure 3.5: Study results: (a, b, c) average trial time and (d, e) error rates across different conditions. T-L, T-R, B-R and B-L represents Top-Left, Top-Right, Bottom-Right and Bottom-Left, respectively.

Error Rate. There was a statistically significant difference in error rate (Figure 5.6f and e) based on the corners that the participants used ($\chi^2(3, N = 12) = 10.3, p < .05$). Post-hoc pairwise comparisons showed that using the bottom-right corner, with an error rate of 20.7%, was significantly more error-prone than others (top-left: 13.2%, top-right: 14.5%, bottom-left: 14.7%). No significant difference was found for other pairwise comparisons. The analysis revealed a significant effect of Angular Segments on the error rate ($\chi^2(2, N = 12) = 6, p < .05$). Accessing items with 3 segments, with an error rate of 12.1%, was significantly less error-prone than with 5-segments (16.3%) and 7-segments (19.0%). There was no significant difference for other pairwise comparisons. Results also revealed a significant effect for Distance Segments ($\chi^2(2, N = 12) = 20.16, p < .05$). The error rate was 9.8%, 15.4% and 22.1% for 3, 5 and 7 Distance Segments, respectively, where all pairwise comparisons showed a significant difference.

Subjective Rating. The overall NASA-TLX ratings were less than 3.5. Results were analyzed using a Friedman test with Wilcoxon signed rank tests for pair-wise comparisons. The Friedman test yielded a significant difference in Corner ($\chi^2(3, N = 12) = 30.63, p < .001$), Angular segments ($\chi^2(2, N = 12) = 18.43, p < .001$) and Distance segments ($\chi^2(2, N = 12) = 19.16, p < .001$).

The participants rated the top-left corner as the easiest (M = 1.59) one to access items, followed by the top-right corner (M = 2.17) and bottom-left corner (M = 3.58). The bottom-right corner was rated as the hardest one (M = 5.75) (all $p < .05$). For Angular Segment, 3-segments were rated as the easiest (M = 2.08), followed by 5-segments (M = 3.0) and 7-segments (M = 5.0) (all $p < .05$). Similarly, for Distance Segment, 3-segments were rated as the easiest (M = 2.0), followed by 5 segments (M = 3.0) and 7-segments (M = 4.42) (all $p < .05$).

Discussion. The results revealed that selecting an item located at the bottom-right corner required longer trial time and was more error-prone than selecting items located at other corners. This is most likely due to the screen occlusion caused by the right-hand index finger for the right-handed participants. Additionally, the result analysis on other factors can be anticipated: trial time and error rates increased with increasing number of angular segments and distance segments. A higher error rate (e.g., around 15.8%) was observed across the factors. This is primarily caused by the occlusion-prone bottom-right corner as well as higher numbers of angular segments and distance segments that we used in our study. This rate could be reduced by determining suitable design parameters (e.g., the average error rate for top-left, top-right and bottom-left corners with 3 Angular Segment and 3 Distance Segments is 3.53%). Additionally, using the bottom-right corner for single step tasks such as "next", "cancel" or "reset" shall be suggested. As suggested in [118], the results could be mirrored for left-handed participants where the bottom-left corner is likely to be less efficient due to finger occlusion.

3.3 Evaluating Page-Flipping Interface

Page-Flipping interface leverages users' spatial memory to recall items that are placed in a hierarchical layout using corner-command mappings. It also combines command invocation and value selection into a single drag action. Researchers have presented other techniques such as marking menus [69] or radial menus combined with sliders [83] to support similar tasks. This study compares page-flipping interface with a functionally equivalent radial menu, as well as a standard smartwatch touch technique using swipe and tap, for both discrete and continuous selection tasks on smartwatches.

Task Type. This study explores selection performance of three techniques with two types of tasks: discrete and continuous target selections. Besides the discrete item selection tasks, that were used in the previous study, continuous tasks are often required on smartwatch interactions (e.g., adjusting music volume or changing display brightness). Therefore, this study includes 3 discrete tasks: (1) select a letter from a set of letters; (2) select a number from a set of numbers; (3) select an icon from an icon set; and 3 continuous tasks: (1) change the size of a triangle to match with a given triangle; (2) change the color of a filled triangle to match with a target color; and (3) change the stroke weight of a triangle to match a target stroke width.

Technique. The following techniques were studied with the six previously described tasks:

(Page-flipping.) Results from the previous study revealed that using the top-right and top-left corners for accessing items is faster and less error-prone than the other two corners. Therefore, this study included the top-left corner for discrete tasks and top-right corner for continuous tasks. This study used 3 angular segments and 5 distance segments as it showed faster trial time (1.14s) with less error rate (8.6%).

With page-flipping interface, a user first sees a discrete item (e.g., Letter 'E' in Figure 3.6a) or continuous value (e.g., blue color in Figure 3.6d) on the screen that they need to select. After reading this, the user can start dragging the top-left or top-right corner to reveal the list of discrete items (Figure 3.6b) or continuous values (Figure 3.6e). For discrete tasks, the currently highlighted value is shown with a different color (e.g., green). For continuous tasks, a preview (e.g., dark blue triangle) is included beside the target showing the user's currently acquired continuous value. The user can continue dragging the corner until it matches with the target discrete item or continuous value. When the user believes they have found the item or value (Figure 3.6c and f), they can lift-off their finger to commit the selection.

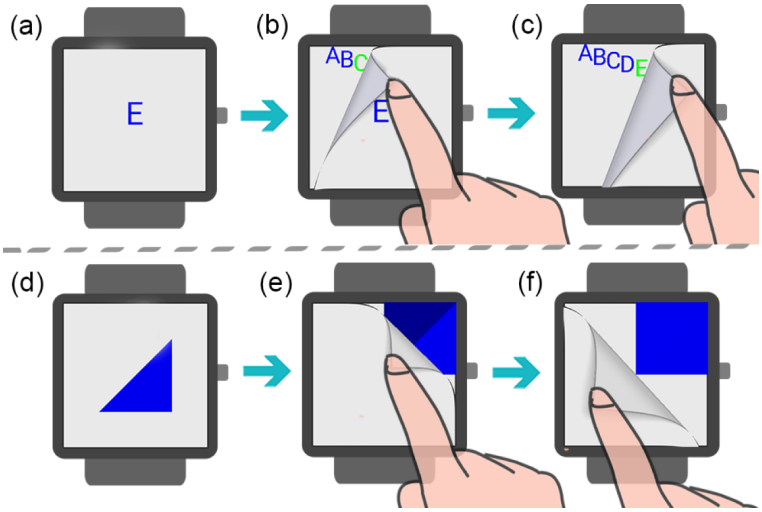

Figure 3.6: Page-flipping interface and workflow: (up) select a letter; and (below) change color. Note that we implemented all six tasks, other pictures are omitted to save space.

(Radial Menu.) The study initially considered Control Menus [102], FlowMenus [40] and FaST Sliders [83], which used radial or marking menus [69] for command selection followed by continuous value adjustment. However, the choice was constrained by (i) the small screen size that made scalability and navigating a deep hierarchy difficult [141]; and, (ii) drawing marks as in marking menus without a menu pop-up is likely to conflict with default swipe gestures. To mitigate these challenges, the study used a one-level radial menu design plus a slider-based value selection, and embedded a trigger mechanism. It adopted the design from [83], which enabled Radial Menu to be used as a technique for command invocation and continuous value selection.

In this technique, a user first sees an instruction screen showing a target item or value (Figure 3.7a and f). Dwell time was used to activate the menu. The user then long-presses on the screen center to trigger a menu where items are arranged in a radial layout around the initial touch position (Figure 3.7b and g). Menu items for discrete tasks (e.g., letter, number and icon) are displayed on the right side and items for continuous

tasks (e.g., weight, color and size) are placed on the left side. Without releasing the finger, the user can swipe to a direction to select a command (e.g., 'number' and 'weight' in Figure 3.7c and h, respectively). This action triggers a sub-menu with a list of available options for discrete tasks (Figure 3.7d) or the target continuous value that the user needs to select (blue triangle in Figure 3.7i). Like the page-flipping interface, a preview of the currently selected value (green triangle in Figure 3.7j) is displayed on the screen. To avoid the finger occlusion problem, the sub-menu is shown on the opposite side of the previous swipe direction. That is, swiping right opens the sub-menu to the left and vice-versa. For discrete tasks, a horizontal line is used to indicate the current finger position. An item is highlighted with green color if the line is on top of it (Figure 3.7e). For continuous tasks, the targets are always placed at the top-right corner. The user adjusts their finger position to match the preview with the target value (Figure 3.7j). Releasing the finger confirms the selection.

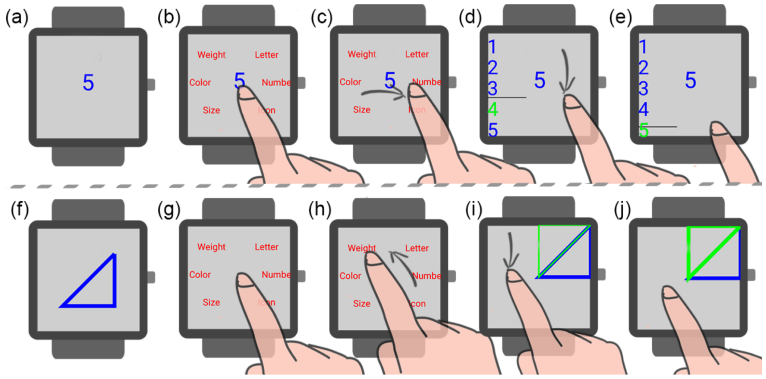

Figure 3.7: Radial Menu interface and workflow: (up) select a number; and (below) change stroke weight.

(SwipeTap.) The standard swipe and tap were included. This technique used the Android Wear 2.0 interface design patterns (e.g., swipe to invoke menus and tap to select) and elements (e.g., seek bar and scroll list).

At the beginning of a trial, this technique includes an instruction screen showing the target item or value (Figure 3.8a and f). A swipe-left gesture reveals a list of scrollable menu items (Figure 3.8b and g). In both discrete and continuous tasks, the user can tap on an item to access sub-menu items (Figure 3.8c and h). For the discrete task, they can then scroll the sub-menu items and select an item by tapping on it (Figure 3.8d and e). For continuous tasks, a target item, a preview and a seek bar are displayed on the screen (Figure 3.8i). The user can adjust the value by moving the seek bar handle (Figure 3.8j). When the user believes they have matched the preview with the target, the selection is triggered by a finger release action.

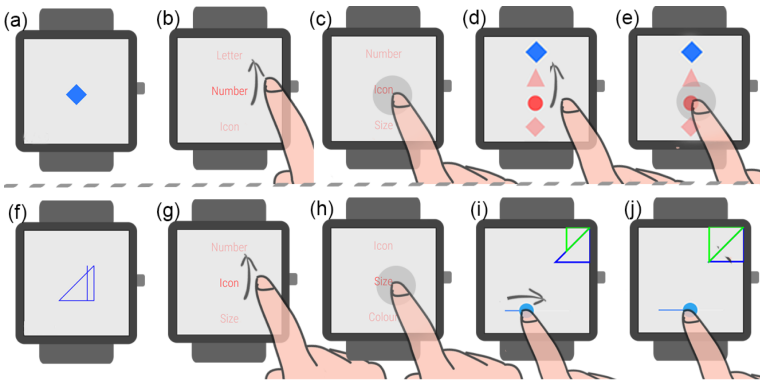

Figure 3.8: SwipeTap interface and workflow: (up) changing size; (below) selecting an icon.

Participants, Task and Experimental Design

12 participants (4 females, average age 26.9) took part in this study. All participants were right-handed and had no prior experience using smartwatches. The same apparatus was used as in the previous study.

At the beginning of a trial, the participants saw an instruction screen showing a target either for a discrete or continuous task and the current trial number. An Android app was developed to show experimental conditions. The app started the trial timer when participants tapped on the instruction screen. Participants then performed the command invocation and value selection tasks with one of the three techniques: Page-flipping, Radial Menu or SwipeTap. The 6 menu items (i.e., Letter, Number, Icon, Weight, Size, Color) were placed for both discrete and continuous tasks. The 5 items in each sub-menu (e.g., 'A', 'B', 'C', 'D', 'E' for 'Letter') were included for discrete tasks. For continuous tasks, the current value was shown based on the distance of curled edge to the corner (Page-flipping condition), the finger swipe distance (for Radial Menu), and the seek bar sliding distance (for SwipeTap technique). The timer for the trial was stopped when the participants selected the correct item. Selection attempts in a wrong menu or sub-menu item were ignored. The trial continued until the participants successfully selected the target item or value.

The study used a 3 $\times$ 2 within-subjects design for the factors Technique (Page-flipping, Radial Menu, SwipeTap) and Task Type (Discrete, Continuous). Participants were asked to repeat each condition 15 times (target value or item in each trial was randomly determined). In total, there were 270 trials per participant. The study counterbalanced Technique across participants and randomized the order of Task Type.

The study recorded trial time for each trial. It was further divided into Prepare Time: the time from the trial start to the first touch time, Menu Activation Time: from the first touch time to the time when menu appears, Menu Selection Time: time involves selecting an item from menu, and Value Selection Time: time to select a target value in the sub-menu. As expected, Page-flipping took no Menu Activation Time and Menu Selection Time (i.e., dragging a corner to a direction directly triggers a sub-menu for value selection).

Two types of error were recorded. A Type 1 Error was logged when participants took a wrong selection attempt to invoke a menu item. A Type 2 Error was registered when participants selected a wrong sub-menu item or value. The participants were asked to complete the tasks as fast and accurately as possible. They were asked to fill a NASA-TLX form for every technique, and their overall preferences (1 – least preferred most and 7 – most preferred). The study session lasted around 40 mins including practice trials.

Results

The data was analyzed using repeated measures ANOVA and Bonferroni corrected paired t-tests for pair-wise comparison to compare the techniques.

Trial Time. It was found that participants spent 2.73s, 3.49s and 5.38s on average to complete a successful trial with Page-flipping, Radial Menu, and SwipeTap, respectively. A repeated measures ANOVA yielded a significant effect on Technique ($F_{2,22} = 187.02, p < .01$) and Task Type ($F_{1,11} = 246.22, p < .01$). Post-hoc pairwise comparisons showed a significant difference for each pair (all $p < .01$). It was also found that participants were significantly faster with the discrete tasks (M = 3.26s) than with the continuous tasks (M = 4.47s). There was an interaction effect between Technique and Task Type ($F_{2,22} = 102.94, p < .01$).

The trial time for discrete and continuous tasks were further examined separately. For discrete tasks, the average task completion time for Page-flipping, Radial Menu, and SwipeTap were 2.56s, 2.97s and 4.25s, respectively. For continuous tasks, the average task completion time for the three techniques were 2.91s, 4.00s, and 6.51s. A one-way repeated-measures test yielded a significant effect of the techniques on both discrete tasks ($F_{2,22} = 106.58, p < .01$) and continuous tasks ($F_{2,22} = 198.44, p < .01$). For both task categories, each pair of techniques were significantly different (all $p < .05$).

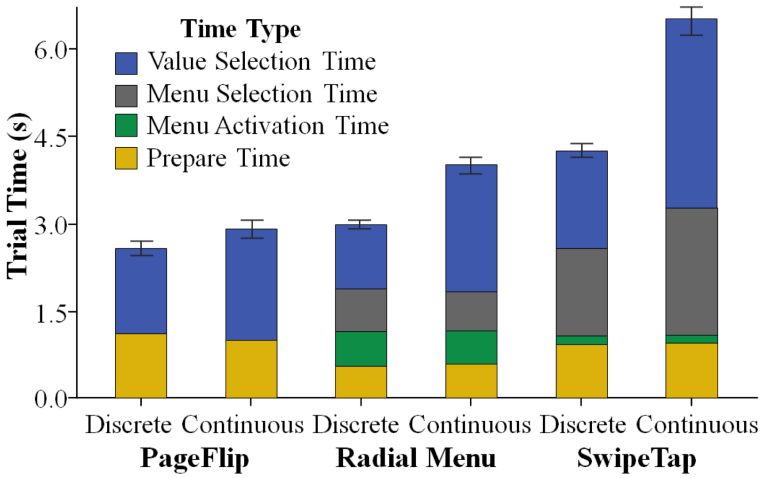

Figure 3.9: Average trial time for both discrete and continuous tasks across three techniques.

Prepare Time. Prepare Time was significantly shorter with Radial Menu (M = 0.56s) than the other two (both $p < .01$). SwipeTap (M = 0.93s) had significantly less Prepare Time than PageFlip (M = 1.05s, $p < 0.05$). No significant effect of the TaskType on Prepare Time was found.

Value Selection Time. A significant effect of Technique ($F_{2,22} = 60.80, p < .01$), TaskType ($F_{1,11} = 177.89, p < .01$) and their interactions ($F_{2,22} = 62.52, p < .01$) for Value Selection Time was found.

For discrete tasks, a one-way repeated-measure test yielded a significant effect on Technique ($F_{2,22} = 51.08, p < .01$). Pairwise comparisons showed that Radial Menu (M = 1.10s) used significantly less time than the others. Additionally, Page-flipping (M = 1.46s) required significantly less time than SwipeTap (M = 1.72s) (all $p < .01$). A significant effect was also found on Technique ($F_{2,22} = 63.68, p < .01$) for continuous tasks. Pairwise comparison showed that SwipeTap (M = 3.24s) used more time than the others (both $p < .01$), but Page-flipping (M = 1.91s) and Radial Menu (M = 2.17s) had no significant difference ($p = .067$).

Error Rate. A Friedman test was used to examine error rate with a Wilcoxon test for pairwise comparison. The two types of error were analyzed separately.

Type 1 Error: There was a significant difference between Techniques ($\chi^2(2, N = 12) = 10.67, p < .01$) and post-hoc pairwise comparisons showed that using Page-flipping (0.74%) was significantly less error-prone than Radial Menu (3.70%) and SwipeTap (2.13%). Other pairwise comparisons didn't show any significant difference. Also, there was no significant difference among the Task Types ($\chi^2(1, N = 12) = 1.6, p = .21$). Discrete (2.28%) and continuous tasks (2.10%) were equally error-prone.

Type 2 Error: The results revealed a significant effect for Technique ($\chi^2(2, N = 12) = 16.95, p < .001$). Post-hoc pairwise comparisons showed that accessing items with Page-flipping caused significantly more error (14.72%) than Radial Menu (8.8%) and SwipeTap (6.3%). There was no significant difference for other pairwise comparisons. The results also found a significant effect of Task Type ($\chi^2(1, N = 12) = 11.00, p < .001$) on error rate. Discrete tasks were less error-prone (5.25%) than continuous tasks (14.63%).

Subjective Rating. The overall TLX ratings for Page-flipping were less than 3.5, while Radial Menu required higher Effort (¿ 3.5), and SwipeTap required higher Physical Demanding and Effort (both ¿ 3.5). A Friedman test yielded a significant difference in Technique ($\chi^2(2) = 7.64, p < .05$). A Wilcoxon signed ranks test found that participants preferred Page-flipping (M = 4.41) more than the other two techniques (Radial Menu: 3.17, SwipeTap: 2.08, $p < .05$). No other pairwise comparison was significant.

Discussion

The results indicate that Page-flipping interface is an efficient candidate to be used for designing value selection tasks on smartwatches. Page-flipping improves selection time for both discrete and continuous

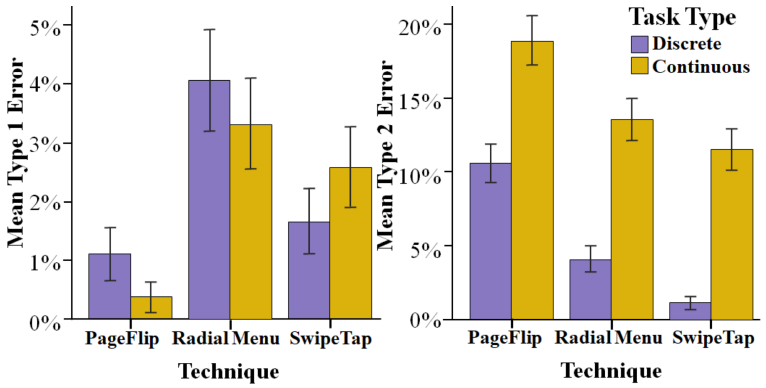

Figure 3.10: Average Type 1 and Type 2 Error rate on different techniques and tasks.

tasks. It has the advantage of having no menu activation time and menu selection time. Radial Menu had the significantly shortest prepare time, which indicates that the participants reacted faster with this technique after seeing the targets. This might due to the finger dwell time that gave them extra time to spatially recall where the menu item was. A 600ms dwell time, that was used based on the system's default settings, caused longer menu activation times. It was also found that the Radial Menu was faster in selecting discrete items. It leverages the users' finger position to automatically highlight a sub-menu item when the user selects a menu item. For instance, Radial Menu automatically highlights '3' after selecting 'Number' menu as shown in Figure 3.7. This auto-highlight feature also helps Radial Menu to be faster as users need to travel shorter distances to access other items (e.g., from '3' to '1' or '3' to '5'). Finally, the SwipeTap had longer menu selection time and value selection time as it required multiple swipe and tap operations to invoke items.

It was also observed that Page-flipping had less Type 1 Errors, meaning users barely selected a wrong menu item. This is understandable for two reasons. First, discrete and continuous tasks were placed separately in two opposite directions, on the left and right corners, respectively. Second, Page-flipping design allows participants to switch fluently between items by changing the angular direction (e.g., from 'E' in 'Letter' to '5' in 'Number'). Such fluent switching between items was not supported by the other techniques. It is worth to acknowledge that the current Radial Menu implementation does not allow cancellation by returning to the center as it could conflict with the 1D sliding operations. Such operations might help reduce Type 1 error, but at the cost of increased trial time.

Page-flipping caused more Type 2 Errors. There might be two reasons. First, discrete items require precise and accurate selection actions as the items were placed in a small semi-circular layout. Second, when selecting continuous values, the preview and target were partially covered by the curled page, making it harder for users to identify the currently obtained value. These visual design drawbacks should be carefully

considered to improve the technique's accuracy. Since targets are only visible with curled pages, it is recommended that the menu items should be placed in a more ordered way to foster users' spatial memory and improve selection efficiency. Some participants had difficulty adjusting color or stroke weight to match the targets, regardless of selection technique.

The study did not compare the learning effort for these three techniques. It is worth mentioning that for novice users, the current design of Page-flipping interface requires much longer exploration time than the other two techniques as the commands are only visible with curled pages. Additionally, the participants spent a relatively long time in the practice session to get familiar with the menu layouts, especially, for the Page-flipping and Radial Menu. This encourages future work to analyze the performance of the techniques when the users already built spatial mappings of the menus.

3.4 Applications Using Page-Flipping Gestures

This section includes three Page-flipping applications to demonstrate its possibility for novel smartwatch interactions. These applications utilize one or several unique features that Page-flipping interface supports. For instance, Page-flipping could be designed to support a stacked-page layout where items can be placed into multiple layers. Additionally, Page-flipping gestures can be used to indicate users' intentions while using smartwatches. For instance, a user can drag a corner to a short distance and hold the finger there to examine a command. A further dragging action can invoke the command or push-back gesture can be used to cancel it. The user may also drag the corner directly to an item if she is familiar with the commands (Figure 3.11).

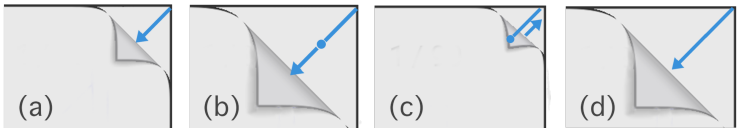

Figure 3.11: A user (a) starts dragging the corner and holds; (b) continues to drag the corner after holding; (c) pushes back the corner after holding; (d) drags the corner without holding.

Message Edit

Text editing is usually tedious requiring multiple steps of menu invocation and selection process. The page-flipping interface can be used to edit short messages on-the-go. For instance, a user wants to remind her colleagues of a meeting schedule. She first enters "Meeting at 10:30 AM" with her smartwatches' speech input. She is not satisfied with the default font size and color, so she edits the message by dragging the top-right corner to change the font size and color, to make it more visible (Figure 3.12a). Dragging to one direction picks a color from several options (Figure 3.12c) and dragging to another direction from the same

corner continuously adjusts the font size (Figure 3.12b). As she finds the changes are not suitable after the first edit, she drags the top-right corner on the second layer to reset it (Figure 3.12d). When the user is satisfied with the edit, she drags the top-left corner to select a name from the contact list (Figure 3.12e) and the message is sent upon the finger release. The user is also able to drag the bottom-right corner and flip the whole page (Figure 3.12f), to create a new message in an efficient way.

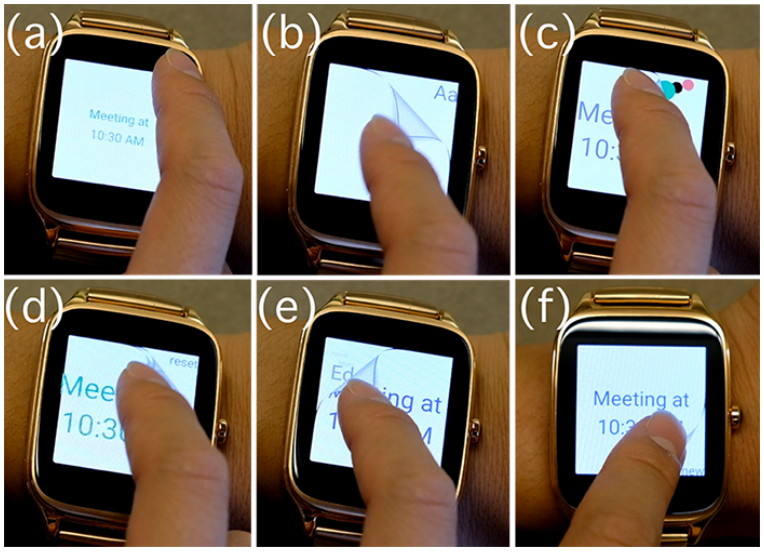

Figure 3.12: Message editing with page-flipping gestures.

App Notification, Preview and Switching

Displaying an app notification could occupy screen space from users' current task on the smartwatch. The page-flipping interface provides an alternative way for showing notifications and switching to the app. A page corner is curled automatically when there is a notification (Figure 3.13a). The corner takes less space, thus not affecting users' current task. Meanwhile, the corner can be kept curled to make sure users do not miss it. The user can drag the corner towards the center to preview the notification content (Figure 3.13b), continue dragging further to open the notification (Figure 3.13c) or push the corner back to remove the notification (Figure 3.13d).

Figure 3.13: App notification, preview and switch with page-flipping gestures.

Pattern Stencil

A pattern stencil technique was designed using the page-flipping gestures. The application integrates a double click action to demonstrate that the page-flipping gestures are compatible with other touchscreen gestures. A user wants to design a stylish letter on her smartwatch for a birthday card. She double-clicks on a pre-selected picture and invokes a "brush" command. She uses her finger to brush on the picture and draws a "Z" (Figure 3.14a). The user then drags the top-right corner to invoke the "copy" command (Figure 3.14b). She flips the whole page to the second layer, where the brushed content is already pasted and ready to be used (Figure 3.14c). This action is similar to tracing on paper or pasting a temporary tattoo, thus easy to learn. Such a technique can also be used to create stylized textured brushes, and cut out a photo.

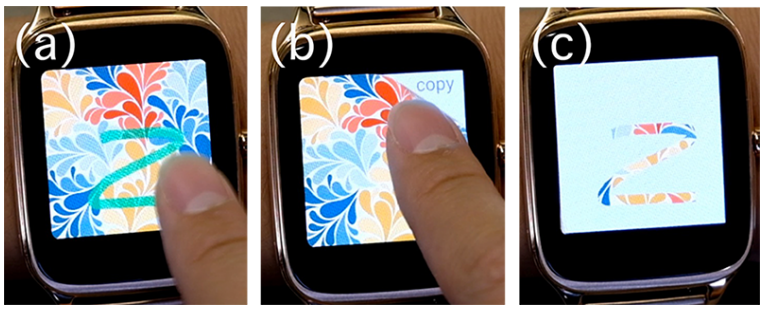

Figure 3.14: Create a textured letter with page-flipping gestures.

3.5 Chapter Summary

This chapter explored the design and performance of Page-flipping gestures, that leverages corner-command mappings and supports command invocation and value selection in a single corner-drag action on wearable touchscreen. The gestures are originally used in book reading activities. The rich information expressed by the gestures, such as finger flipping direction and distance, can be transformed and mapped with menu operations with a suited layout.

Besides of the efficiency, the advantage of leveraging the page-flipping gestures on wearable touchscreen, is that it provides users an intuitive feelings when operating the menu. The gestures and the interface metaphors are familiar to the users, and both mental and physical effort required by performing the gestures are comparable to, and even less than traditional tap and swipe gestures.

Designing the page-flipping gestures on touchscreen faces several key usability challenges such as Discoverability, Affordance and Learnability, especially for novice users. Like most gestural input on touchscreens, it is hard for novice users to find available gestures or commands. It is essential to design a tutorial mode for novice users. For instance, a corner could automatically be curled to show available or recommended

commands upon the task context and users' actions. Further strategies could help novices learn quickly. For example, consistent command-corner mappings for frequent commands or categorizing discrete and continuous commands into left and right corners, as in the second study, could be used to facilitate spatial memory and improve learning. Using many angular dragging directions with one corner might increase users' mental and physical effort. Although participants are familiar with the page-flipping gestures of other metaphors (e.g., books), the use of the gestures for command invocation and value selection are new to them. UI designers could consider incorporating page-flipping gestures as a complementary feature to existing touch input, which could make such page-flipping gestures common to users.

Although design like page-flipping gestures is shown to be intuitive to use and improve the input efficiency, the fundamental challenges of wearable touchscreen still exist. Gestural input that can be performed around the device raises more attention as an alternative way to mitigate the input challenges on the wearable devices. It overcomes the limitation of the input space on device, and enriches the expressiveness via leveraging the dexterity of the hands. This could potentially provide an input solution, for wearable devices that are with, or without touchscreens.

Chapter 4

Body-Worn Display with In-Air Gestures

An alternative way to mitigate the on-screen input challenge is using in-air gestures. Compared to touch-screen input, gestural input takes the advantage of allowing a wide range of operating space around the devices, without requiring precise pixel-level locating. Gestural input can be expressive and adaptive to diverse usage contexts. For instance, gestures can range from coarse hand movements such as hand waving, to fine-grained finger movements and micro-gestures.

Exploring gestural input for mobile and wearable devices is not new. Prior research has shown that a mobile device or environment can be instrumented to track gestures performed around the devices (e.g., in the air, on the body, and on physical surfaces) to enrich the interaction design. The gestural interactions have been shown promising to mitigate the input challenge on wearable devices [3]. However, previous work lean towards examining gesture spaces driven by technology. The drawback is designers often need to adapt users to system limits and comfort the way we interact with smartwears to a set of arbitrary conventions or procedures [94]. Such interfaces are often inconsistent to our normal behaviors. For instance, current smartwatches usually embed a series of motion gestures detected with accelerometers. Users can switch menus by quickly flicking their wrists. It seems fine but may look awkward to many users like they try to "shake a mosquito off the thing".

This chapter focuses on exploring an alternative method to design in-air gestures that provides intuitive feeling to users via bridging the gap between novel smartwear interactions and real-life experiences shared among users. This chapter discusses a solution via using hand generated acoustics. Non-vocal acoustics that are produced using our hands are common in daily lives, such as when snapping or rubbing our fingers,

tapping on objects or even when using an auxiliary object to generate the sound. Such naturally occurring acoustics can be captured and leveraged in wearable device interactions.

4.1 Acoustic Signatures

Acoustic signatures are generated using hand-based sound events and therefore can provide a large and rich vocabulary, especially, if we include acoustic features such as tempo and rhythm. A catalog of acoustic signatures can be defined based on the sound sources generated via different hand gestures. Their input attributes can be analyzed and leveraged for wearable device interactions. In this way, common hand activities such as finger snapping, and hand clapping, can be transformed into inherent input gestures.

To gain initial insights on the types and attributes of acoustic signatures, a design workshop was run with eight senior students and one professor from the music department at a local university. They are familiar with sound generation theory and processes. The design session was structured as follows. We first explained the goal of the project and mentioned how non-voice acoustics can be produced with hand actions (i.e., snapping or clapping). Participants were then asked for written suggestions or sketches of potential acoustic signatures. They were instructed to list all the sound sources they can imagine without considering recognition or technical issues. We discussed and refined the proposed signatures together with the participants. The session took approximately 30 minutes to complete.

In total 56 acoustic signatures were collected. A subset of that list is presented in Figure 4.1, which is not intended to show an exhaustive set, but those deemed possible and popular (listed at least twice by participants). They were grouped according to the following two key axes, handedness and location.

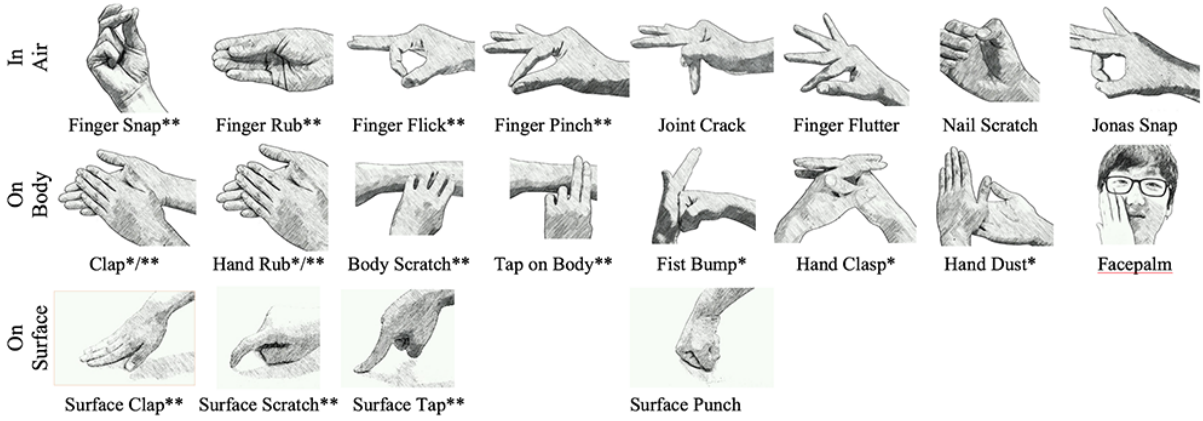

Figure 4.1: Acoustic signatures collected from musicians (* indicates two-handed, ** indicates signatures evaluated in this section).

4.1.1 Handedness

This category defines the number of hands (one-handed, or two-handed) involved in producing a sound. *One-handed signatures* usually require the use of multiple fingers. Some are explicit (e.g., snapping, joint cracking, tapping) where the gestures can be performed at a relatively large distance from the device and the sound generated is recognizable by nearby users. Others are finer grained signatures (e.g., finger rubbing, nail scratching) which are more subtle. One-handed signatures can be performed on either the wearing or the non-wearing hand. During the design session, most participants demonstrated the gestures using their dominant hand.

Two-handed signatures require both hands to produce a sound. Examples include hand clapping or clasping where one hand comes in contact with the other. These gestures, however, can hardly benefit from sound source location to the device as they are restricted to hand position. One-handed signatures can be transformed into two-handed ones if both hands simultaneously perform the action, offering the opportunity for bi-manual interactions on smartwatches.

4.1.2 Location

This category defines where the gestures are performed (in-air, on-body or on-surface). In-air signatures are those performed by fingers without touching additional body parts or surfaces. Examples of such gestures include finger snapping, rubbing and pinching.

On-body signatures produce sounds with hands or fingers contacting other body parts (including the other hand). Tapping and scratching for instance, are two common signatures in this category. In these cases, forearms are often used as they provide relatively large and flat surfaces.

On-surface signatures are similar to those on-body but contact is with physical objects. A variety of sounds can be produced with the same gesture by varying surface types. For instance, flicking on a table would generate a different sound than flicking on water.

Participants expressed their impression of using acoustic signatures for smartwatch usages. All of them were very enthusiastic about using such gestures. Many of our participants mentioned that such input would allow them to access their smartwatch without using the small touch screen. Additionally, they indicated that accessing information with acoustic signatures would be faster than on-screen operations. However, a few participants raised the issues of not being able to perform certain gestures. For instance, one student reported that he was not able to snap. Some others raised the social acceptance issues in public places. They stated that the "small, quick and less noticeable" gestures such as finger rub are more acceptable in public placed rather than explicit two-handed gestures such as clapping.

4.2 Capturing Acoustic Signatures

A prototype, SoundCraft, was built[1] using a 4-microphone array on a small wrist-worn platform. This enables sound detection, localization, enhancement, and classification by placing each of the four microphones in the four corners, and running a series of acoustic processing algorithms.

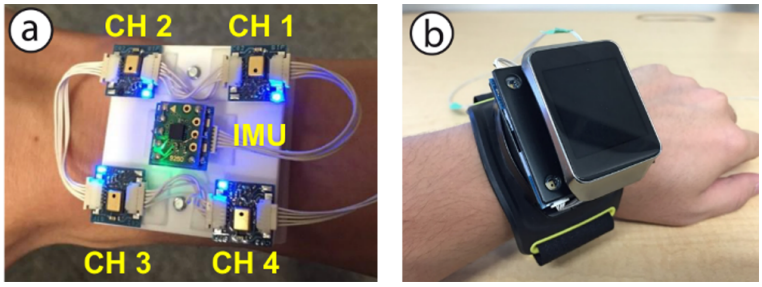

Figure 4.2: (a) Four microphones placed at 1.5 inches apart at the corners of the device, and a IMU in the middle; (b) a watch display attached to create the SoundCraft prototype.

4.2.1 Hardware

We use four digital MEMS microphones (Knowles SPM0406 [2]) each placed at one corner of a platform (1.5 × 1.5 inches, Figure 4.2). The microphones operate synchronously with a central micro controller (RASP-ZX [3]), which is powered by and communicates with a Linux machine via USB connection. The system is set to record the data at a 16 kHz sampling frequency and 24-bit ADC Dynamic Range. We also mounted a 6-axis Inertial Measurement Unit (IMU) (BMI150 [4], Figure 4.2a) that records data at 2 kHz sampling frequency and 16-bit ADC dynamic range, synchronously with the microphone.

4.2.2 Software

The Linux machine receives and processes acoustic signals. It transfers sound source information (i.e., location and classification) over sockets to a Samsung Mini S4 phone. An Android wear watch is used for demo applications which communicates with the phone via Bluetooth.

4.2.3 Acoustic Processing

Our aim was to implement acoustic processing that operates with microphones at very close proximity, as well as to adapt to noise changes when the user moves between environments. Therefore, the key challenges

[1]The hardware and algorithm were developed with the help from Honda Research Institute, Japan.
[2]www.Knowles.com/eng/Products/Microphones/SiSonic%E2%84%A2-surface-mount-MEMS
[3]www.sifi.co.jp/system/modules/pico/index.php?content_id=36
[4]www.bosch-sensortec.com/bst/products/all_products/bmi160

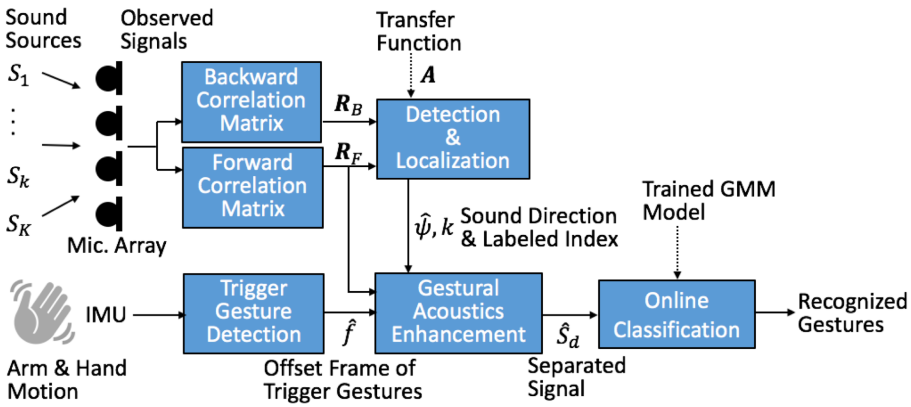

Figure 4.3: Block diagram of SoundCraft's audio processing.

in the acoustic processing for recognizing acoustic signatures involve: i) designing a suitable algorithm that separates the source locations when the microphones are at proximal location; ii) detecting low power acoustics in noisy environments, and; iii) enhancing the acoustics by estimating current environmental noise. For (i) and (ii), we adopted a robust target signal subspace method, *MUltiple SIgnal Classification (MUSIC)* [109] with extensions to the generalized Eigenvalue decomposition introducing correlation matrices of estimated noise [88]. MUSIC originally uses standard eigenvalue decomposition so that high power sounds can be detected. In our work, we extend it to use generalized eigenvalue decomposition with a dynamic backward and forward noise correlation matrix to improve detection of acoustics in a noisy environment. We detect an acoustic event onset by defining the frames just before the observed frames as 'noise'. For (iii), we introduce wrist twists as a "trigger gesture" detected by the IMU, to explicitly notify the smartwatch of environment changes. After the trigger, the background noise information is updated and used for a *Minimum Variance Distortionless Response (MVDR)* beamformer [116], which results in enhanced acoustics. The block diagram shown in Figure 4.3 summarizes the acoustic processing components used in this section. The system contains two pipelines: detection and localization of acoustic events, and enhancement of the detected acoustics for classification. We describe the system stepwise as follows.

Sound Source Model

To describe the system mathematically, we define $X_m(\omega, f)$ and $S(\omega, f)$ as the acoustic signal input of the m-th channel ($1 \leq m \leq M$) of a M-microphone array and a sound source signal after a *Short Time Fourier Transform (STFT)*, respectively (where ω is the frequency bin index, f is the time frame index). Assuming the frame is sufficiently long and $S(\omega, f)$ is at location ψ, the observation model is described as:

$$X_m(\omega, f) = A_m(\omega, \psi)S(\omega, f) \tag{4.1}$$

where $A_m(\omega, \psi)$ is a *Transfer Function (TF)* at the frequency ω from the m-th microphone to the sound source located at ψ. The TF models the characteristics of the surroundings relative to the intrinsic properties of the microphones with regards to sound propagation. TFs are usually used as prior information and obtained in advance either via actual measurement or geometrical calculation.

Since we use a planar microphone array, we consider only the azimuth (from 180° to 180°) and positive elevation (from 0° to 90°) in relation to the device. Moreover, the sound source distance is not considered since the small size array has a short Fraunhofer distance $d_F(\omega)$ computed as:

$$d_F(\omega) = \frac{2{D_M}^2}{\lambda(\omega)} \tag{4.2}$$

where $\lambda(\omega)$ and D_M are the wave length at the frequency bin ω and the size of the array, respectively. A distance greater than $d_f(\omega)$ is considered as "far field", making the distance estimation difficult. In our case, the microphone array on the smartwatch, 0.038m sized square, has $D_M \approx 0.054$m, resulting in a $d_F(\omega) \approx 0.135$m for 8 kHz and 0.051m for 3 kHz, which is too short for capturing spatial position around the watch. Additionally, we assume that there is only one acoustic signature at a time in one location.

Let $S_k(\omega, f)$ denote the k-th spatial acoustic ($1 \leq k \leq K$) where K is the total number of acoustics at a time. The purpose of detection, localization, and enhancement of sound sources is to detect all $S_k(\omega, f)$ under a noisy environment.

Computation of Backward and Forward Correlation Matrices

As shown in Figure 4.3, the system first defines forward and backward correlation matrices of the current observed and previous frames, respectively, which are used for sound source localization and enhancement. The correlation matrices are averaged over F frames to make them robust against instant noise. F is empirically determined as $F = 50$.

Let $X(\omega, f) = [X_1(\omega, f), \cdots, X_M(\omega, f)]$ denotes $X_m(\omega, f)$ of all channels. The forward correlation matrix of the observed signals is computed as:

$$R_F(\omega, f) = \frac{1}{F} \sum_{i=0}^{F-1} X(\omega, f-i) X^*(\omega, f+i) \tag{4.3}$$

and the backward correlation matrix is computed as:

$$R_B(\omega, f) = \frac{1}{F} \sum_{i=1}^{F} X(\omega, f-i) X^*(\omega, f-i) \tag{4.4}$$

where $()^*$ is a complex conjugate transpose operator.

Sound Source Detection and Localization

We adopt *MUSIC* [109] to detect and localize acoustic signatures relative to the microphone array. This block in Figure 4.3 labels acoustics with direction information.

In this work, we focus on onset detection of acoustic signatures. At each onset, the backward correlation matrix contains only noise (i.e., background without acoustic signatures), and the forward correlation matrix contains both noises and target acoustics. Therefore, we introduced the following generalized Eigenvalue decomposition to whiten the noise information of the backward correlation matrix from the forward correlation matrix:

$$R_F(\omega, f)E(\omega, f) = R_B(\omega, f)E(\omega, f)\Lambda(\omega, f) \tag{4.5}$$

where $E(\omega, f)$ and $\Lambda(\omega, f)$ are the Eigenvector matrix and the Eigenvalue matrix, respectively. Let $E(\omega, f) = [E_1(\omega, f), \cdots, E_M(\omega, f)]$ denote the Eigen vectors. The spatial spectrum is given as:

$$P(f, \psi) = \frac{1}{\omega_H - \omega_L + 1} \sum_{\omega=\omega_L}^{\omega_H} \frac{|A^*(\omega, \psi)A(\omega, \psi)|}{\sum_{m=L_{s+1}}^{M} |A^*(\omega, \psi)E_m(\omega, f)|} \tag{4.6}$$

where L_s is the number of sound sources at a time frame. and are the frequency bin indices that represent the maximum and minimum frequency considered, which are set as $500Hz \leq \omega \leq 2800Hz$. Let $\hat{\psi}$ demote ψ that maximizes $P(f, \psi)$ at the f-th frame. The frames that satisfy $P(f, \hat{\psi}) \geq T_p$ are defined as activity periods of target acoustics, and the sequence of $\hat{\psi}$ with respect to f is the direction of detected acoustics, where T_p is a threshold. Moreover, we track $\hat{\psi}$ with respect to time and direction to obtain $S_k(\omega, f)$. We simply conduct thresholding if the consecutive $\hat{\psi}$ is sufficiently close with respect to time and direction in order to regard the two $\hat{\psi}$ as the same acoustic signal. All $\hat{\psi}$ regarded as the same signal, and labeled by $S_k(\omega, f)$.

Detection of Trigger Gestures

Meanwhile, we use a beamformer to spatially de-noise and enhance the detected acoustics for classification. This improves the robustness in noisy environments.

Using a trigger mechanism provides practical support and is not unusual for commercially available commercial systems such as "Alexa" in Amazon Echo and "Siri" in Apple. To update the noise information when environments change, we use a trigger gesture. We experimented with the nine hand gestures, with signals shown in Figure 4.4. We selected the wrist twists as it showed sufficiently larger angular velocity of y-axis $\dot{\theta}_y(f)$ than others. We simply detect wrist twists with the following threshold:

$$\max_{0 \leq i \leq F} |\dot{\theta}_y(f+i)| \geq T_\theta \tag{4.7}$$

where $\dot{\theta}_y(f)$ is a threshold. The last frame where Eq.(4.7) is satisfied is defined as the offset of the trigger gesture, and the frame is defined as $\hat{f}$. The noise information is updated after the trigger. Namely, the forward correlation matrix at the $\hat{f}$-th frame (just after the trigger) is memorized as the current noise information, which is denoted as $R_F(\omega, \hat{f})$, and used for the enhancement of the acoustic signature.

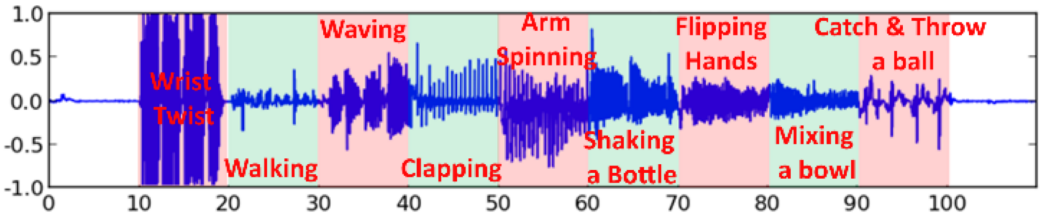

Figure 4.4: Angular velocity of Y-axis of the in kdeg/sec.

Enhancement of Localized Sound Sources

We introduced $MVDR$ with the selected forward correlation matrix $R_F(\omega, \hat{f})$ by the trigger gesture and the location of the sound source $\hat{\psi}$. The sound source location above provides the direction $\hat{\psi}$ and the label index k. When a sound source is detected, the corresponding TF TF is selected from the estimated $\hat{\psi}$ and k, denoted as $A_k(\omega, \hat{\psi})$. The $MVDR$ based enhanced signal is computed as follows:

$$\hat{S}_k(\omega, f) = \frac{A_k^*(\omega, \hat{\psi}) {R_F}^{-1}(\omega, \hat{f})}{A_k^*(\omega, \hat{\psi}) {R_F}^{-1}(\omega, \hat{f}) A_k(\omega, \hat{\psi})} X(\omega, f) \tag{4.8}$$

where $\hat{S}_k(\omega, f)$ is the estimated $S_k(\omega, f)$. Since we use $R_F(\omega, \hat{f})$ which contains the current environmental noise, Eq.(4.8) can enhance the k-th acoustic by beamforming in the $A_k(\omega, \hat{\psi})$ direction and subtracting the environmental noise.

Sound-Source Classification

We train a $GaussianMixtureModel(GMM)$ with 64 components for each of the enhanced acoustics. The GMM captures the acoustic information of the individual gesture, namely $S_k(\omega, f)$. Training parameters are summarized in Table 4.1. The trained $GMMs$ are used during online classification together with the separated acoustic signal. The likelihood score for each model representing a particular sound gesture is computed using the separated acoustic data. The corresponding acoustic model with the highest score is selected as the most likely acoustic signature.

Sampling frequency	16kHz
Frame length	25ms
Frame period	10ms
Pre-emphasis	1 - $0.97z^{-1}$
Feature vectors	12-order MFCCs, 12-order MFCCs, and 1-order E
GMM	64 Gaussian components

Table 4.1: System parameters used in the system.

4.3 Localization and classification Accuracy

Three studies were conducted to evaluate how accurately the prototype can localize and classify acoustic signatures, both in non-noisy and noisy environments.

4.3.1 Study 1: Localizing acoustic signatures

This study examined how accurately the prototype can localize acoustic signatures in a non-noisy environment. It used a 2D discrete target selection task where wedge shape items were arranged in a circular layout (Figure 6b and c). An external screen was laid horizontally and vertically to mimic azimuth and elevation conditions, respectively. These settings alleviate confounds due to the visuo-motor mapping.

One in-air (finger snap) and one on-surface (surface tap) acoustic signature were selected, based on the most frequently mentioned gesture by the participants in the design workshop. The study design used 4, 8, 12 and 16 discrete wedge shape laid out in a half-circle, giving $45°, 22.5°, 15°, 11.25°$ angular widths for the items. In a natural smartwatch viewing position (i.e., close to the body), users have limited in-air angular space ($\sim 180°$) in the horizontal direction. To be consistent with both azimuth and elevation conditions, Only a 180° angular space was considered for both these two axes.

A $2 \times 2 \times 4$ within-subject design was used for factors Axis (Azimuth and Elevation), Acoustic Signature (Finger Snap and Surface Tap) and Angular Width ($45°, 22.5°, 15°, 11.25°$). The presentation order of Axis and Acoustic Signature were counterbalanced among the participants using a Latin square design. The order of the Angular Width was randomized.

12 right-handed participants (2 females, mean age 26.4 years) took part in the study. They wore the prototype on their non-dominant hand and moved it close to the bottom center of the screen (Figure 4.5b-c). A target was shown on the screen with a blue wedge and the participants were asked to move their dominant hand close to the target and perform a gesture. Once the acoustic signal was detected on the target, the blue wedge color changed to green and the screen showed the next target location. An incorrect selection highlighted the actual selected wedge in red. Participants performed 30 repetitions (target segment was randomly picked) for each condition, resulting in a total of 480 trials per participant. With practice trials,

the study session lasted approximately 50 minutes.

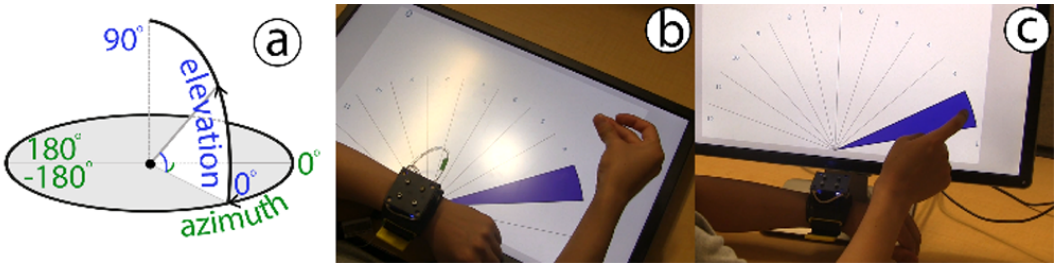

Figure 4.5: Experiment interface for 12 segments.

The data was analyzed using a repeated-measures ANOVA and Bonferroni corrected paired t-tests for pair-wise comparisons. A significant effect was found on Axis ($F_{1,11} = 39.786, p < .01$) and Angular Width ($F_{3,33} = 82.897, p < .01$), and interaction between these two ($F_{3,33} = 9.601, p < .01$). There was no significant effect of Acoustic Signature ($p > .05$).

Figure 4.6 shows the average localization accuracy across the twelve participants. Overall, it achieved an average accuracy of 99.37% (std. = 0.45%) with 45° segments on both azimuth and elevation dimensions. As expected, 11.25° segment on these dimensions returns the lowest average accuracy of 83.77% (std. = 5.02%). Results also indicated higher accuracy across all conditions (≥90%) when the segment is larger than 15°.

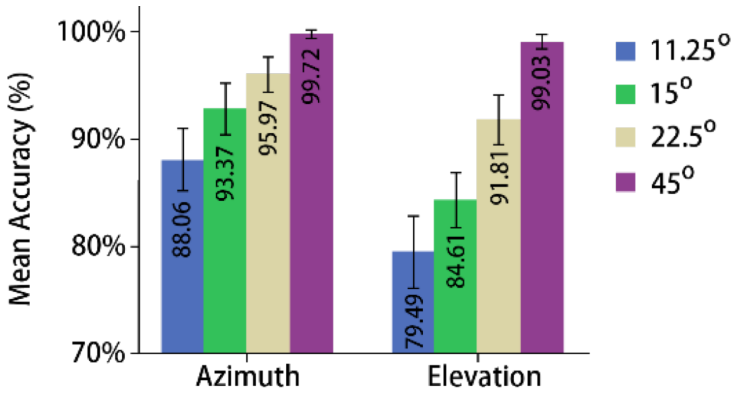

Figure 4.6: Average localization accuracy across 12 participants on Axis and Angular Width. (Error bar: 95% CI).

It was observed that the prototype localized the sound events significantly more accurately in azimuth (avg .= 94.28%, std .= 4.33%) than in elevation (avg .= 88.73%, std .= 7.94%). Tap (avg. = 91.33%, std. = 6.24%) is more accurate than Snap (avg. = 86.13%, std. = 8.59%) in elevation dimension, but performs equally well in azimuth (avg. = 93.77%, std. = 4.90% and avg. = 94.79%, std. = 3.60% respectively).

Results from this study reveal several key information. First, the findings suggest that the prototype

detects acoustic signatures in azimuth more accurately than in elevation. This is anticipated either due to the chosen alignment of the microphone array, or users' better perception of degree segments on the horizontal plane than the vertical. Further experimentation is needed to confirm this. Second, selecting a target with a Snap, on average, is less accurate than with a Tap. This is expected as the sound source from a Snap gesture is harder to locate precisely as it is generated from the thenar muscles at the base of the thumb, and not at the location where the thumb and middle fingers meet. Third and most importantly, the results indicate localization accuracy degrades under 22.5° angular width. Therefore, angular targets cannot be smaller than this size.

4.3.2 Study 2: Classifying acoustics signatures

This study tested the classification accuracy with the 11 acoustic signatures listed in Figure 4.1 in a non-noisy environment. A paper box was used as surface.

A new group of 12 right-handed participants (2 female, mean age 25.2 years) were recruited for this study. They were asked to perform the gestures next to the smartwatch while wearing the device. The study was conducted in a quiet laboratory with an average sound level of $50dB$, where the ambient sound was produced from mechanical devices such as air conditioning, computers or people talking outside the laboratory. The room was kept quiet (e.g., no door opening/closing) during the study. This environment allowed us to include more gestures and evaluate the classification in the best case.

A smartwatch program guided the participants to perform gestures, and informed the server application to start recording when the sound event was detected. It was observed that the non-impulsive sounds such as finger rub and hand rub last 0.5-1.0 seconds while the impulsive sounds such as hand clap and finger snap last only 0.1-0.2 seconds. Therefore, the number of feature frames obtained by an acoustic signature varies according to its type. To obtain approximately the same number of feature frames for training, the impulsive sounds were conducted at least 3 times compared to the non-impulsive ones in a trial. The order of gestures was randomized across participants. The program recorded 20 sound files for each gesture.

After completing the training phase, the participants took rest for 30 mins and then recorded data for testing a random gesture order. In each trial, they were asked to perform a gesture once and then wait for the next trial. It was repeated 5 times to collect 5 testing data points for each acoustic signature. The study lasted roughly 75 minutes.

A GMM was trained and used for classifying the testing gestures. The results revealed an average accuracy of 90.15% across all 12 participants and 11 gestures. One-way ANOVA yields significant effect between gestures ($F_{10,121} = 10.965, p < .01$). A Tukey post hoc test revealed that Finger pinch that

		Finger				Hand		Body		Surface		
		Snap	Rub	Flick	Pinch	Clap	Rub	Scratch	Tap	Clap	Scratch	Tap
Finger	Snap	56	1	0	0	2	0	0	1	0	0	0
	Rub	0	56	4	0	0	0	0	0	0	0	0
	Flick	0	2	57	0	1	0	0	0	0	0	0
	Pinch	0	14	14	29	0	0	0	3	0	0	0
Hand	Clap	2	0	0	0	53	0	0	5	0	0	0
	Rub	0	0	0	0	0	60	0	0	0	0	0
Body	Scratch	0	0	1	0	0	0	59	0	0	0	0
	Tap	2	0	3	1	2	0	1	50	1	0	0
Surface	Clap	0	0	0	0	0	0	0	0	60	0	0
	Scratch	0	0	0	0	0	0	0	0	0	60	0
	Tap	0	0	0	0	2	0	0	0	3	0	55

Figure 4.7: Confusion matrix of classification results across 11 acoustic signatures and 12 participants, 60 trials per gesture.

produced small and less noticeable sounds provided significantly lower accuracy (avg. = 48.33%) compared to others gestures (all $p < .01$). There was no significant difference for the other pairs (all $p > .05$). Figure 4.7 shows a confusion matrix for the gestures we tested. It was found that the non-impulsive gestures such as finger rub, hand rub, body scratch and surface scratch have a higher average (avg. = 97.91%) than the impulsive ones (avg. = 85.71%). This raised challenges on collecting training data with equal feature frames for all acoustic signatures.

The study also collected users' preference of using in-air, on-body and on-surface gestures. 6 out of 12 participants rated finger snap to be the best in-air gesture while 4 preferred the finger rub. None of them listed finger pinch as their preferred gesture. For on-body gestures, 7 favored hand clap and 3 preferred hand rub. Furthermore, 6 participants preferred surface tap for on surface gesture, 3 preferred surface scratch.

4.3.3 Study 3: In-situ evaluation with background noise

This study evaluated the prototype in noisy environments with a variety of background noise (i.e., near vending machines or an operating 3D printer) (Figure 4.8). More specifically, the study examined the impact of background noise on the prototype's localization and classification. The noise subtraction technique discussed before was applied, where a trigger gesture, i.e., wrist twists, was used to update the background noise information. In addition, the collection and training process were run in-situ and the system classified and localized the acoustic signatures in real-time.

6 participants took part in this study (all male, mean age 25.5 years). To simulate environments with

constant background noise, three participants were taken close to a set of vending machines and the other three were taken in a room with a running 3D printer. In both locations, the average sound level was $\sim 70dB$. With the sound subtraction algorithm, no sound event was detected from the background noise. For this study, two top-ranked gestures were selected from in-air (finger snap, finger rub), on-body (hand clap, hand rub) and on-surface (surface tap, and surface scratch) categories. The same procedure was used as in Study 2 to train the classification model per user.

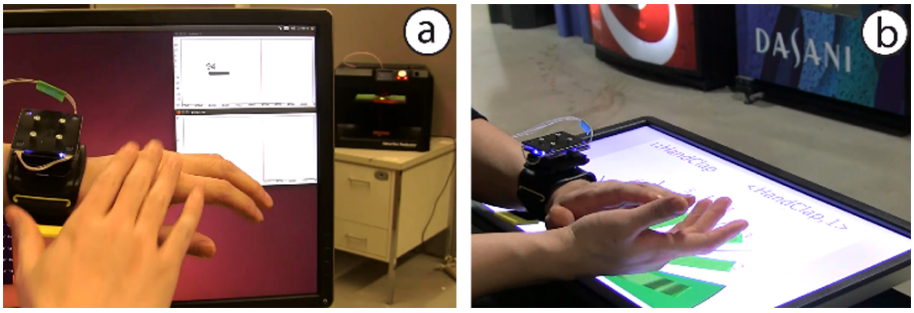

Figure 4.8: (a) The system handles noises such as sound from a 3D printer. (b) User evaluation in front of a vending machine.

The testing session used a target selection task similar to Study 1. Only the azimuth condition was included as the prototype detected acoustic signatures more accurately in this dimension. The 22.5° angular width was chose for targets as the localization accuracy degrades after this size. The targets were showed at a random position in a 180° circular layout. An external screen was positioned horizontally on a table to display the layout, trial number and the target acoustic signatures.

The participants were asked to place their hand wearing the device at the bottom center of the screen. The other hand was used to perform the acoustic signature on top of the target which was displayed on the monitor. For hand clapping and hand rubbing, the targets were always displayed at a fixed location (i.e., on the right bottom corner of the layout) due to constrained movements of the hand wearing the device. Additionally, paper tape was attached along eight angular directions on the screen to ensure enough audible sound produced with scratches. Once the acoustic event was detected, the sound was processed to display localization and classification results on the screen. Each acoustic signature was repeated 5 times at random locations. The session lasted approximately 30 minutes.

Figure 4.9 shows the confusion matrix across the acoustic signatures and the classification accuracy for the tested gestures. Results revealed that out of 180 (6 participants $\times$ 6 gestures $\times$ 5 repetition) gesture testing trails, the system successfully classified 158 samples into a correct category, yielding an average accuracy of 87.78%. Similar trends to those in Study 2 was found where gestures that are continuous in nature (such as finger rub) provided higher accuracy than the discrete ones (e.g., surface tap).

Results showed that system achieved an average of 88.89% localization accuracy. The prototype estimated the location of Tap and Rub sound events more accurately (93.33%) than others in noisy environments. It was also found that the prototype detects Clap and Snap sounds with a lower accuracy. As mentioned before, it's hard to predict the exact sound source location generated with these gestures, thus, making them less accurate to localize.

		Finger		Hand		Surface	
		Snap	Rub	Clap	Rub	Scratch	Tap
Finger	Snap	27	2	1	0	0	0
	Rub	0	27	0	3	0	0
Hand	Clap	3	0	27	0	0	0
	Rub	0	0	0	30	0	0
Surface	Scratch	1	2	0	1	26	0
	Tap	0	0	7	2	0	21

		Localization Accuracy
Finger	Snap	86.67%
	Rub	93.33%
Hand	Clap	80.00%
	Rub	90.00%
Surface	Scratch	90.00%
	Tap	93.33%

Figure 4.9: (a) Confusion matrix across 6 gestural acoustics. 5 testing samples for each, yielding 30 samples per participants. (b) localization accuracy for these gestural acoustics.

4.3.4 Evaluation Summary

Overall, the results indicate that prototype can localize and classify a set of acoustic signatures with high accuracy, in non-noisy and noisy environments. Impulsive acoustic signatures require more instances to get enough feature frames during training. Additionally, the sound generated with the gestures that have different initial and final finger contact positions (e.g., snap) are less accurate than others.

4.4 Applications with Acoustic Signatures

Several scenarios were implemented to demonstrate use of acoustic signatures in smartwatch interactions. Note that to make these interactions fully operable, specific delimiters to indicate that an acoustic signature is being issued (instead of environmental sounds) and sound source training are needed.

4.4.1 Rapid access to smartwatch content

Smartwatch users often require information access on-the-go, even while the other hand is busy, such as holding a coffee cup. Acoustic signatures facilitate input with either or both hands to quickly send device commands.

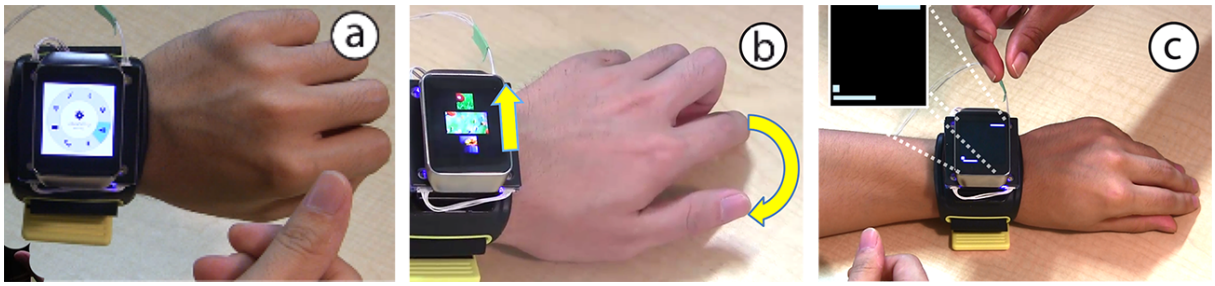

Figure 4.10: (a) User rubs fingers to select an item from a 2D pie menu. (b) One-handed content navigation. (c) Ad-hoc multi-user interaction.

Physical Surface for One-Handed Interaction - Acoustic signatures can be generated using a physical surface such as a table (e.g., hand tapping), turning it as available input space for one-handed interaction. This makes it possible to use smartwatch in single-handed mode. For instance, it can track directional finger scratching sounds on a table, either from top-to-bottom or in reverse (Figure 4.10b). These actions can be mapped with navigation and scroll activities on the smartwatch. For instance, a user browses an image gallery with the hand wearing the device. A finger tap on the table opens the content.

Delimiter for One-handed Interactions - Researchers have demonstrated the use of motion sensors (e.g., IMU's) to control smartwatch input [122]. However, to operate these, a delimiting action is necessary. Acoustic signatures can serve as input delimiters. Such a scenario was implemented wherein the user can snap the wearing hand finger, to enable and disable IMU functions to browse a contact list (Figures 4.11). Another acoustic signature (in this case a finger clap) places a call to the person selected in the list.

2D Pie Menu - Operating a menu system with many items and across multiple layers can be challenging on smartwatches. Instead of direct touch or swipe gestures on the touchscreen, SoundCraft allows users to shift the input space around the device, thus expanding the item selection zone. Several acoustic signatures can be used for commands. We use a 2D pie menu application to demonstrate this usage (Figure 4.10a). Users navigate the menus by rubbing their fingers in the corresponding directions. Performing a snap opens the menu items and a flick moves back to the previous layer.

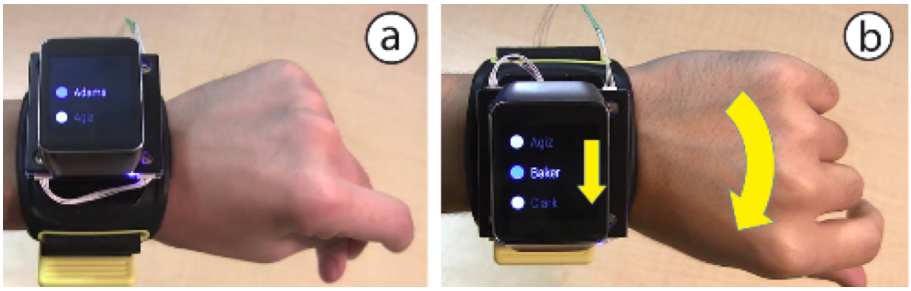

Figure 4.11: (a) User snaps to activate IMU function and (b) tilts the hand to scroll items.

4.4.2 In-situ content creation on smartwatches

Smartwatches are primarily used to consume content. It has the potential to expand functionalities to support content creation anytime-anywhere, such as drawing. Using acoustic signatures, a user can leverage the large space surrounding the smartwatch for content creation. A demo application was developed to show the use of acoustic signatures (i.e., finger rub) to sketch (Figure 4.12a) and navigate content in space.

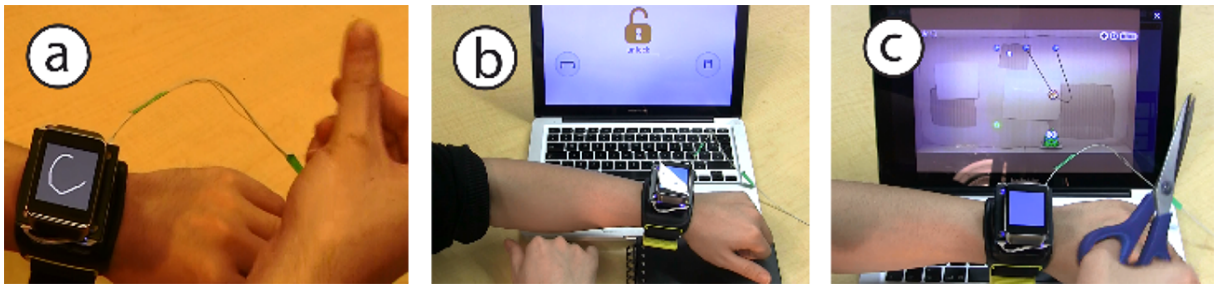

Figure 4.12: (a) A user sketches on the smartwatch with finger rubs. (b) The user unlocks the screen with a chain of acoustic signatures. (c) The user "cuts" the rope with a scissor in a game.

4.4.3 Smartwatch authentication

The hand wearing the device is often left idle while the non-wearing hand is operating. This leaves out the opportunity for a/symmetric bimanual input. SoundCraft allows classifying and localizing sounds generated using both hands, opening possibilities for bimanual smartwatch interactions. We demonstrate a smartwatch authentication application using bimanual input (Figure 4.12b). In this application, a user performs acoustic signatures in asymmetric patterns to log into his laptop. The user taps with both hands, on a book and table, generating sounds on the right and the left side of the watch, respectively. A matched sequence of sound types and locations unlocks the screen.

4.4.4 Ad-hoc gaming on a smartwatch

Multi-user game - Acoustic signatures can be produced by people at different directions. This capability enables smartwatches to support tasks in co-located ad-hoc collaboration. This application shows a two-player pong game using acoustic signatures, to extend the smartwatch into a multiplayer device (Figure 4.10c). The directions (e.g., inward and outward) of sounds relative to the watch is used to differentiate players and the location of the Finger Snap is mapped to controlling the paddle movement

Physical tools for gaming - This example demonstrates the use of a physical tool to produce acoustic signatures and play computer games. Users can use a scissor to perform the "cut" operation in a popular game, 'cut-the-rope'. A user places the hand with the prototype to the bottom-center of a game console

and holds a regular scissor to play the game. Snipping sounds produced by the scissor (Figure 4.12c) are classified and localized to cut the ropes at different places.

4.5 Chapter Summary

Utilizing angularly localized acoustic signatures provides valuable Input gestures on smartwatch. A dictionary of acoustic signatures was elicited through a design workshop, revealing opportunities for a broad range of spatial interaction scenarios. The evaluations ensured that the suitable algorithms reveal that such proximal sensor placement works, for tasks such as unique angularly localized signatures (i.e., snapping vs. rubbing). The classification and localization capabilities of the device allow us to explore a rich set of interaction techniques on the smartwatch in both non-noisy and noisy environments.

The demonstrated applications of the gestures show that such gestures provide efficient alternatives to the touchscreen input. This is especially useful when it comes to wearable devices, as for one reason, current touchscreen interface on wearable devices are not optimized to support efficient interactions, and for another reason, gestures from existing daily activities and living environments provide users the natural feeling of interactions and match the attribute of wearable devices that can used any time, any where. Meanwhile, the gestures extend the interaction design space on wearable devices, enabling novel scenarios and applications.

Nonetheless, designing such gestures face a lot of challenges. These are normally related to the accuracy and robustness of the sensing approaches. In the presented cases, vibrational signals embody rich information to express gestures, but are pretty noisy. For instance, when designing finger swiping gestures, one has to consider the distinction of bumpy surfaces, and when designing signature acoustics, the system's noise robustness has to be taken care. Systematic evaluations are required to validate the sensing approach and the feasibility of using the gestures. Moreover, designers also have to consider the cost of embedding new sensors to the wearable devices. Supporting finger swiping gestures requires no extra hardware as it uses the embedded motion sensors, while detecting acoustic signatures leverages an array of four MEMs microphones, that are possible to be embedded in the future wearable devices.

In-air gestures (e.g., around the device) is efficient and expressive, providing a viable approach to mitigate the input challenges on wearable touchscreen. However, performing the gestures may still feel socially awkward especially in public space. This may require a long period of refinements before the gestures become socially acceptable and users feel comfortable of using the gestures. On the other hand, when devices are getting smaller and embedded into the body, our body becomes more capable for (i) interactions will be no longer device centric, but rather body centric. Devices would be unnoticeable and unobtrusive, that frees the hand from the device centric interactions, and allow users to put more focus on interacting with

everyday objects; (ii) Those embedded devices enhance our body with sensing capabilities. For instances, hand movements in daily life can be tracked. Objects that hands are touching or holding can be recognized. This provide potentials to design hand gestures with everyday objects.

Chapter 5

Device as On-Body Sensors

Except smartwatch, touchscreen becomes less prominent on wearable devices as there is less need to have a full interactable display to provide the desired experiences and services to the user, and this brings more design flexibility in terms of the wearable size and structure. This kinds of wearable device are acting more as on-body sensors, that augment people and enable tracking and collecting data about the wearer activity or physiological conditions such as fitness, health and sports. To design the interface of this type, we have to face the expressiveness and false triggering challenges for leveraging on-body sensors to design gestural input.

This chapter discusses a solution leveraging finger swiping gestures on daily bumpy surfaces. Vibrational signals that are generated when a finger is swept over an uneven surface can be reliably detected via low-cost sensors that are in proximity to the interaction surface. Such signals can be transformed into interactions that provide an alternative input approach to wearable devices.

5.1 Why Finger Swiping Gestures

Our living environments are surrounded with many different bumpy surfaces (Figure 5.1). It is un-rare that we swipe our fingers on the surfaces, to vibrate the fingers rhythmically. In most cases, these express no specific meanings, either for public or for personal. These happen occasionally and unconsciously when people are focused in thinking, or at leisure. Such gestures are considered as good candidates for Inherent Input. A valid approach is converting the vibrational signals emitted when swiping a finger over an object or surface into an interaction that can occur in users' immediate physical environment. Previously, researchers have tried using contact microphone(s) to capture the mechanical vibrations that transmit through objects [48]. With wearable devices, this is achievable by using Inertial Measurement Units (aka IMUs) embedded

in the devices to capture the vibrational signals transmitting through the swiping fingers to the wearing positions on hand, such as watches and rings (Figure 5.2a).

Figure 5.1: Examples of daily bumpy surfaces.

Although such a concept has not thoroughly exploited the vibrational signals from ubiquitous Inertial Measurement Units (IMUs, e.g., combination of accelerometer and gyroscope), these seem optimal for such forms of interactions as they are embedded in most wrist-worn and finger-worn devices, thus not requiring additional instrumentation of the user's body or environment. They also have the advantage of operating with countless natural and fabricated textured surfaces, as shown in (Figure 5.2b) and (Figure 5.2c). For example, swiping over a book binder coil can move forward or backward through a digital presentation.

Figure 5.2: Illustration of vibrational signals transmitting through the swiping hands.

These interactions are influenced by a number of factors, including the location of the IMU (finger or wrist), the properties of the natural or fabricated surface (in particular the number of textured ridges, their height, etc.) and the nature of the swipe (direction, for example). This chapter provides a thorough exploration of factors that affect the input with wrist- or finger-worn IMUs. In particular, the examination of these factors needs to consider the unique challenges with IMUs: they have a lower bandwidth and sampling rate than acoustic sensors, and are less sensitive to vibrations, as signals get dampened while traveling through fingers or the hand.

5.2 Capturing IMU-Based Finger Swiping Gestures

The level of expressiveness produced by the input depends on how well the sensor can register vibrations from finger swipes across physical textures. Instead of using any commercially available devices, a customized "smartwear" is devised. This eliminates any possible confounds resulting from the different hardware implementations and capabilities of the devices and thus allows for device-independent comparison between a finger-worn and a wrist-worn IMU. The emulated wearable prototype is shown in Figure 5.3. It uses a commercial low-cost IMU (Bosch BNO055[1]) which is powered by a custom-made controller board. Sensor data is sampled at only 100Hz (which is much less than what is possible with acoustic sensors, but comparable to what is achievable with popular wearable devices such as the Samsung Gear Live smartwatch which reads accelerometer data at up to 200Hz). The data is sent to a laptop using the ZigBee wireless transceiver on the controller board.

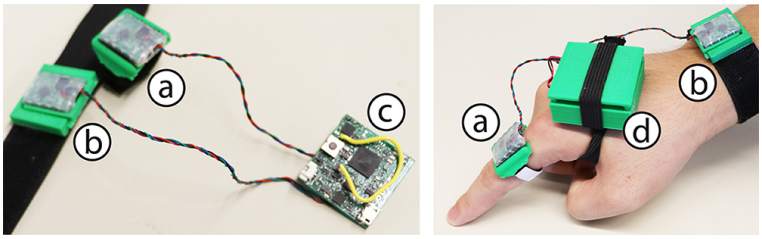

Figure 5.3: Prototype. (a) IMU sensor for finger. (b) IMU sensor for wrist. (c) MCU board. (d) MCU board and battery.

In pilots it was found that swiping the index finger over an object takes roughly 0.5 seconds, from start to finish. Accordingly, to ensure that the software (implemented with Java) captures the complete swipe motion, including the important moment when the finger crosses a bump which is indicated by a peak value in device acceleration, the size of signal extraction window is defined to 64 frames (0.64s). The acceleration data points in each window are then transferred into the frequency domain using the Fast Fourier Transform (FFT). Since the results of FFT are mirrored, only the values of the first 32 bins are converted into decibels and used as features to classifying the IMU signals. Furthermore, following McGrath and Li's method [82], a number of additional features are calculate to be able to reliably distinguish between a swipe on purpose and any causal hand movements. Additional features include: the standard deviation, skewness and kurtosis of accelerations, the distance between the minimal and maximal values in two consecutive windows, the finger's swiping direction, the forearm's pointing direction, and the finger's pointing direction. To overcome the drift in the sensor and to reduce accumulated errors, a first-order Butterworth high-pass filter is applied on the raw data (using a cutoff frequency of 0.1Hz). The resulting feature vector is then used to train an SVM to

[1]https://www.bosch-sensortec.com/bst/products/all_products/bno055

identify swipes on different bumpy surfaces (similar to most related work).

5.3 Feasibility Evaluation

Six "everyday" objects that could be appropriated for finger swiping interactions were used to evaluate the device's feasibility. The objects are made of different materials and/or provide bumpy surfaces of different character (e.g., distance between "crests" and "valleys", uniform or non-uniform height and width of "crests"). These include: a book with a metal ring binder, a plastic bottle with pronounced grooves and ridges, a plastic comb, a metal dish rack, a human hand, and a conch shell, all shown in Figure 5.4a.

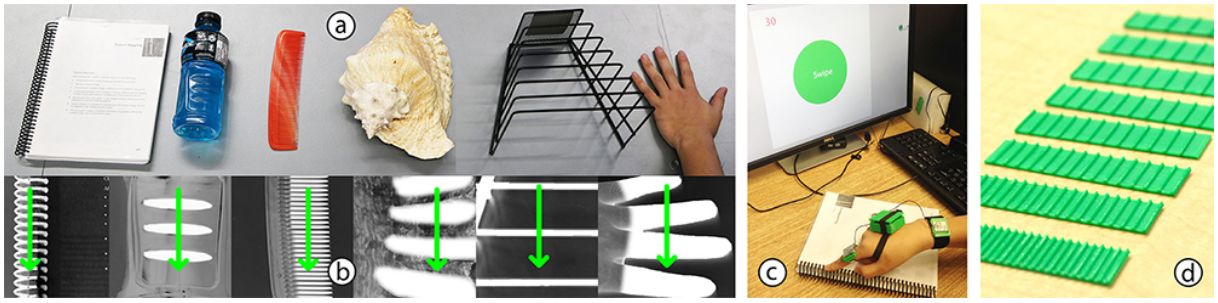

Figure 5.4: (a) The tested objects. (b) Highlight of the parts on the objects where participants swiped. (c) Setup with screen prompt. (d) 3D-printed stripes with varying bump density as used in one of our later explorations.

5.3.1 Participants and Procedure

Twelve participants were recruited (7 male; all right-handed; between 21 and 30 years old). Results from informal explorations and from a pilot study indicated that a naturally performed and unconstrained finger swipes across the selected objects lasted roughly 0.75 seconds. This information was used to reduce the need of extensive pre-processing of the data delivered from the sensors before analyses and opted to visually prompt the participants to swipe at regular intervals, during which sensor data was recorded. A countdown counter was displayed on a monitor in front of the participant (depicted in Figure 3c) to guide the start of each swipe. They were instructed to start a swipe when the prompt turned green and finish the swipe before the prompt turned red after 1.5 seconds. Thus, providing enough time for comfortable and natural swipe behavior, yet limiting the amount of recorded sensor data. The compliance to the prompt and any swipes that started or ended outside the time frame when recording was on (a swipe counter was shown on the monitor) were monitored.

All participants performed swipes on all six objects. They were instructed to swipe with the index finger of the dominant hand and showed where to swipe at each of the objects, as indicated with green arrows

in Figure 5.4b. They were also instructed to position the object at a comfortable distance at the table, if necessary fixate it with the non-dominant hand (e.g., when swiping on the light comb or bottle), and to swipe in a vertical direction, e.g., from far away toward the stomach. When swiping on the hand, participants were instructed to rest their non-dominant hand on the table and to slightly spread its fingers.

Participants performed 65 recorded swipes on each object, had 10 to 20 practice swipes with each new object, and a short break after each object. The order of the objects was randomized between participants. Data were collected from a total of 12 (participants) $\times$ 6 (objects) $\times$ 65 (repetitions) = 4680 swipes and ended up with 9360 swipe recordings, 4680 from the finger sensor and 4680 from the wrist sensor.

5.3.2 Training and Classification

According to the notes during data collection, 179 data ($\sim$3.8%) that the participant did not start or end within the active data recording time frame were manually removed from swipes. At most, 15 swipes for a participant and object combination had to be removed. Thus, after the removal there were still a sufficiently large number of swipe samples for each participant and object combination (min 50 samples). On the remaining samples (4501 from each sensor), Chang and Lin's [15] LIBSVM toolkit was used to tune the required SVM-parameters that produced high cross-validation scores and train a 6-class classifier (swipes on six objects) for each participant and sensor combination. Below, the overall accuracy was reported, i.e., the mean accuracy calculated across the 24 classification rounds (12 participants $\times$ 2 sensors).

Results

The overall classification accuracy was 89.4%. Patterns in the data from the wrist sensor allow us to correctly determine which object was swiped in 90.2% of the cases, data from the finger sensor provide an accuracy-level of 88.7%. For all objects we could achieve a classification accuracy well above 80%. The overall classification accuracy ranged from 84.6% for the shell with the finger sensor to 96.3% for the dish rack with the wrist sensor.

It was suspected that the lower performance with the shell may be attributed to its non-uniform "wavy" surface: both undulation height and undulation distance vary where participants swiped. With the exception of the hand, the other objects have a uniform surface. The classification accuracy for the different objects and object-sensor combinations are listed in the top part of Table 5.1.

With these encouraging results it is interested to see whether the classification accuracy could be improved by reducing the number of objects. Accordingly, the shell was removed, which had the lowest accuracy and has a very similar bump-density as the bottle (cf. Figure 3b) and used a 5-class classifier. Without the shell,

		Book	Bottle	Comb	Shell	Rack	Hand	Mean
6 obj.	Wrist	90.7%	90.0%	89.0%	85.1%	96.3%	90.1%	90.2%
	Finger	89.6%	88.1%	89.8%	84.1%	93.5%	86.9%	88.7%
	Mean	90.2%	89.0%	89.4%	84.6%	94.9%	88.5%	89.4%
5 obj.	Wrist	90.9%	94.9%	89.7%	–	96.5%	90.6%	92.5%
	Finger	90.5%	90.3%	91.4%	–	93.0%	88.6%	90.8%
	Mean	90.7%	92.6%	90.5%	–	94.8%	89.6%	91.6%

Table 5.1: Classification accuracy, with and without the shell.

the overall accuracy is now 91.6% (wrist: 92.5%, finger: 90.8%). The accuracy for each of the five objects is around 90% or well above, as listed at the bottom of Table 5.1.

In summary, these results are within the same range (or higher) than reported in previous projects [45] [49] [48] [108] where special purpose hardware was used and sensor data was sampled at very high frequencies ($\geq$1.6kHz). The results demonstrate that designing and using finger swiping interactions for a low-frequency IMU (100Hz) – as typically found in smartwear devices – is indeed feasible and can be used to identify objects the user swipes across.

5.4 Exploring Finger Swiping on Fabricated Textures

An extension to the finger swiping interaction is using fabricated objects with bumpy surfaces. As consumer-level 3D printers are becoming popular and universally available, fabricating objects are getting common and part of the life activities. Performing swiping gestures on fabricated bumps could be more efficient and accurate, as the bumpy surfaces are computationally designed and generated with desired attributes. Additionally, these fabricated objects could be attached to the environments, and be carried on body, such that the proposed inherent interactions can be more accessible. Fabricating the bumpy surfaces involves designing of the texture properties and their use contexts, including, for instances: 1) the spacing between the bumps on the surface, 2) the direction of swipes (horizontally vs. vertically), 3) the swipe style (swiping with finger tip vs. swiping with finger nail), 4) the height of the bumps on the surface, 5) surface stability (stable on a table vs. on unstable ground), and 6) swipe device (swiping with bare finger vs. swiping wearing a glove). This section examines the 6 factors and reports how they would affect the accuracy of the swiping gestures.

5.4.1 Bumping Space

The bumps on a multi-bump surface can be closely or sparsely distributed across the surface. While the distribution of bumps can be non-uniform, which is the case for many everyday objects, it is necessary to

explore uniform spacing on fabricated bumps. To gain initial insights, sensor data were collected from swipes across eight stripes with different bump intervals: 1.5, 2.5, 3.5, 4.5, 5.5, 6.5, 7.5, and 8.5 millimeters. Each bump was 1mm high. The stripes are depicted in Figure 5.4d. 12 new participants swiped 65 times across each stripe.

To evaluate the classification accuracy, a 2-class classifier was trained for each of the 28 pairs of stripes for each participant and sensor. The overall accuracy (i.e., the mean calculated across the 12 (participants) $\times$ 28 (pairs) $\times$ 2 (sensors) = 672 classifiers) was 90.5%. The accuracy for the wrist sensor and finger sensor was 91.1% and 89.9% respectively.

Figure 5.5 shows the mean classification accuracy for each of the 28 spacing pairs. The accuracy ranged from 80.2% (finger, 6.5 vs. 7.5) to 96.8% (wrist, 1.5 vs. 7.5). It was surprising to find such high accuracies even for pairs that only differ by 1mm. However, in general, the classification accuracy increases with increasing spacing difference (1mm: 84%, 2mm: 90%, 3mm: 92%, 4mm: 93%, 5mm: 94%, 6mm: 95%, 7mm: 95%).

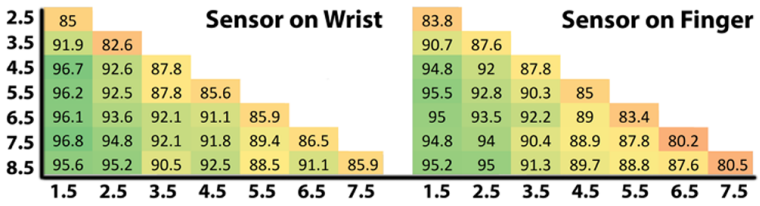

Figure 5.5: Color scaled maps of pairwise classification accuracy of the eight different bump densities.

5.4.2 Swiping Direction and Swiping Style

A user can swipe across a surface in numerous ways, using different amount of pressure, swiping from different directions (vertical, horizontal), using fingertip, finger pads, or a sharp or stiff devices such as a stylus or a pen. This section explores the swipe style and the swipe direction factors by testing the fingertip-style and the nail-style in the horizontal and in the vertical directions, as shown in Figure 5a and b. To simplify the procedure, the exploration was limited to "up-to-down" swipes for the vertical orientation and "left-to-right" swipes for the horizontal orientation. Furthermore, to exclude any possible effects caused by a particular bump spacing, the study used a stripe with one 1mm high bump and a flat stripe within each of the four direction-swipe style combinations (Figure 5.6). Twelve new participants swiped 65 times with each of the four direction-swipe style combinations.

A 2-class classifier (bump vs. flat) for each of the four direction-swipe style combinations for each participant and sensor. The overall classification accuracy (i.e., the mean calculated across the 12 (participants) $\times$ 4 (combinations) $\times$ 2 (sensors) = 48 classifiers) was 95.6%. The accuracy for the wrist sensor and finger

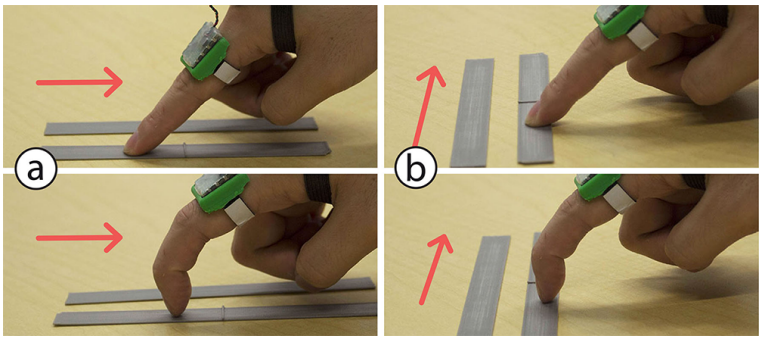

Figure 5.6: Vertical (a) and horizontal (b) swipe direction with fingertip-style (top) and nail-style (bottom).

sensor was 95.3% respectively 95.9% and the nail-style resulted in an accuracy of 95.5% and the fingertip-style resulted in an accuracy of 95.8%. A larger difference was found between the two directions, 93.4% for vertical and 97.8% for horizontal.

Looking at the differences between the four direction-swipe style combinations for the two sensors, as shown in Figure 5.7, reveals that some combinations yield lower accuracies than others. The classification accuracy with the finger sensor is higher when swipes were performed using the fingertip as opposed to the fingernail for both the horizontal and vertical directions.

However, the opposite is true in the case of the wrist sensor: classification accuracy was actually higher for both directions when participants swiped using the fingernail. Figure 5.7 shows that the difference between the two swipe styles is greater in the vertical direction with the finger sensor but, more so, that the greatest difference between the two swipe styles occurs in the horizontal direction with the wrist sensor. Possible interplays between different factors such as these demonstrate the complexity of these type of swipe interactions and they clearly show the need for further investigations regarding the many factors that need to be considered when designing finger swiping interactions.

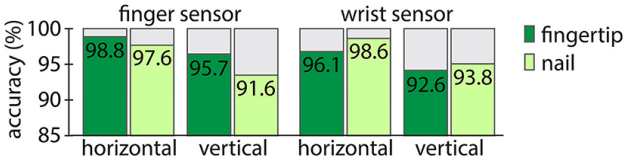

Figure 5.7: Classification accuracies for the four direction-swipe style combinations for the finger sensor and wrist sensor.

5.4.3 Bumping Height, Surface Stability, and Swipe Device

One of the fundamental properties that might determine the classification accuracy is likely to be the height of the bumps on a surface. Additionally, exploring the effect of wearing a glove, which dampens the signals

during a swipe can extend usage scenarios, e.g., where an operator may be working with heavy machinery. Similarly, interactions on non-stable surfaces may be desired in many working situations, thus the effects of surface stability is also explored.

Again, the study used stripes with one bump, that was either 0.2, 0.4, 0.6, 0.8, 1.0, 1.2, 1.4, or 1.6mm high and did also include a flat stripe. 12 new participants were asked to swipe across each of the nine stripes 65 times while wearing a glove (maid of wool) when the stripes were positioned on a table and when they were mounted on a 3D-printed pen, as illustrated in Figure 5.8. Pilot testing made evident that in order to swipe from a stretched finger posture (Figure 5.8b) when holding the pen, the user had to cross the bump using a contracting, or "curling", finger movement towards the palm. The resulting vibrations were too weak for the wrist sensor (likewise when using the opposite movement from curled to stretched finger). Accordingly, the wrist sensor data was abandoned and participants were asked to swipe from stretched to curled finger posture.

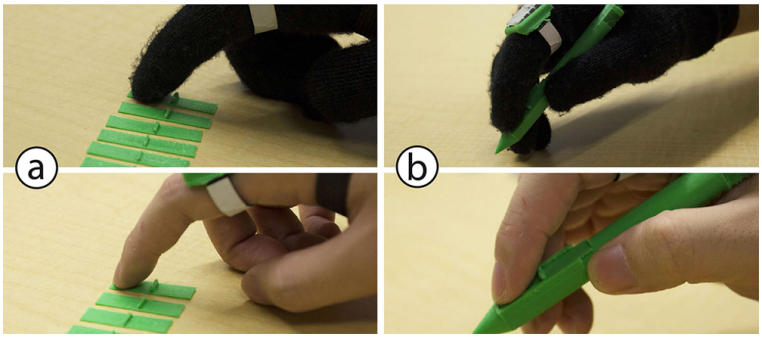

Figure 5.8: Stable (a) and (b) unstable swipe surfaces with glove (top) and with bare finger (bottom).

A 2-class classifier was trained for each of the 36 pairs of stripes from each participant's swipes under the four condition combinations: Pen & Bare Hand, Pen & Glove, Table & Bare Hand, and Table & Glove. The overall classification accuracy (i.e., the mean calculated across the 12 (participants) $\times$ 36 (stripe pairs) $\times$ 4 (condition combinations) = 1728 classifiers) was 86.2%. The classification accuracy for the stable (table) and unstable (pen) surface was 86.8% and 85.5%, respectively. The accuracy with and without a glove was 86.1% respectively 86.2%.

Figure 5.9 shows the accuracy results for each pairwise comparison of the different bump heights. The accuracy ranged from 71.2% (Pen & bare Hand, 1.4 vs. 1.6mm) to 96.8% (Table & Bare Hand, 0.0 vs. 1.6mm). Again, as with the achieved accuracy for the spacing factor, it was somehow surprising to find accuracies in this high range given that the studied height differences were at most 1.6mm. Understandably, the smaller the difference, the lower accuracy was obtained. Generally, for each combination of the four condition combinations, it was found that with a height-difference around 1mm results in an accuracy of

90% or above.

These results suggest that the recognizable height for a bump needs to be higher than 1mm to guarantee an accuracy of 90% or above. More interestingly, it was found that it was possible to reliably distinguish between two bumps (with accuracy > 90%) as long as their heights differ with 1mm or more. The accuracy for swipes performed on the table was generally higher than for swipes on the pen. However, this was only true when the bumps were higher than 1mm. This suggests that swiping on bumps that are higher than 1mm can cause the position of the pen to shift, thus affecting the sensor data. It was surprising that wearing a glove did not hamper classification accuracy. This could be a positive result indicating the usefulness of the approach – even in cases where the vibrational signal may be dampened. However, it is also plausible that the effect may not appear in untested conditions (e.g., with a thicker glove, such as when skiing).

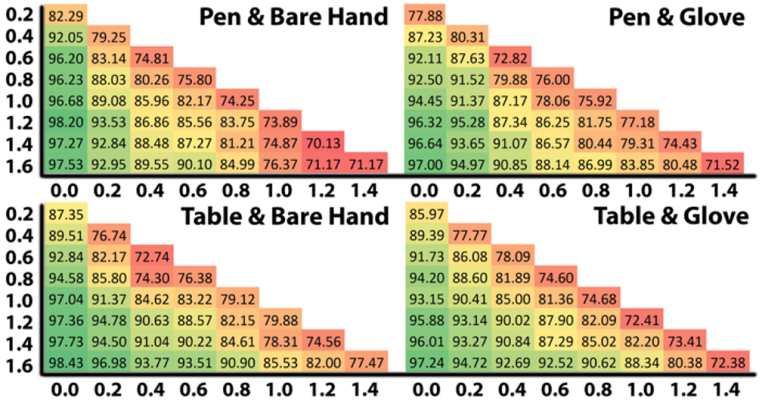

Figure 5.9: Color scaled map of pairwise classification accuracy of the nine different heights for the four stability-device conditions.

5.4.4 Exploratory Study Summary

The studies reveal some interesting findings. For example, swipe direction has an effect on the accuracy of our system. The accuracy is higher in the horizontal orientation than in the vertical orientation, which indicates that swiping across a bump in a vertical orientation generates less distinguishable vibrational signals. While the reason behind this is not fully understood, observations suggest that this is partially because the biomechanics of the index finger allow for vertical operations more easily than horizontal ones, the latter of which causes strong vibrational signals. The studies also find wearing a glove does not affect the performance of our system. This is somewhat surprising as the damping effect is expected to be more noticeable when swiping with a glove. More investigation is needed to investigate the effect of gloves made with different material, as well as the effect of the location of the sensor (e.g. whether the sensor is worn outside or inside the glove). Applications of this knowledge include using gloves in industrial or medical settings. Finally, the

IMU sensor is sensitive enough to pick up finger crossings over a small bump (e.g. as small as 1mm in our implementation). This opens an interesting space for designing distinguishable planned bumps using height as a parameter. User feedback suggests that people prefer small and dense bumps for the sake of comfort when swiping. It is thus important to balance the trade-off between the richness of distinguishable bumps and system usability.

5.5 Scenarios

The finger swiping input is an example of Inherent Interaction, that triggers a number of novel usage scenarios of smartwatches. Although the scenarios can also be made possible through the instrumentation of objects using sensors. This section demonstrates that such efforts can be largely reduced or avoided using IMU-based finger swiping interactions.

5.5.1 Touch Input on Un-instrumented Objects

Cooking often results in wet hands that may prevent the user from interacting with a touchscreen. The bumpy surfaces of many kitchen items can be considered good candidate textures for finger swiping interactions. In the implementation, swiping edges of a cutting board can be used for interacting with a nearby tablet. Such interactions allow users to swipe their finger from the edge of the cutting board to the kitchen counter-top to navigate through their favorite recipe book (Figure 5.10a). This allows users to use their tablet without having to dry their hands.

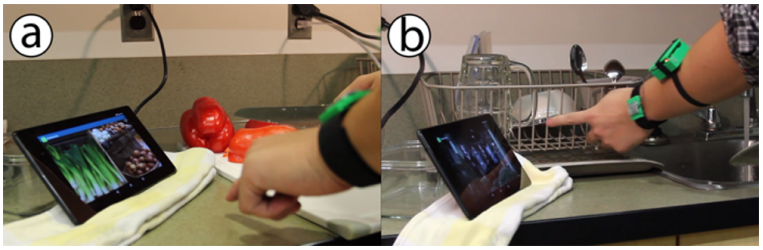

Figure 5.10: (a) A swipe across the edge of a cutting board to switch pages in a digital recipe book. (b) A swipe across the dish rack to navigate within videos.

In the implementation, users can swipe left to advance a page in the recipe book and swipe right to return to the previous one. Similarly, users can swipe up or down to adjust the music volume. Swiping across the edge of a cutting board generates a distinguishable vibrational signal that can be differentiated from the same swiping gesture carried out on a different object, such as a dish rack. The system is configured to allow users to launch a video player by swiping across a dish rack (Figure 5.10b). Once launched, users can swipe

the dish rack to switch between videos. Users can also swipe the tray of the dish rack to pause and start the video.

5.5.2 Contextual Actions on a Single Object

Objects with non-uniform textures can generate distinguishable vibrational signals on different parts of the surface of an object. This allows users to trigger different contextual actions using a single object. Finger swiping interactions is implemented on a conch shell to create an engaging environment for kids exploring sea life in a museum exhibit, for example. Via their smartwatch application, they can swipe across the bumpy surface of the whorl to explore the science of conches. Alternatively, swiping across the spire plays a video showing the characteristics of the corresponding conch (Figure 5.11a).

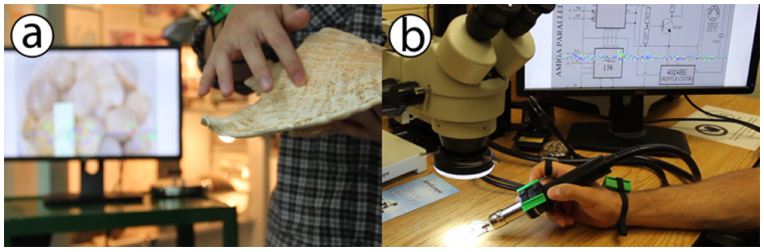

Figure 5.11: (a) Swipes on different parts of a conch shell to navigate through exhibition images and videos. (b) Instrumenting a soldering iron with fabricated textures can enable rapid interaction with circuit diagrams.

5.5.3 Instrumenting Objects Using Fabricated Textures

Fabricated textures can be placed on objects that do not have a bumpy surface to enable finger swiping gestures. For example, users can easily turn a soldering iron into an interactive device to facilitate work in situations where the user needs to examine a series of circuit diagrams on a computer monitor during hands-busy tasks (e.g., operating the soldering iron). Instead of shifting the hands between the soldering iron and a computer mouse, users can attach two or three fabricated textures to the iron's barrel, as shown in Figure 5.11b. Users can swipe different textures while holding the soldering iron to zoom into the diagram. For convenience, users could also attach a fabricated texture on a laptop to turn the light on and off in the room.

5.6 Chapter Summary

Finger swiping gestures are occasionally observed from daily activities. By extracting and classifying the vibrational signals generated from finger swiping on surrounding bumpy surfaces, we can transform the

actions into gestural input. The bumpy surfaces can be found in our living environments, and can also be fabricated with 3D printers. This chapter evaluates the feasibility, and design factors associated with using embedded IMUs on smartwatches and smartrings to detect finger swiping gestures. Such setup allows users to perform on-hand interactions in various real-life scenarios, and thus provides an efficient alternative gestural input approach to wearable devices.

This chapter discusses around gesture design and validation with on-body sensors. The approach of detecting swiping gestures shares in common with the work in previous chapter, in the way that they both exploit vibrational signals generated with hand gestures. These are the most common signals associated with our daily activities. These signals range widely from audible sounds such as when we speak, to inaudible and even ultrasonic. They operate with low and high frequencies that happen within and around us. This formalizes the idea that the vibration signals can be leveraged to detect daily hand activities, supporting interaction design with wearable/implantable devices.

As conventional screen based interaction is getting less prominent and even disappearing, designing alternative output channels on the miniature devices becomes more crucial. The miniature size brings challenges, as well as opportunities on designing output mechanisms that is close, and directly applied to skin. Besides the on-body sensing setup, on-body actuation could also be enabled by embedding electro-mechanical components and structures in the devices. This setup allows us to expand the design space of output channels, by considering non-visual approaches such as providing haptic feedback.

Chapter 6

Device as On-Body Actuators

As devices are getting smaller and conventional visual display centric interfaces are getting less prominent, it turns out to be more essential to design viable output channels on the device. Existing work on exploring non-visual feedback used to use sound and/or vibrations. However, these feedback are often used for notification purpose and limited in information expression. Besides, these feedback are decoupled with users' input activities. Not only embedded sensors, devices that are worn on the body can be composed of small sized mechanical actuators and structures, enabling the possibilities of designing different haptic feedback applied on users' skin.

This chapter proposes a design of passive kinesthetic force feedback as a viable way for device output. By designing different force profiles, the expressiveness of the output channel can be enriched. To evaluate the feasibility of the approach, a ring like prototype was built and used in user studies.

6.1 Passive Force Feedback on Smart Ring

Smart rings have become important peripherals within the ever-growing ecosystem of wearable devices [33]. Unlike smart phones or smartwatches, smart rings support subtle, socially-acceptable, always-available, eyes-free interaction due in large part to their miniature size and form factor. However, given their compact size, input and output capabilities on smart rings are still limited. Existing research with smart rings has primarily focused on leveraging smart rings for input [16] [39] [60] [92] [136] [138], with less effort devoted to output. The existing work on ring-based output typically uses light [21] [85] [103] , sound [106], vibration [21] [28] [61], skin drag [58], or poking [106], which require substantial user attention, and is often decoupled from the input mechanism.

Passive kinesthetic force feedback can be used as a viable output method for rotational input on smart

rings. Smart rings often leverage rotational input, mimicking the natural behaviors often performed with traditional rings [5] [96]. When enhanced with force feedback, such ring rotating behaviors can provide feedback that can be perceived without continuous visual attention. This output not only fits naturally in a ring form factor, but also complements existing smart watch output mechanisms with increased bandwidth and creates opportunities for new interactions. With such an output channel, different friction force profiles can be designed, programmed, and consequently felt by a user whenever they rotate the ring. Depending on the needs of an application, these force profiles can make it harder to rotate the ring or completely lock it in place. Such functionality can be mapped, for example, to the time remaining until wearer's next meeting, offering a convenient, always-available, calendar application (Figure 6.1).

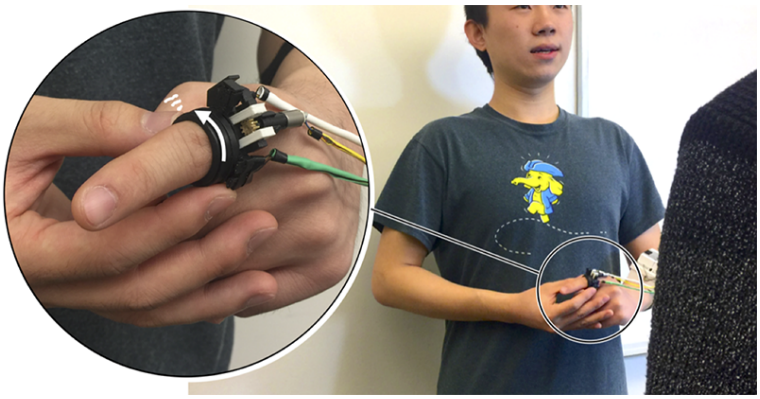

Figure 6.1: A user chats with his colleague while rotating the ring (without looking at the ring). As the ring exhibits some rotational stiffness, he knows that his next meeting starts soon.

6.2 A Ring Prototype with Passive Force Feedbacks

The prototype is composed of a ring, a braking system, and necessary electronics (Figure 6.2). The ring was 3D printed using GPBK02[1] resin on a Formlabs2 printer. It has an outer race that can be rotated in either direction. A small DC gear motor (TGPP06-D[2]), in combination with a rack and pinion gear mechanism was used to move a rubber brake in contact with the outer race. When the brake is engaged, users feel a high friction force resisting their rotation. The gear motor provided sufficient torque to lock the outer race into a full stop position. The gear motor was controlled using a TB6612FNG[3] Motor Driver Carrier that was connected to an Arduino Micro board and communicated with a MacBook Pro laptop.

The brake's rest position is approximately 1 mm above the outer race to ensure the brake can be engaged quickly to minimize latency in providing feedback. The brake moves at a linear speed of 20 mm/s with

[1] www.formlabs.com/store/us/form-2/buy-materials/?RS-F2-GPBK-02=1.
[2] www.ttmotor.com/productshow.php?sid=212&id=123.
[3] www.sparkfun.com/products/9457

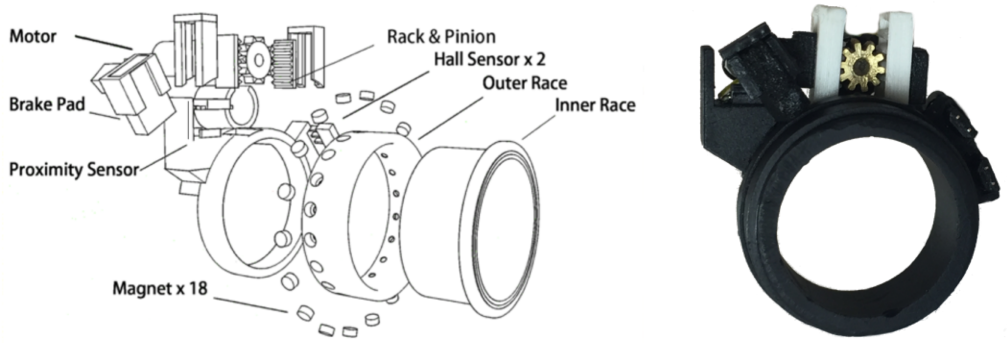

Figure 6.2: Left: A prototype assembly explosion diagram of the prototype. Right: The front view of the prototype ring.

a minimum distance of approximately 0.1 mm (measured using a high-speed camera). A QRE1113GR[4] reflective proximity sensor (Figure 6.2) was used to monitor the brake position during braking and ensure that the brake came back to the rest position when disengaged from the outer race. This provides the system with information about the amount of the braking force based on the distance the brake traveled. Although, a pressure sensor could be used to measure the braking force, the present implementation was sufficient to render many different force profiles and resulted in a smaller form factor.

The rotational angle of the outer race was tracked using magnets and two A1324[5] Linear Hall Effect sensors. Eighteen neodymium disc magnets (2 mm diameter $\times$ 1 mm height) were placed inside the outer race and were evenly spaced 20° apart from each other with alternating magnetic poles. With this setup, the sensor readings achieve maximum (positive pole) or minimum values (negative pole) whenever a magnet is directly underneath them. The Hall Effect sensors were positioned such that they were 30° apart relative to the center of the ring, allowing for the detection of the rotation direction (Figure 6.3). The outer race's angular displacement within the two adjacent magnets was inferred using linear interpolation of the peak and valley values. This enabled the prototype to achieve approximately 1° sensing resolution. An Arduino Uno sampled the analog values of the Hall Effect sensors at 1000Hz.

6.3 Force Profiles

To demonstrate the capabilities of this new output channel, five force profiles were designed and implemented (Figure 6.4). The profiles were triggered based on rotation angle. Once triggered, the profiles were rendered over rotation angle (Ramp-Up/Down), time (Hard Stop, Resistant Force), or both (Bump). Each force profile was inspired by an existing rotatable object (e.g., soda bottle cap) or mechanical knob.

[4]www.pololu.com/file/0J117/QRE1113GR.pdf
[5]www.allegromicro.com/ /media/Files/Datasheets/A1324-5-6-Datasheet.ashx

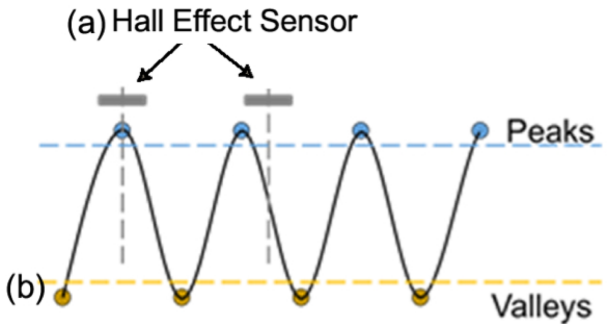

Figure 6.3: (a) Two Hall Effect sensors are used to detect rotational displacement and direction. (b) The Hall Effect sensor signal.

No Force. The outer race is free to rotate without any resistive force applied by the brake. The only force felt by the user is the light friction between the inner and outer race. The resisted torch in this case is ∼0 Nm.

Hard Stop. When the outer race is locked, the ring is unmovable in a certain position. A Hard Stop prevents the ring from being rotated, so it can be triggered after the user rotates the ring a certain number of degrees. This causes the outer race to be immovable by the user. We implemented the Hard Stop by rapidly engaging the brake by running the motor for 50 ms to depress the brake against the outer race, which resists a torque up to 0.06 Nm. After running the motor, the pad stays in place against the outer race to maintain resistance against rotation. In our implementation, the maximum braking force the brake pad can apply to the outer race is 3 N.

Resistant Force. The Resistant Force represents a force that requires effort from the user to overcome. It falls between the Hard Stop and No Force. Our implementation resists a torque of 0.03 Nm. With the Resistant Force, the outer race can still be rotated, but requires extra effort from a user to overcome the friction force. Rotating the ring allows the user to feel the force and associate it with a certain event. Similar to the Hard Stop, it could be used to deliver specific messages to a user. Different information could be encoded in the braking force, with a light resistant force representing one piece of information, and a stiffer force representing another.

Ramp-Up. The friction force applied to the outer race increases as the ring rotates. Ramp-Up starts at 0° and ends after the outer race was rotated 180°. The peak resisted torque is 0.04 Nm. From the user's perspective, the ring becomes harder to rotate the more the ring is rotated. Similar to the other force profiles, Ramp-Up can be associated with specific events or messages. By changing the slope of the 'ramp', as well as the duration of the ramp, different information can be encoded and conveyed to the user. Alternatively, this profile can be used to assist with fine-grained motor control for continuous input or to simulate the force that would be found while interacting with physical objects, e.g., closing the cap on a soda bottle.

Ramp-Down. Ramp-Down is the opposite of Ramp-Up, whereby the ring becomes progressively easier to rotate. In our implementation, Ramp-Down starts with a resisted torque of 0.04 Nn, and gradually decreases the braking force to that found with the No Force profile as the user rotates the ring. As with Ramp-Up, the slope and duration of the ramp can be modified.

Bump. The outer race stops at the bump, which requires a stronger rotational force from the user to overcome. A haptic bump is distinguishable and can be used to represent certain events. Information can also be encoded through the number or density of the bumps. Additionally, the 'force' of the bump as well as the 'width' of the bump can be modified to convey more or less information to the user. The bump can also be used to reduce attention on tasks requiring fine motor control. For example, discrete targets can be located inside two adjacent bumps to prevent the user from slipping off the target. In our implementation, the friction force ramps up rapidly when the outer race reaches a certain position and the friction force increases rapidly to 0.03 Nm resistive torque in 150 ms, and rapidly ramps down after a short distance (e.g., 5°).

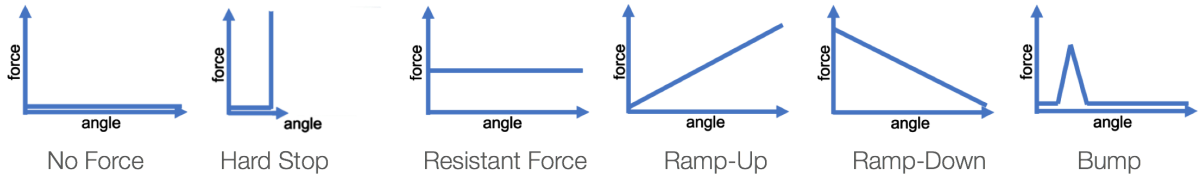

Figure 6.4: Force profiles designed and implemented.

6.4 Evaluation of Force Profile Perception

To explore whether passive kinesthetic force feedback can be an effective, recognizable output channel within the context of smart ring use, a user study was conducted. It examined how well participants could perceive and distinguish the force profiles previously described.

16 participants (8 females), between the ages of 22 and 30, participated in the study. All participants were right-handed.

Apparatus and Task Conditions

While walking, the movement of their hands and body may impact one's ability to accurately perceive some force profiles. Thus, to allow for the evaluation of the ring within more ecologically-valid scenarios, a treadmill was used to. In the walking condition, participants had to perform each experimental task while walking on a motorized treadmill at a speed of 3 km per hour. In the standing condition, participants

performed the tasks while standing stationary on the treadmill. A 27-inch computer monitor was placed in front of the treadmill, facing each participant, to display the experimental user interface to them (Figure 6.5).

In addition to identifying which profile was being presented, on some trials, participants also performed a secondary task to induce cognitive load. This task was introduced to divert participants' attention from the force pattern identification task, simulating a scenario such as interacting with the ring when talking to a colleague or listening to a presentation. When the secondary task was presented (Cognitive Load), participants were asked to perform both tasks in parallel. A modified Stroop test [111] was used, where the name of a color was shown using a random font color (e.g., the word "red" shown using a yellow font color). To ensure the two tasks were performed simultaneously, instead of sequentially, the text and color were randomly rendered from a pool of five colors (e.g., red, yellow, green, black, and blue) every two seconds. Participants were asked to count how many times there was a match between the text and font color. Two seconds was chosen based on results from an earlier pilot study to ensure that participants had enough time to process the task. When the secondary task was not used (No Load), participants were not presented with the Stroop task and only indicated which force profile they felt.

In the Resistant Force and Ramp-Down conditions, as the force was expected to be felt immediately after participants attempted to rotate the ring, the brake was engaged immediately after the trial began. Ramp-Up, in contrast, began with no force. Both Ramp-Down and Ramp-Up started at 0° and ended after the outer race was rotated 180°. Hard Stop and Bump were rendered at the 40° position. The position was determined based on data from an earlier pilot study, where a single clutch of the ring would rotate it 40° and still provide a sufficient leading distance so that it would not be confused with No Force. As the brake pad has to move into position at the beginning of each trial, the brake pad was moved a random distance before moving it to the correct position to avoid the possibility that the vibration of the brake pad would indicate the current force profile.

During the experiment, participants wore noise canceling headphones to block the noise generated by the ring's motor, yet enable them to listen to the audio feedback from the experimental software. The experimental software was written in Python, and was run on a MacBook Pro laptop.

Procedure

Participants were shown the prototype and were asked to wear the ring on the index finger of their non-dominant hand. They were then told that they would be presented with one of the force profiles and would need to indicate which force profile it was. After being shown the prototype device and putting it on their finger, each force profile was presented to the participant. Each participant was allowed several practice

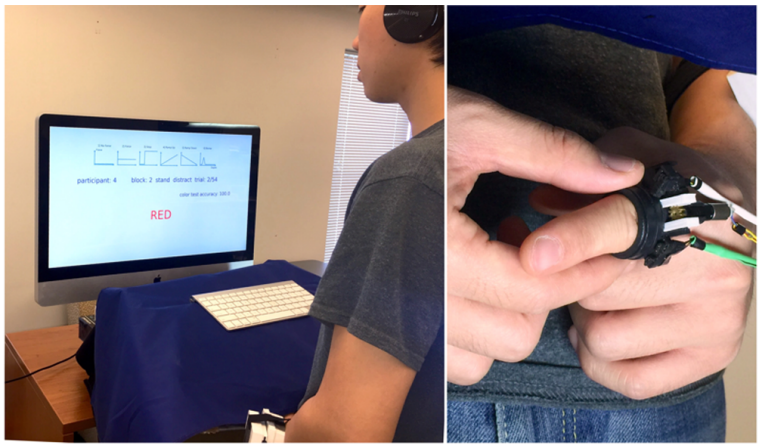

Figure 6.5: Force profiles designed and implemented.

trials in each condition to familiarize themselves with the force profiles.

During each trial, participants were asked to rotate the outer race using their dominant hand to feel the force profile. Participants were allowed to try a profile as many times as they wanted until they felt confident they could report which one it was. To end the current trial, participants used their dominant hand to press the space bar on the keyboard to finish the trial. They then verbally told the experimenter which force profile was presented. To begin the next trial, participants pressed the space bar again. In the condition, where a secondary task was presented (i.e., the modified Stroop test), participants performed the two tasks in parallel. The percentage of correct responses to the cognitive task was shown on the monitor and participants were asked to maintain an accuracy above 90%. Each participant successfully maintained the 90% accuracy threshold. Breaks were encouraged at the end of each condition.

During the study, participants' hands were covered using a cardboard box to avoid visual cues from the ring potentially influencing their responses. To feel the force profiles, participants were asked to rotate the ring towards their body. Each force profile, except for the Hard Stop could be felt again after the race had been rotated an excess of 180°, at which time a beep indicated the end of the profile. Hard Stop could not be felt again as the outer race was locked at 40°.

Upon completion of the study, participants filled out a post-experiment questionnaire where they indicated subjective ratings for the recognizability of the force profiles (1: very hard to recognize, 7: very easy to recognize). The experiment lasted approximately 60 minutes.

Experimental Design and Measures

The experiment employed a 2 × 2 × 6 within-subject factorial design, with Mobility (Walking and Standing), Secondary Task (Cognitive Load and No Load), and Force Profile (Hard Stop (S), Resistant Force

(RF), Ramp-Up (RU), Ramp-Down (RD), Bump (B), and No Force (NF)) as independent variables. The experiment was comprised of three blocks of trials, with each block consisting of 3 repetitions. During each trial, participants performed tasks in one of the Mobility × Secondary Task × Force Profile combinations. The Mobility × Secondary Task combination was counter-balanced among participants. The Force Profile was presented in a random order. The experimental design was thus 2 Mobility × 2 Secondary Task × 6 Force Profile × 3 Blocks × 3 Repetitions × 16 Participants = 3456 trials.

Dependent measures included the profile recognition accuracy (i.e., the number of correctly identified force profiles), the response time (i.e., the time elapsed from the start of the force profile to the depressing of the space bar), and the number of attempts required to identify each force profile. The response time for Hard Stop and Bump was measured from the moment when the force was detectable.

Results

The data were analyzed using repeated-measures ANOVA and Bonferroni corrected paired t-tests for pair-wise comparisons.

Profile Recognition Accuracy. The average accuracy across all conditions was 94.0% (SD = 10.5%; Figure 6.6 right). The repeated measures ANOVA yielded a significant effect of Mobility ($F_{1,15} = 17.76, p < .01$), Secondary Task ($F_{1,15} = 11.57, p < .01$), and Force Profile ($F_{5,75} = 10.3, p < .01$). An interaction was also found between Mobility and Secondary Task ($F_{1,15} = 5.75, p < .05$), indicating that mobility has a slightly smaller impact when there is cognitive load (Figure 6.7 left). Recognition accuracy was significantly higher when participants were standing (M = 95.7%, SD = 8.8%) than walking (M = 92.2%, SD = 11.7%; $p < .05$) and when no secondary task was present (M = 95.31%, SD = 8.54%; $p < .05$). Hard Stop (M = 99.5%, SD = 2.4%) was significantly higher than Resistant Force (M = 90.6%, SD = 13.3%), Ramp-Up (M = 91.3%, SD = 9.8%), and Ramp-Down (M = 87.7%, SD = 14.3%; $allp < .05$). No significant difference was found between Hard Stop, Bump (M = 98.4%, SD = 3.9%), and No Force (M = 96.4%, SD = 7.2%; all $p > .05$) or between Ramp-Down, Ramp-Up, and Resistant Force (all $p > .05$).

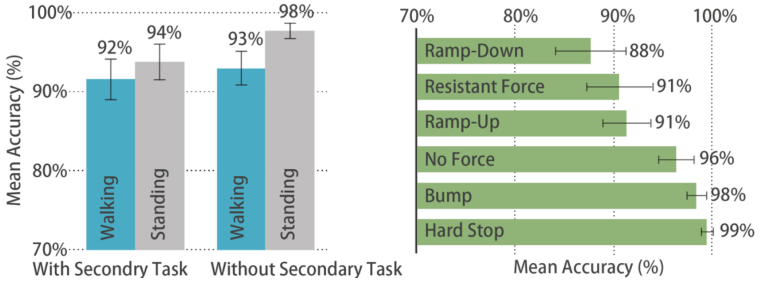

Figure 6.6: Profile Recognition Accuracy. Left: Secondary Task and Mobility. Right: Force profiles. (Error bars show 95% CI in all figures).

Confusion matrices of the recognition accuracy of different force profiles under the Mobility and Secondary Task conditions (Figure 6.7) revealed that the Resistant Force was the major source of confusion with Ramp-Up and Ramp-Down when the task was performed when walking or with the Secondary Task.

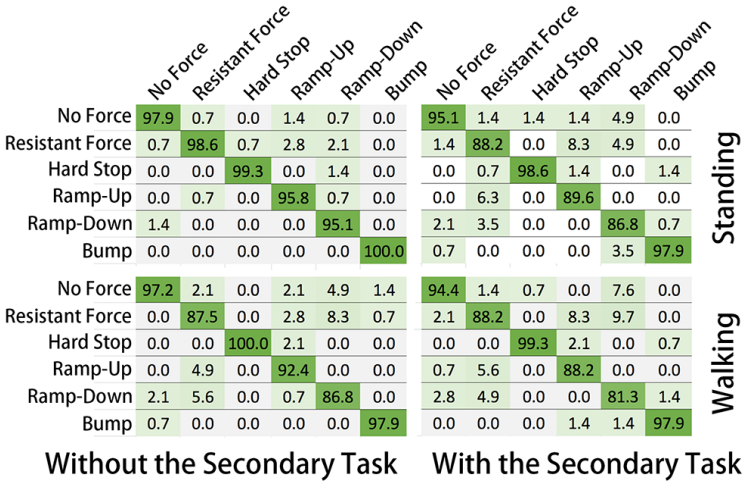

Figure 6.7: The confusion matrices of the Profile Recognition Accuracy (%), by Secondary Task and Mobility.

Response Time The average response time was 3.1 seconds (SD = 1.3 seconds). A repeated-measures ANOVA yielded a significant effect of Secondary Task ($F_{1,15} = 13.17, p < .05$) and Profile ($F_{5,75} = 83.62, p < .05$). There was no significant effect of Mobility ($F1, 15 = 1.644, p = .219$), nor any significant interaction effects (all $p > .05$).

The response time for walking and standing were 3.2 seconds (SD = 1.3 seconds) and 3.1 seconds (SD = 1.4 seconds) respectively. Surprisingly, response time was faster with the secondary task (M = 2.8 seconds, SD = 1.1 seconds) than without it (M = 3.4 seconds, SD = 1.5 seconds). Participants reported that they felt the faster they performed the task, the fewer number of colors they needed to memorize.

As expected, the response time for Hard Stop (M = 1.7 seconds, SD = 0.6 seconds; all $p < .05$) was the shortest, followed by Bump (M = 1.9 seconds, SD = 0.6 seconds; all $p < .05$). This was to be excepted as these two profiles were distinguishable earlier in each trial, after only 40° of rotation. The remaining force profiles required participants to rotate the ring for longer, increasing the response times. No significant difference was found between No Force (M = 3.7 seconds, SD = 0.9 seconds), Resistant Force (M = 4.0 seconds, SD = 1.2 seconds), Ramp-Up (M = 3.9 seconds, SD = 1.1 seconds), and Ramp-Down (M = 3.6 seconds, SD = 1.2 seconds; all $p > .05$; Figure 6.8 left).

Number of Attempts On average, participants took only 1 attempt (SD = .09) to correctly guess each profile. There was no significant effect of Mobility ($F_{1,15} = .22, p = .644$), Secondary Task ($F_{1,15} = 1.48, p = .24$), or Force Profile ($F_{5,75} = 1.52, p = .23$). Unsurprisingly, Hard Stop resulted in exactly one attempt as

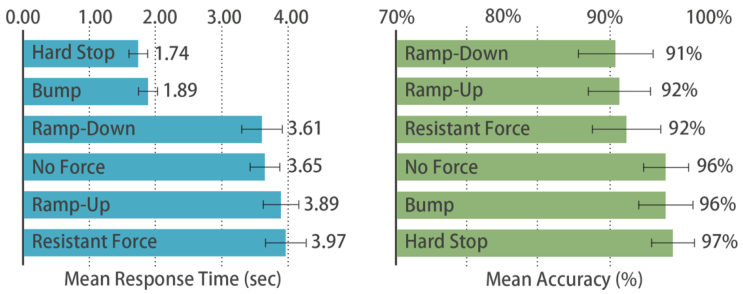

Figure 6.8: Left: The average response time (in seconds). Right: The secondary task accuracy for each force profile.

the ring was not rotatable once the profile was executed.

Secondary Task Accuracy The overall accuracy of the Secondary Task was 94.1% (SD = 8.2%). There was a significant effect of Mobility ($F_{1,15} = 11.667, p < .05$) and Profile ($F_{5,75} = 4.413, p < .05$).

Participants completed the secondary task more accurately when standing (M = 95.7%, SD = 7.5%) than walking (M = 92.5%, SD = 8.6%). Regarding the effect of Force Profile, the secondary task received higher accuracies with Hard Stop (M = 96.9%, SD = 5.8%), No Force (M = 96.2%, SD = 6.1%), and Bump (M = 96.2%, SD = 7.3%), than Resistant Force (M = 92.4%, SD = 9.1%), Ramp-Up (M = 91.7%, SD = 8.5%), and Ramp-Down (M = 91.3%, SD = 10.1%). Post-hoc comparisons only revealed a significant difference between Hard Stop and Ramp-Down ($p > .05$; Figure 6.9 right).

Subjective Ratings. Study results were analyzed using Friedman signed-rank tests with Wilcoxon tests for pair-wise comparisons. The Friedman test yielded a significant difference in Force Profile ($\chi^2(5) = 43.74, p < .001$). Overall, median ratings for all scenarios were above 5 (with 1 indicating the profile was very hard to recognize and 7 being very easy to recognize). This suggests that all or most of the participants agreed that the force profiles were easy to perceive (Figure 6.9). Bump and Hard Stop were rated very easy to perceive (i.e., both received a median of 7), followed by No Force. Participants rated these three force profiles significantly easier to perceive than Resistant Force, Ramp Up, and Ramp Down (all $p < .005$). Post-hoc tests found no significant difference between the two groups of force profiles (all $p > .05$). As the subjective ratings are consistent with the recognition accuracy results, this confirms the effectiveness of passive kinesthetic force feedback as a new output channel.

Participants were welcoming of this new output technique as well. They described it as "interesting" (P2, P8, P9), "awesome" (P6), "cool" (P15), "promising", (P16), "exciting" (P11), and "amazing" (P3). They told us that they could imagine new applications that could be enabled by this type of haptic feedback (e.g., "I am looking forward to seeing new applications" (P14)). Participants also saw potential for such a ring in scenarios such as "sports & yoga" (P7) or during "fitness" (P10). Two participants also noted the intimate

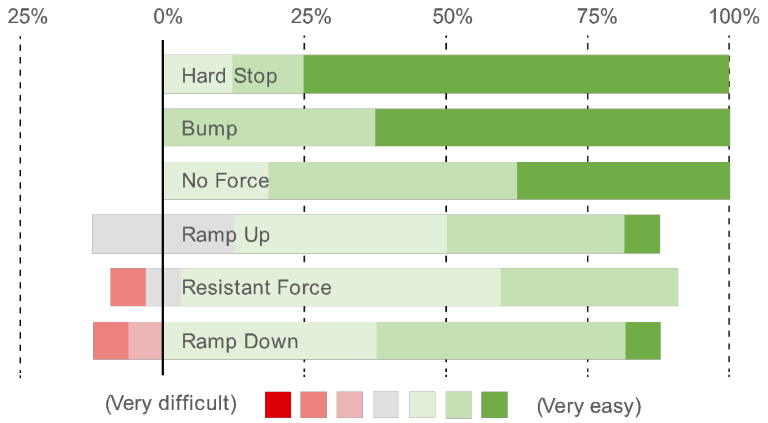

Figure 6.9: Participant responses to the ease of recognizability of the force profiles. Graphs are centered around the neutral response, with the proportion of positive and negative responses on the right and left side, respectively.

nature of the ring, suggesting it could be used "between lovers" (P14) or for "private communication" (P10).

Evaluation Summary

The user study indicated that most force profiles could be easily distinguished, even under conditions where users' physical or mental workload was high. Walking or performing a secondary task had a negative impact on participant's ability to accurately perceive the haptic feedback. A promising finding was that physical or mental workload did not significantly impact response time. Surprisingly, response time was even shorter when participants were asked to perform a secondary task, requiring extra cognitive load.

The unique properties of the different force profiles allow them to be suitable for different applications. For example, Hard Stop and Bump seem more are appropriate to indicate urgent messages, as they can be recognized quickly. Ramp-Up and Ramp-Down seem most suitable if one wants to mimic physical feedback during physical interactions. Therefore, the value of the force profiles value may lie in the realistic feelings that could be provided to users in applications where haptic feedback is important (e.g., games), or in designing novel metaphors for the ring (e.g., closing an application is accompanied by the Ramp Up to mimic the closing of the lid on a soda bottle).

The study also demonstrated how clear each force profile was via the number of attempts that were required to complete a trial. In situations where two or more force profiles were indistinguishable by participants, e.g., Ramp-Up and Resistant Force, the participant may have spent more time on decision making than physically rotating the ring multiple times to get a clear feeling. In either case, response time may have been longer, but less attempts would have been made, i.e., the classic speed-accuracy tradeoff. As the average number of attempts made was close to one, the participants could readily feel the haptic feedback

patterns. Similarly, decision making did not take extra time away from participants while identifying the right force profile. This confirms that passive kinesthetic haptic feedback does not divide attention to the degree that it imposes a significant cognitive load on users.

Smart rings are expected to be used on-the-go, while users are performing another task and have their attention divided. It was thus important to understand if interacting with the ring through the passive kinesthetic haptic feedback would impact the performance of the user's task. The results demonstrated that the average accuracy of the secondary task was around 94%. This suggests that ring-based passive kinesthetic haptic feedback may not significantly impact the performance of a second, parallel task. On the other hand, physical workload did have an impact on haptic perception: the accuracy was higher when standing than walking. These results were like caused by the movement of the user's hands and body, but still indicate that passive haptic feedback could be useful for multi-tasking. If a passive kinesthetic haptic feedback-enabled ring is to be used in a context-aware application that detects physically activity, one may want to alter the force patterns that are supported so as to improve recognition rates.

6.5 Applications with Passive Force Feedback

To demonstrate potential usage scenarios for ring-based, passive kinesthetic haptic feedback, and explore the range of tasks that it may be best suitable for, we implemented four applications. The applications exemplify novel interactions techniques that could enhance common, everyday tasks.

Calendar

It is common that individuals check the time on their smartphone or smartwatch to plan for the next appointment in their calendar. Frequently looking at your watch, however, is considered inappropriate in many social settings. With the prototype ring, the amount of friction force and rotation allowed can be used to indicate the time remaining until one's next meeting. For instance, if there is over an hour until the next meeting, the ring can freely rotate for a full rotation (Figure 6.10), but if there are only 15 minutes, the ring can be made to feel stiff, and would stop rotating after a 90° rotation. If one was late to a meeting, the ring could become unmovable. Such an application would employ three of the patterns tested in the prior study (No Force, Resistant Force, and Hard Stop) and could utilize greater gradations of resistant force to provide more expressiveness.

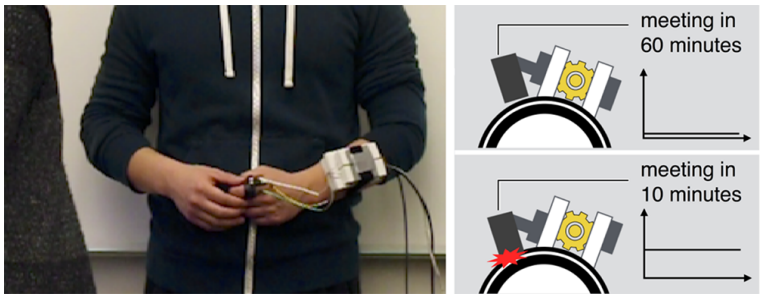

Figure 6.10: With passive force feedback, a user can subtly check their calendar while chatting.

Rotary Combination Lock

Providing precise rotary input on a smart ring can be challenging, as pointing at a small angular target requires fine motor control or continuous visual attention []. This challenge can be mitigated by providing haptic landmarks around the targets using the Bump force profile. To demonstrate this capability, we implemented a rotary combination lock to allow a wearer to unlock their personal computing devices (e.g., smartphone or laptop) using the ring (Figure 6.11 left). Passwords can be entered as a series of three rotations that alternate direction, followed by a fourth direction change to confirm the inputted sequence. The device provides Bump feedback every 45° of rotation. Eyes-free input is also possible as the user can memorize how many times the dial needs to be turned across the haptic landmarks in a certain direction. If the correct sequence of rotations is entered, the ring will spin freely (No Force) to indicate success. A Hard Stop would be used to indicate a failed attempt.

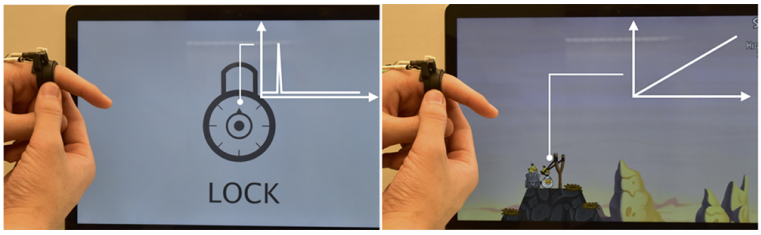

Figure 6.11: With passive force feedback, (Left) a wearer can unlock their laptop by using their ring as a combination lock, or (Right) control the angle and power of a slingshot while gaming.

Gaming

Inspired by the popular Angry Birds mobile game, the ring can also be used for traditional gaming input, by mapping the rotational nature of the device to input. Using the ring, the wearer can rotate the outer race to indicate the angle of the birds' slingshot. After a one-second dwell, the mode is switched to input the power of the slingshot. During pull-back, the Ramp-Up profile informs the wearer that the slingshot is approaching the maximum force (Figure 6.11 right). The wearer can then quickly rotate the ring in the

opposite direction, which switches to No Force, and gives the wearer the sensation of a large spring force being released as the motor disengages the brake. This example showcases the novel haptic output responses that can be generated in response to user input to provide a richer gaming experience.

Eyes-Free Call-Display

If the wearer is at a movie theater with their phone on silent and they receive a phone call, they may want to know who is calling before deciding whether to leave and answer the call. If they take the phone from their pocket to see the screen, the glow it emits will disrupt the other viewers. Instead, when the phone vibrates, the wearer can twist the ring to query the caller. As the wearer has memorized predefined mappings for frequent callers, they know that if they twist the ring and feel the No Force profile, it is an unknown caller, whereas if they feel the Hard Stop profile, it is their wife calling and they should answer the call (Figure 6.12).

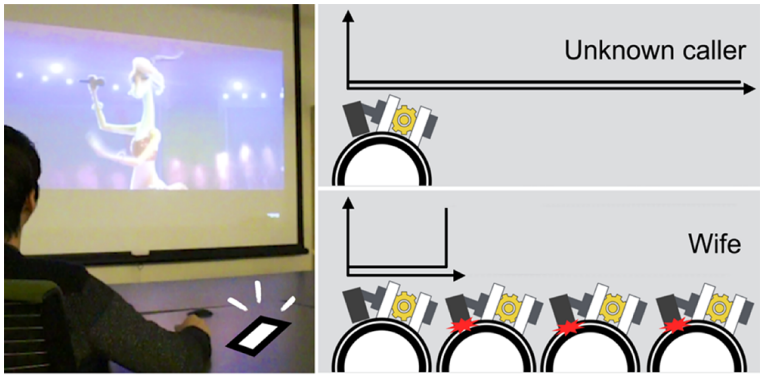

Figure 6.12: With passive force feedback, a user can check who is calling by associating different force profiles to different incoming callers.

6.6 Chapter Summary

The chapter described an example of output channel leveraging passive force feedback on smart ring. It is coupled with rotational input on the ring. With such feedback, different friction forces can be designed, generated, and felt by a user when they rotate the ring. A set of novel interaction techniques demonstrate the unique capabilities enabled by this novel haptic output channel.

The passive haptic feedback provides an alternative approach to design output channels on wearable devices. One benefit of doing this, is it matches with users' daily feedback experiences. Inherent Output like this, could provide new perspective, and hopefully new insights into the feedback mechanisms on wearable devices.

Designing a new output channel, e.g., the haptic feedback in this case, requires adding new components such as motors to the wearable devices. Miniaturization and compactness are important aspects of any wearable [33], especially those found on the finger. This needs further optimization of the structures, and development of micro motors.

When devices are embedded into the body, skin will become more important as a design space for input and output channels. Turning skin into haptic display would be valuable but challenging. Although mechanical actuators and structures have advantages of being accurate and low latency, their nature of being rigid, preventing adapting the approaches to the design of skin-like haptic displays. For instance, the haptic devices would impede skin's natural sensations of physical world. This raises the necessity of exploring different actuation approaches that are better suited to the design of skin-like haptic display.

Chapter 7

Skin as Haptic Display

When devices are embedded into the body, skin will act as an important interface to communicate information with users. Designing output channels on skin is challenging. Some previous work envisioned scenarios of using skin as visual display. This can be realized with thin and stretchable LEDs such as the work presented in [135] and [81], as well as with the technology of smart tattoos, demonstrated in [120]. Nonetheless, less work has been explored on turning skin into a haptic display. As described in the previous chapter, haptic output channels can be used for subtle interactions, without requiring a user's visual attention. However, turning skin into haptic display will face several challenges. Traditional haptic interfaces are based on electro-mechanical structures which are often rigid and bulky. These are not easy to be embedded into, or attached onto skin, and will easily impede the natural sensations of the skin, preventing the user from interacting with the physical world. This chapter discusses liquid flow actuating skin-like haptic display, that enables mixed reality haptics.

7.1 Skin like Haptic Device

This chapter presents a skin like haptic display, which enables virtual haptic feedback without disturbing the user's natural tactile sensations of the physical world while wearing the device. A proof of concept prototype (Figure 7.1), is composed of a thin, flexible latex tube (0.1mm thick) that is lightly stretched over the skin, and provides the tactile sensations of pressure, vibration, and temperature on the fingertip via liquid flow. The sensations are delivered by modulating the temperature, pressure and flow rate of the liquid travelling through the device and across the fingerpad. The haptic device is non-obtrusive, and can readily switch between actively providing sensations, and being 'passive', i.e., supporting natural dexterity and allowing the user to sense and interact with the real world. This approach opens new opportunities

for interaction, for example, allowing the user to seamlessly switch between physical and virtual sensations in mixed reality tasks, and provides a new channel for always-available notifications and other information. This work envisions a future type of skin like haptic display that can be always worn, or implanted on one's body with the support of artificial skins [54] and microfluidic devices [89].

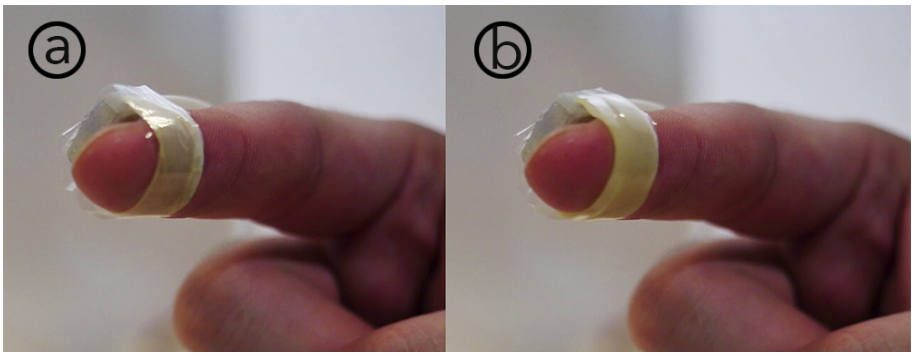

Figure 7.1: A haptic display that is thin and slightly stretched over the skin, that is (a) not active, (b) active with liquid flow applying pressure.

7.2 Mixed Reality Haptics Using Liquid Flow

There have been little efforts to design haptic devices that can also support a user's ability to perceive physical sensations. The term mixed-reality haptics, was used to describe devices that can enable virtual haptic feedback without impeding the user's haptic sensations of the physical world on the same location of the body (i.e. fingertip) while worn. Such devices are akin to mixed-reality displays, which support a user's ability to view both physical and virtual imagery. Before describing the specific device, here outlines two main design considerations when constructing the prototype - the use of liquid flow, and the form factor.

7.2.1 Liquid Flow

A challenge of mixed-reality haptics is to design a device that allows the skin to perceive both virtual and physical stimuli. Any mechanical or rigid device that covers the skin would thus not be suitable. One possibility is to use a retracting device to stimulate the skin on demand, and retract when not in use. However, such an approach would require significant power and accuracy and the miniaturized motors would likely be rigid and bulky. The use of liquid and liquid flow, has several beneficial properties that lend well to providing mixed-reality haptics.

Liquid flow has a variety of states that can be described with physical and transport properties such as pressure, velocity, viscosity, (in)stability, and temperature. By dynamically adjusting the properties of liquid

flow inside a tube, a range of haptic feedback sensations can be created. Due to the nature of liquid flow and the design of the system, some of these haptic sensations can be applied independently or simultaneously. For instance, a user could sense changes in both temperature and vibration at the same time as the temperature of the flowing water changes, and the flow is restricted and released quickly to provide the vibration.

The use of liquid to deliver haptic sensations also allows the end-effector that delivers the sensations to be located away from the equipment that drives the flow of the liquid. As liquid is incompressible, the latency for many sensations (e.g., vibration, pressure) can be relatively low, despite there being long distances between an end-effector and its associated equipment. For other properties (e.g., temperature), the distance to the end effector can impact the latency, but, when using liquid, this can be mitigated through the use of higher flow rates and thinner tubing. If a sealed end-effector is located away from the equipment controlling the flow, it can also be used in a variety of environments (e.g., under water, in dirty or oily environments, and so on). Lastly, if the majority of the end effector is made of flexible tubing, it would be robust to daily usage and small impacts. Even if components become damaged, they could easily be replaced with passive plastic and rubber parts. In comparison, the small, rigid electromechanical actuators associated with traditional haptics damage relatively easily and are often costly and difficult to repair.

7.2.2 Form Factor

With strategic tube routing, liquid flow could potentially be used to provide haptic sensations on any area of the body. In the implementation, we focus on a finger worn device. The fingertip is particularly sensitive to haptic stimulation [50], making it a suitable target area. Demonstrating mixed-reality haptics on the fingertip will also allow us to explore usage scenarios which require dexterous use of the hands or fingers, which traditional haptic devices impede.

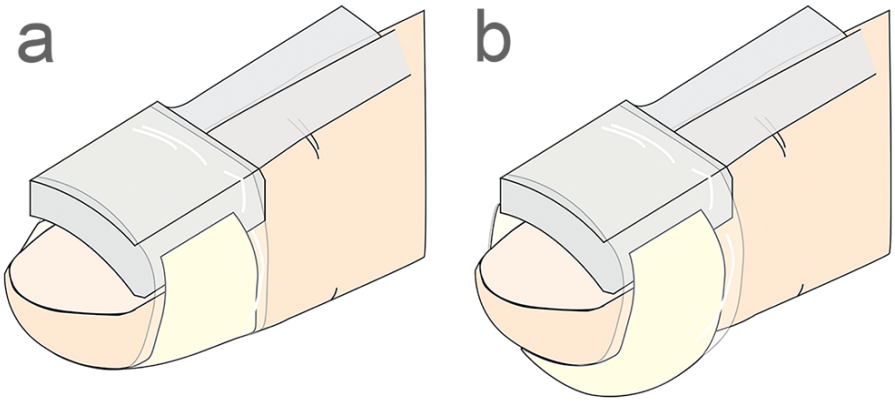

Figure 7.2: Diagram of the prototype as worn on the finger: a) non-active state; b) applying pressure to the finger by pumping water into the latex tube.

Fluid was delivered to the fingertip using a dedicated hydraulic circuit running through a latex tube (Figure 7.2). One potential implementation of liquid-flow haptic feedback is to offload the hydraulic circuit to existing hydrostatic or hydrodynamic systems the user is already wearing. Exoskeletons, while once part of science fiction [23], have recently become a reality, with both industry and medicine [27] testing their utility. It is possible that these existing fluid-based exoskeletons could be modified to include the ability to provide haptic feedback to the fingertip in addition to their regular assistive function.

There is also potential for future liquid-flow haptic devices to be implemented using active microfluidics [124]. Using very thin films, micropumps, and microvalves, it may be possible to deliver haptic sensations directly to the fingertips using low volumes of liquid. This approach shows potential, as it is low powered, very small, and may be able to be implantable directly under the skin in the distant future [54].

7.3 Prototype

The prototype consists of a purpose-built hydraulic circuit (Figure 7.3) connected via flexible PVC tubing to a fingertip-worn ring (Figure 7.2). The hydraulic circuit controls the flow of the liquid, to provide sensations of pressure, temperature, and vibration. Pressure and temperature sensors attached to the tubing monitor the state of the liquid and provide input to the system to ensure that accurate sensations are being rendered. We use water as the liquid medium due to its availability, inert nature, and low cost, although other liquids could potentially be substituted, potentially altering the sensations which are received. While the current form-factor is relatively small and unobtrusive, it does require a dedicated hydraulic circuit and tubing running to the fingertips. In the future, we foresee this approach becoming less cumbersome and more easily integrated.

7.3.1 Hydraulic Circuit

The hydraulic circuit that drives the movement of the water through the ring was custom built to efficiently deliver haptic sensations to the fingertip (Figure 7.4). Water is stored in two reservoirs, one contains hot water, the other cold. Each reservoir has a peristaltic pump [1], which draws water from the reservoir at a controlled speed, computed from the desired pressure, vibration, or temperature. The water flows from the pumps and is combined in a drip chamber [2]. This drip chamber not only mixes water that is at two different temperatures, but also dampens the pressure fluctuations introduced by the peristaltic pump. The water travels from the drip chamber, through the PVC tubing (inner radius: 1mm) to the finger-worn ring before

[1] https://www.adafruit.com/product/1150
[2] https://www.sciencedirect.com/topics/medicine-and-dentistry/drip-chamber

passing through a controllable solenoid valve [3] that stops the flow of water. This allows the device to increase pressure or produce vibration sensations. When the valve is open, the water flows into a terminal reservoir to be later recycled. The latex tube empties when the pump stops and the valve is open, or maintains constant pressure when the valve is closed. Currently, the reservoirs are manually emptied and refilled, but with a more complex system, the water could be recycled within a closed circuit.

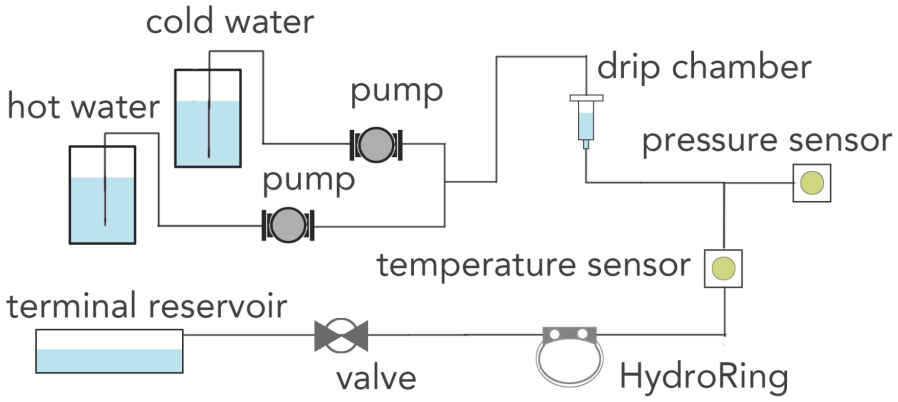

Figure 7.3: Schematic of the system. Water is pumped from the hot and cold water reservoirs, through the drip chamber, and passes through the latex tube before emptying into the terminal reservoir.

The two peristaltic pumps are controlled using an Arduino Uno with an attached Motor Driver board [4] that allows the speed of the pump to be dynamically controlled. The same Arduino UNO also controls the solenoid valve that modulates the flow of liquid to the terminal reservoir. A second Arduino oversees the pressure and temperature sensors (pressure sensor - MS5803-14BA [5] and infrared thermometer - MLX90614 [6]) that monitor the current state of the ring. Both Arduinos are connected to a single PC which contains the logic that monitors user input and sensor values and controls the flow rates and valve states.

7.3.2 Ring

The ring is comprised of a small custom 3D printed plastic structure (12 × 12 × 4 mm) worn on the back of the finger, and a thin latex tube that is 9mm wide which wraps around the fingertip and connects to the rigid structure behind the finger on either side of the fingertip. As latex is very flexible, any increases in pressure will cause the latex to expand both toward, and away from, the actuated finger. To constrain the expansion toward the finger, a thin film of clear Low-Density Polyethylene (LDPE) was wrapped around the latex tubing and finger. As LDPE is not as elastic as latex, this constrains the expansion of the latex tubing

[3] https://www.sparkfun.com/products/9673
[4] https://www.adafruit.com/product/1438
[5] https://www.sparkfun.com/products/12909
[6] https://www.melexis.com/en/product/MLX90614/Digital-Plug-Play-Infrared-Thermometer-TO-Can

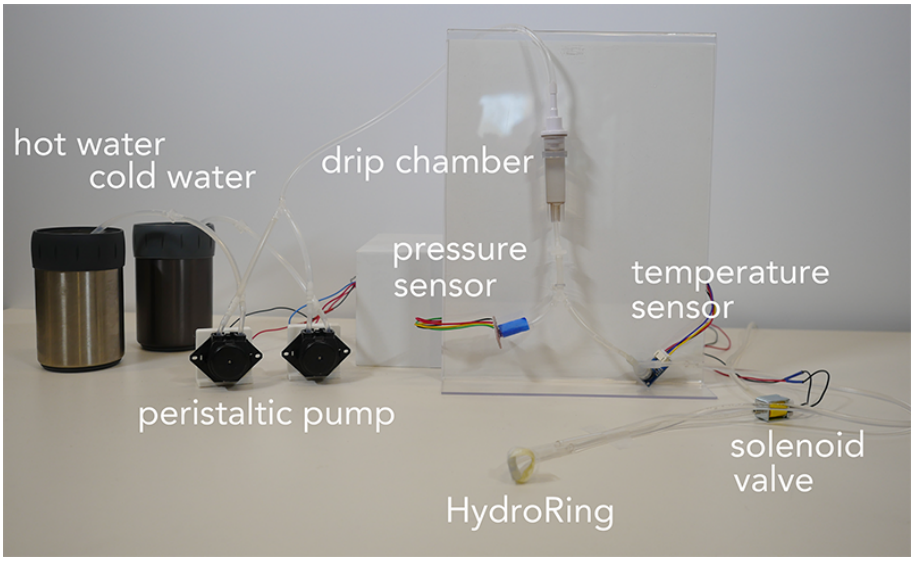

Figure 7.4: Overview of the prototype system showing the hydraulic circuit.

toward the finger-pad, increasing the pressure felt on the finger and reducing the overall size of the actuated device.

Custom software written in Java monitors the sensors and coordinates the control of the pumps and valves. The software is run on a desktop PC, and communicates with the Arduinos over USB.

7.3.3 Haptic Sensations

An advantage of using a fluid is that it can produce a range of haptic sensations. Below we describe how the device is used to render vibration, pressure, and temperature.

Vibration

To render vibration, the terminal solenoid valve is opened and closed in rapid succession as the water is pumped through the system. By varying the incoming flow rate as well as the frequency at which the solenoid valve opens and closes, the system is able to control both the frequency and amplitude of the vibration. The system is able to render vibrations from 1Hz to 50Hz while running a single pump at 12VDC constantly. Beyond 50Hz, the water does not circulate fast enough through the system and pressure builds up. It is worth noting that the vibration amplitude decreases as the frequency increases, while the absolute amplitudes are also determined by the water flow rate (as affected by pump speed, tube size, etc.). The latency to activate the vibration sensation is less than 200ms.

Pressure

Pressure is produced by closing the terminal solenoid valve and preventing the water from flowing back into the terminal reservoir. As the volume of water increases, the pressure within the tubing does as well. Because the latex tubing is the most elastic component within the prototype, this volume of water causes the latex tubing to expand towards the finger, yet still be constrained on one side (by the LDPE), causing the user to feel the sensation of pressure on their fingertip.

The system can produce pressures ranging from 0.1N to 2.6N (measured with a force sensor [7] put in between the fingertip and the latex tube). The minimum pressure (0.1N), represents the pressure felt from wearing the ring in its relaxed form. We observed a linear relationship between water pressure inside the tube via the pressure sensor reading and the measured force applied to the fingertip. Thus the inner water pressure sensor is used to monitor and adjust the rendered pressure sensation. As the water takes some time to reach and fill the latex tube, there is some latency in achieving high pressures. Currently, the device takes approximately 3 seconds to change from no pressure to maximum pressure, with smaller changes taking less time. With a stronger pump, this time to reach the desired pressure may decrease, but the accuracy in controlling the pressure may be reduced.

Temperature

Temperature output is produced by controlling the speed of two pumps that draw water from insulated reservoirs. One reservoir contains hot water held at $50 - 60°$C, while the other contains cold water held at $1 - 2°$C. To control the ratio of hot to cold water, a PID controller [8] monitors the water temperature via the infrared temperature sensor, and controls the relative speed of each pump. Manual tuning of the PID parameters ensured that the temperature reached the target value as quickly as possible, but did not overshoot (so as not to expose the wearer to temperatures that are too hot or too cold). The PID parameters also ensured the stability of the flowing water at the target temperature, to reduce undesired oscillations.

Using this approach, the system is able to deliver water in the range from $2-55°$C, but we limit the output to $15 - 40°$C to ensure users' comfort. Because the temperature change requires the liquid to travel from the reservoir to the fingertip, and the priority of not overshooting and maintaining temperature stability, its latency is higher than the pressure and vibration stimulus generation. The system takes approximately 6 seconds to change the temperature by 5 degrees. This latency could be reduced with a stronger pump, or by shortening the tubing connect the fingertip device to the reservoir.

[7] https://www.sparkfun.com/products/9673
[8] https://github.com/tekdemo/MiniPID-Java

7.4 Evaluation

Two studies were carried out to evaluate the design and prototype. The first examined a user's ability to learn and recognize different levels of temperature, pressure, and vibration produced by the device. The second study evaluated the extent to which such skin-like haptic display impedes a user's natural touch perceptions of surface texture, pressure, temperature, and vibration while the device is worn in passive mode.

7.4.1 Recognition of Sensations

The objective of the first study was to determine how well users could differentiate different levels of rendered tactile sensations produced by the prototype after a brief training period. This study serves to validate that the prototype is able to reliably generate haptic sensations and to evaluate users' ability to perceive and recognize the sensations. Twelve participants (8 male) between the ages of 22 and 36 years participated in the study.

Apparatus

The experiment was performed using the prototype previously described to render the sensations. A traditional desktop computer ran the experimental software, showed feedback to participants, and controlled the haptic rendering.

Three prototype sizes were available: the best fitting ring was chosen by using the largest ring where the latex tube would lightly stretch over the fingertip of the dominant hand while the finger was in a resting state.

Experimental Design

This experiment evaluated participants' ability to recognize stimuli using the three modalities that the prototype is capable of rendering (i.e., pressure, temperature, vibration). For each modality, the functional range of stimuli that the ring could provide was divided into three, five, or seven levels of granularity (values for stimuli at 7 levels is shown in Table 7.1). Participants completed 3 repetitions of each of the three granularity levels for each of the three modalities for a total of 135 testing trials per participant (i.e., 3 levels of granularity (3 trials at level 3) + (5 trials at level 5) + (7 trials at level 7) = 15 trials $\times$ 3 repetitions of each stimulus $\times$ 3 modalities pressure, temperature, vibration = 135 testing trials per participant).

The presentation order of modalities was counterbalanced among participants using a Latin square, as was the presentation order of each granularity level. Within each block of trials, the presentation order of stimuli was randomized.

Sensations	Levels	Unit
Pressure	0.3, 0.39, 0.50, 0.64, 0.83, 1.07, 1.4	N
Vibration	2, 3, 4, 7, 12, 20, 31	Hz
Temperature	15, 19, 23, 27, 31, 35	°C

Table 7.1: Levels of each stimulus rendered for the 7 level condition.

Procedure

After being outfitted with the prototype, participants began the first block of the experiment, for the first assigned modality. In each block, participants were shown a training set of stimuli corresponding to the current granularity level (i.e., in the 3 levels of granularity condition they were shown the stimuli from 1 – 3, in order; in the 5 levels of granularity condition, they were shown the stimuli from 1 – 5 in order; etc.). They were then shown this training set of stimuli again. Then, they were shown a testing set of stimuli, which was one of the stimuli from the current granularity level, and were asked to indicate, using a keyboard, which level the stimuli corresponded to. This process was repeated for all remaining stimuli in the current granularity level. Once all the testing set stimuli were presented, the participant was shown the training set of stimuli again and completed another testing set of stimuli. This process was repeated until the participant had been exposed to a total of three sets of testing stimuli (with additional two sets of training stimuli interspersed). Once a block was completed, the participant then moved onto the next granularity level and modality.

Figure 7.5: Apparatus of study 1. The user's view of the device is occluded, and they wear headphones to mask the noise of the pumps and valves.

Each time a granularity level was presented during a training set, HydroRing would render the stimuli and the computer monitor would display the number associated to the current granularity level of the stimulus (i.e., in the 7 level condition, the numbers 1 – 7 would be displayed; in the 5 level condition the numbers 1 – 5 were displayed; in the 3 level condition the numbers 1 – 3 were displayed).

Results

Response accuracy (Figure 7.6) was analyzed using a 3 (Modality: pressure, temperature, and vibration) × 3 (Granularity Level: 3, 5, and 7) repeated measure ANOVA, with Bonferroni corrected paired t-tests for post-hoc pairwise comparisons. No Modality × Granularity Level interaction ($p > .05$) or effect of Modality was found ($p > .05$), but a main effect of Granularity Level was significant ($F_{2,22} = 170.9, p < .01$). Post-hoc pairwise comparisons demonstrated that it was easiest to discriminate between 3 levels (M = 98.1%), followed by 5 levels (M = 84.4%), and by 7 levels (M = 53.8%) (all $p < .01$).

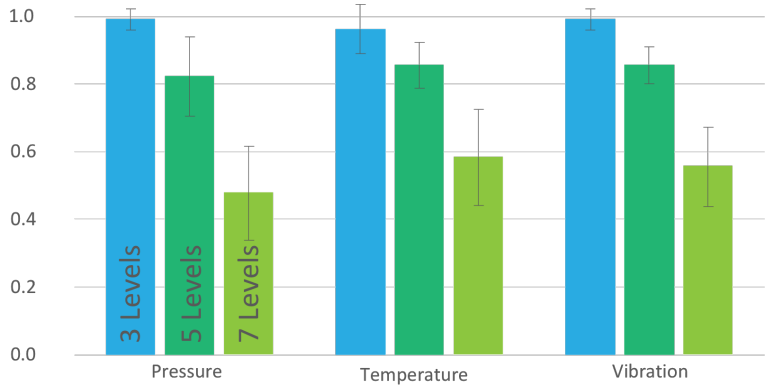

Figure 7.6: Mean recognition accuracy per modality. Error bars show standard error of the mean.

A further analysis on the responses with 7 levels demonstrates that while accuracy levels may be low (around 50%) across all modalities, the participants were often close to the correct answer. Comparing the mean responses against the baseline (Figure 7.7) shows that participant responses tended towards the ground truth, with strong correlations for all modalities.

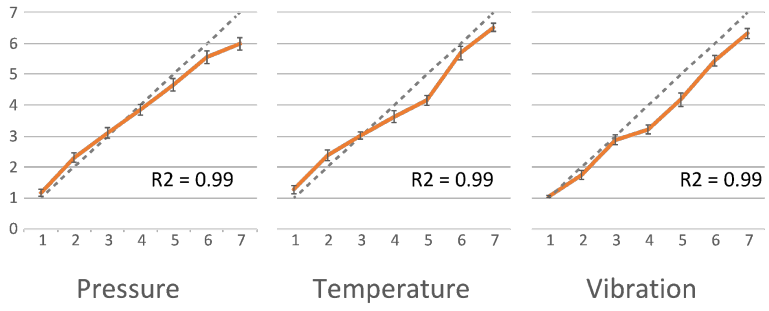

Figure 7.7: Mean perception of each stimuli, compared to the ground truth. Error bars show standard error of the mean.

Discussion

The results demonstrated that the prototype was able to reliably produce haptic sensations at different levels. Participants could accurately distinguish among 3 levels of haptic stimuli on each sensation, and performed relatively well even with 5 levels. However, if accurate perception of the stimuli is needed, subdividing the space into more than 5 levels is not practical.

The results suggest that designers could consider including 3 or 5 items or notification levels, that are associated with different levels of haptic stimuli. However, applications should allow users to receive enough training to become familiar with, and learn the stimuli. Two participants (P4, P9) noted that re-training was beneficial as it helped strengthen their memory and improved their confidence in subsequent trials. It remains a challenge as to how best to design interactive training sessions within applications.

When deciding between many levels of haptic feedback (e.g., 7 levels), users were likely to under-rate their perceived stimuli. Despite this, it was easier for them to distinguish between values at the extreme ends of what the prototype could generate versus those that were similar. Such information could be useful for designing feedback like haptic progress bars that do not require users to perceive absolute values but could indicate a general direction or relative magnitude.

The study design has some limitations that were observed or elicited through participant feedback, which designers should consider. First, participants' perception of pressure, vibration and temperature were likely influenced by the last stimuli they had encountered. For instance, participants may have felt a stimulus was warmer if the previous stimuli was cold. This suggests that the relative change in stimulus level should be considered, not just the absolute stimulus. Second, although participants could rest during the study, some felt that they lost some ability to sense stimuli accurately towards the end of the study due to the repeated trials.

7.4.2 Study 2: Impact on Physical sensations

A second study was conducted to assesses the degree to which the haptic display impedes the wearer's natural tactile sensations. Four common tactile sensations that could be impacted by the use of the prototype were evaluated: pressure, vibration, temperature, and texture. The same twelve participants from the first study participated in the second study.

Apparatus

Several purpose-built devices were constructed to render different levels of each of the desired stimuli [].

Pressure was produced via a small platform which was constrained to move along a single dimension

Sensations	Levels	Unit
Pressure	0.3, 0.6, 1.2, 2.4, 4.8	N
Vibration	80, 110, 150, 200, 250	Hz
Temperature	14, 21, 28, 35, 42	°C
Texture (Bump size)	0, 0.5, 1.0, 1.5, 2.0	mm

Table 7.2: Levels of each sensation used in Study 2.

(normal to the fingertip). The finger was placed underneath the platform with the fingerpad facing upwards. Different masses ranging in weight from 0.3-4.8N were placed on top of the platform to produce a range of pressures. The masses had the same appearance so participants could not visually determine which weight was being added, but differed in the amount of weight that was contained inside.

Vibration was produced with a small vibrotactile motor that could be actuated between at 80 and 250 Hz. The motor was fixed onto a table and participants rested their finger on the tactor. The frequency of the vibration was controlled by regulating the voltage that powered the device.

Temperature was rendered using a 20 × 20mm Peltier module with a heatsink to provide stimuli between $14°C$ and $42°C$. The module and heatsink were affixed to a table and participants were instructed to place their finger on the pad. The temperature of the module was controlled by regulating the current flowing to the device, and participants were instructed to place their finger on their module only after the module had reached the desired temperature.

Texture was rendered using five different 3D-printed texture samples. Each texture sample was created by embedding different sized spheres on top of a solid to create a grid of bumps. The bumps ranged in size from 0 mm (flat and smooth) to 2 mm (rough, bumpy surface). All texture samples had the same overall dimensions of 50 mm × 50 mm × 2 mm.

Experimental Design

Participants completed the within-subjects study under two conditions, a baseline, where they used their bare index finger to perceive the stimuli, and an augmented condition, where they perceived the stimuli using their index finger while wearing the HydroRing in its passive state.

The levels of each stimuli were selected to represent a range of levels frequently encountered in daily life, while remaining inside the range of comfort for a given sensation (Table 7.2). Each level of the stimuli was repeated 5 times, resulting in 5 levels × 3 repetitions × 2 conditions (baseline, augmented) = 30 trials for each sensation. The presentation order of the conditions, as well as the type of sensation was counterbalanced between subjects using a Latin Square design. Within each stimulus, the presentation order of the levels was randomized within each block of trials.

Procedure

Before beginning the study, participants were informed of the nature of the study. Depending on the condition, they were then outfitted with the prototype.

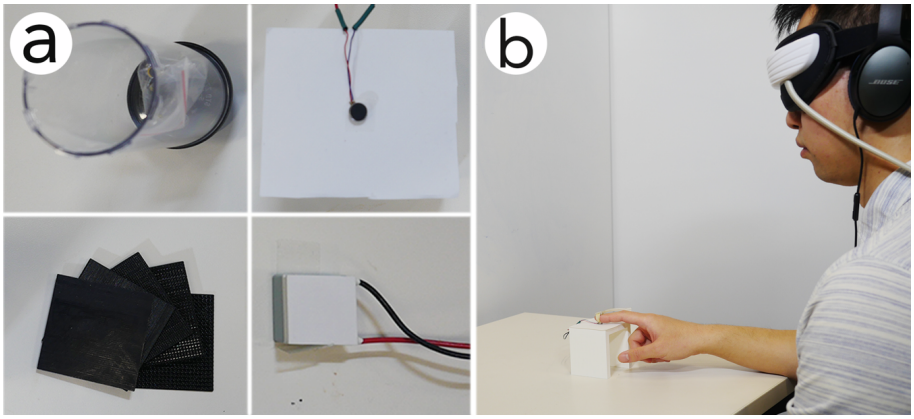

Figure 7.8: Apparatus for testing tactile perception capability; a) the four devices used to produce the sensations of pressure, vibration, texture, and temperature; b) the participant assessing the vibration stimulus while wearing the prototype.

Each sensation was tested independently, and all trials were completed for that sensation before beginning a new sensation. For each sensation, there were two blocks, with the ring and without the ring. The order of the blocks was counterbalanced among the users. Users received 5 minutes of training before beginning the trials for each sensation to get familiar with the five levels of the stimuli. During the test, the presentation order of the stimuli were selected randomly. The stimuli were presented to the user (their hand was guided towards the stimuli), and they were asked to verbally report which level of the stimuli they believed they had felt.

Results

A two-way 2 (Condition: baseline, augmented) $\times$ 4 (Modality: pressure, temperature, vibration, texture) repeated measures ANOVA was conducted, with Bonferroni-corrected paired t-tests for post-hoc pairwise comparisons. There was a significant effect of Condition, ($F_{1,11} = 16.60, p < .01$); as well as Modality ($F_{3,33} = 4.31, p = .01$). There was no interaction effect ($F_{3,33} = 1.08, p = 0.37$). Wearing the ring significantly impacted the user's ability to identify the sensations, with accuracy dropping from 0.876 with the bare finger to 0.839 with the ring. The only significant difference between modalities was between vibration ($M = 0.90$) and texture ($M = 0.81, p < 0.01$); all other comparisons within Modality were not significant ($p > 0.2$).

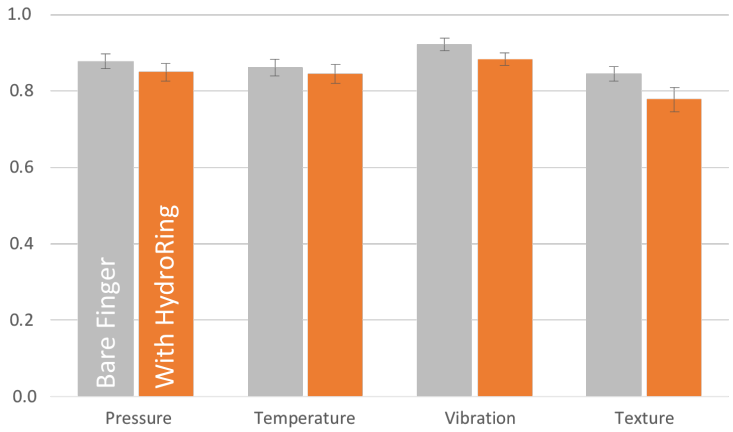

Figure 7.9: Accuracy in perception recognition with and without wearing the prototype. Error bars show standard error of the mean.

Discussion

While the difference in accuracy while wearing the ring was significantly less than without the ring, the actual effect was quite small at only 3.7%. From this small effect, we can conclude that while the device has some impact on the user's perception, the effect is quite minimal. Additionally, some modalities were relatively unaffected (e.g., temperature, pressure), while texture was most impacted. This is likely due to the higher frequency textures being dampened by the latex tubing. Further evaluation is necessary to determine exactly what components of the perception are altered to better characterize how the perception is affected [73].

7.5 Sample Usage Scenarios

While always-available, unobtrusive haptic devices could have many different applications and use cases, here we outline three general uses of such technology that were prototyped in a Wizard-of-Oz approach.

7.5.1 Usage in Daily Activities

The ring form factor makes it suitable for an always-available notification and low-bandwidth information channel. Vibration, pressure and thermal feedback can be used to enrich the information received by the users from a notification. Using the pressure input channel, users can provide simple input using the same channel they received the notification from, providing a tight coupling between input and output. As the actuation of the device results in very little visible movement, the notifications could be quite subtle, and non-disruptive to others around the wearer.

As the device is designed not to be obtrusive, users can continue doing their normal daily activities without worrying that the device will impede their dexterity or tactile sensations. Additionally, as the actuating component of the device is sealed and flexible, the user does not have to worry about damaging the device through normal activities. Users can use the device in messy or wet environments, and while performing fine manipulation or assembly tasks [51].

Figure 7.10: Sample scenarios where mixed-reality haptics could be used; a) while operating existing technology b) performing activities in wet or dirty environments c) performing activities that require manual dexterity.

7.5.2 Augmenting Physical Objects

Mixed-reality haptics could be used to augment existing static objects and structures. They could provide feedback to augment the real world with haptic information, or deliver new haptic sensations. For instance, if the hand were tracked in 3D space and the structure of the room was known, by running your finger over a wall the ring may increase in pressure to indicate where wiring or framing structures are located behind the wall.

The feedback could also be used to enhance existing technology that does not have haptic output capabilities. For instance, when reading a children's book on a tablet, the device could respond and provide haptic feedback corresponding to the elements in the book. For instance, if the book has scenes of a desert, the ring may heat up when the book is touched – if the book has bees, the ring could vibrate to emulate the buzzing. Such sensation may also be used to aid low-vision users.

7.5.3 Mixed Reality Interaction

Current augmented reality devices and applications are largely focused on visual augmentations of the real world, with other sensations left un-augmented. By leveraging mixed-reality haptics, the virtual elements in a scene can not only have a visual representation, but a tactile representation as well. The haptic device can provide contact sensations, as well as vibration and thermal information to enrich the user's perception of the virtual aspects of the augmented scene.

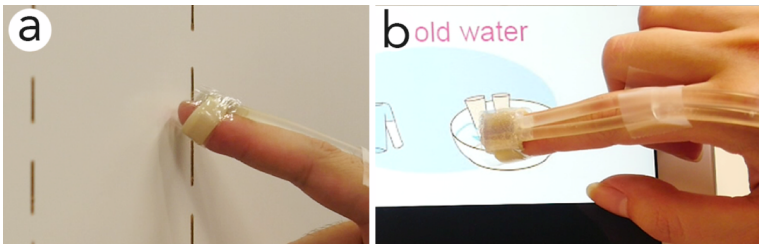

Figure 7.11: Example scenarios using mixed-reality haptics to add feedback to existing objects and devices. a) a user moves their finger over a wall, and feels vibration feedback as her hand passes over wiring hidden behind the wall. b) a user touches an interactive children's book, which provides thermal feedback corresponding to the on-screen content.

Additionally, because the device does not substantially impede the user's natural sensations, they can seamlessly switch between interacting with real objects and interacting with virtual objects.

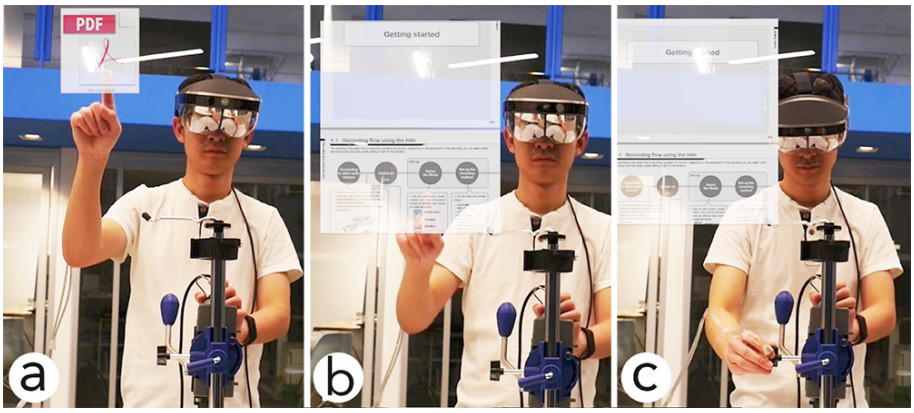

Figure 7.12: Example scenario of adding tactile feedback to an augmented-reality instruction manual. As the user selects items on the display and navigates the content, vibration and pressure provide real-time feedback on their actions (screens are simulated).

7.6 Chapter Summary

This chapter explores a design of a skin-like haptic display and the benefits of enabled mixed-reality haptics. A proof-of-concept prototype was built using liquid flow that run through a thin latex tube which was slightly stretched over the skin. By dynamically adjusting the liquid flow, haptic senstaitons such as pressure, vibration and temperature can be rendered on the end-effector.

The prototype and the studies validated the design while the current approach faced several technical and practicality limitations. The current prototype utilizes hardware such as valves, pumps, and temperature-controlled reservoirs that require a considerable amount of space. Additionally, after flowing through the ring, the water flows into a reservoir which must be manually recycled back into the system. Further work

is needed to develop a prototype that is more self-contained and would allow the water to be recycled. Such a prototype could quickly adjust the temperature of liquid on-the-fly using high-power Peltier modules. Additionally, we anticipate that further hardware developments, particularly in the area of microfluidics [124] will result in hardware devices such as valves and pumps that are smaller, require less power, and can be more readily integrated into wearables.

Full, independent control of all three tactile sensations is not possible with the current implementation of the hydraulic circuit. For instance, increasing pressure requires restricting the flow rate, which prevents different temperatures of water from reaching the ring. Alternative approaches to the design of the hydraulic circuit, and different hardware to drive the flow of liquid, may be able to achieve more seamless and responsive integration of the stimuli. For instance, a higher-powered pump, a variable terminal valve, and a more complex control loop may be able to provide more flexibility to combine sensations.

As the last piece of the design space, this chapter intends to help us examine design challenges, as well as application scenarios that can be enabled with skin haptic display. On one hand, this shows that skin will be playing an important role as interfaces when the implantable technology is mature. On the other hand, the chapter illustrates the feasibility of leveraging liquid flow as actuation source, which makes the example scenarios possible with the development of implantable technologies such as the microfluidic systems. The chapter also envisions the future work on leveraging body fluids such as blood, with the functions of implanted devices inside body.

Chapter 8

Conclusion and Future Work

Wearable devices are evolving rapidly: While they are becoming smaller in size, their computational power is growing stronger. Human technological advancement further empowers this evolution: as these devices grow smaller, a transition occurs as they begin to be implanted in the skin. As traditional screen-based interfaces on wearable devices become less common, they will likely be replaced by tiny devices embedded into the body. Naturally, such evolution will bring profound changes to the way we recognize and perceive the world. The interface paradigms considered in the design of implantable devices are currently weighted towards human languages of symbols, words, and gestures. Nonetheless, it will take a long period of refinement before implantable devices gain considerable market share.

To help users get accustomed to the changing interfaces, forecasting the evolution of implantable devices is key, along with the new types of control mechanisms and interaction metaphors which must be considered for these transformations. This thesis looks into a design space of interface paradigms, with a focus on the input and output metaphors derived from the transitions from wearable to implantable. Upon summarizing the key features, use-case scenarios, and challenges of the interface paradigms, the thesis undertakes a broad exploration of design, implementation, and evaluation of the interfaces.

As introduced in Chapter 1, the statements of the thesis are:

1. With the implantable revolution, conventional screen-centric interactions are becoming less prominent and even disappearing. New interface paradigms are weighted towards human languages of symbols, words, and gestures.

2. An interface design space is sketched based on the input and output metaphors derived from the evolving technology.

3. Leveraging daily interaction metaphors such as the page-flipping gestures helps to compose efficient interfaces on wearable touchscreen.

4. Gestural input becomes more important on miniature devices. Daily hand gestures that generate vibrational signals are viable sources for the design of gestural Input. Acoustic signals are rich input sources for in-air gestures and mechanical vibrations that transport through the body can be detected by on-body sensors.

5. Designing appropriate output channels for implantable devices is crucial. Leveraging passive force feedback, a common perception experience that happens in daily life, provides a valid way to design output channels for non-visual feedback.

6. Skin will become an important interface for communicating information with users. Developing a skin-based haptic display requires non-mechanical structures which are not rigid and bulky and do not impede with users' natural sensations of physical objects.

8.1 Summary

Chapter 1 described the motivation and the thesis' topic. The forthcoming implantable revolution will bring profound changes to the way we recognize and perceive the world. With the decreasing size of wearable devices, visual displays will become less prominent and even disappear. Implantable devices bring interactions closer to the body. With the focus of input and output metaphors, the chapter sketched several interface paradigms that are considered part of the transformation from wearable to implantable (Figure 8.1). This includes *touchscreen as the input and output channel*, *gesture input around the device*, *devices as on body sensors*, *devices as on body actuators*, and *skin as haptic display*. The key features, scenarios, and challenges of these interface paradigms were analyzed.

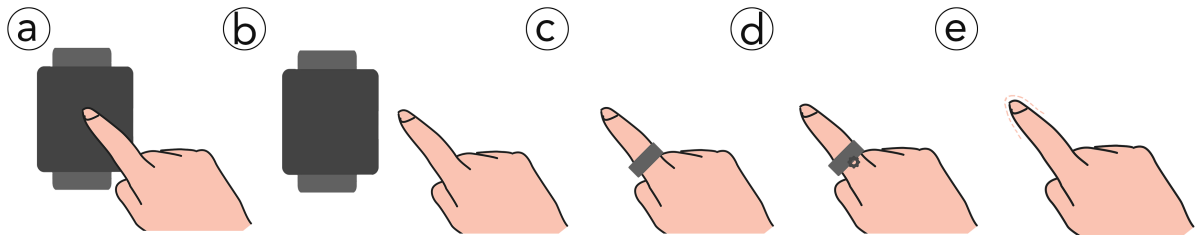

Figure 8.1: Interface paradigms presented in this thesis: (a) Touchscreen as the input and output channel; (b) Gesture input around the device; (c) Devices as on body sensors; (d) Devices as on body actuators; (e) Skin as haptic display.

Chapter 2 discussed the related work in the development of wearable and implantable devices, as well

as recent progress in novel input and output techniques and interfaces on the devices. It was shown that previous interaction design focused on innovation in sensing that could be applied to wearable devices. Gestures used in interaction are often adapted to a set of arbitrary conventions or procedures derived from a variety of approaches to sensing. Previous work informs of the necessity of composing more intuitive and natural interactions that are weighted towards human language of symbols, words and gestures.

Chapter 3 discussed *touchscreen as the input and output channel* and considered how to design interactions on wearable touchscreens that are commercially available. The design in question was inspired by a common hand activity - flipping book pages. By imitating a curled page visual effect and mapping finger flipping direction and distance to a pie shape hierarchical menu layout, a page-flipping interface is implemented on smartwatch and users are able to use page-flipping gestures to select commands and values. Two studies were carried out to investigate the design factors and performance in comparison with standard menu UIs on smartwatch. Using the page-flipping gestures was found to be efficient and intuitive for small touchscreen interactions. The gesture also raised concerns of usability challenges that were discussed in the chapter.

Chapter 4 discussed *gesture input around the device* and proposed an alternative approach to in-air gestures, in response to the challenges faced when interacting with small screen on a wearable. Acoustic signals generated by hands are rich and easy for the user to generate. These signals can be recognized and classified with a watch-size, four microphone array. With this sensing approach, users are able to perform a rich set of hand gestures around the device, enriching the design space for wearable interactions.

Chapter 5 discussed *devices as on-body sensors.* As devices are getting smaller and screens are becoming less prominent, wearable devices increasingly serve as on-body sensors that enable health and motion tracking. To help improve the expressiveness of the hand gestures and avoid false triggering from users' arbitrary actions, this chapter proposed to leverage finger-swiping gestures on surrounding bumpy surfaces that are either already existing, or 3D printed with desired physical properties. A design space of the design factors was investigated.

Chapter 6 discussed *devices as on body actuators.* Designing non-visual feedback on miniature devices becomes more crucial. Besides sensors, devices can be composed of mechanical actuators and structures that can be leveraged to render haptic senstations on skin. Existing haptic feedback such as vibration is often used for notification purpose but is limited in terms of information expression. This chapter discussed having passive kinesthetic force feedback on a finger worn device that is capable of rendering different force profiles. Users are able to perceive the force profiles while engaged with both physical and mental workload.

Chapter 7 discussed *skin as haptic display.* As devices are getting smaller and embedded into the body, skin will play an important role as an interface used to communicate information with users. This chapter presented a hydraulic approach to render haptic sensations including pressure, vibration, and tempera-

ture through a thin latex tube that is slightly stretched over the skin. Compared to conventional electric-mechanical approaches, the presented skin-like haptic display is able to render haptic sensations when needed, without impeding users' natural sensations.

8.2 Future Work

The future work following this thesis will be further exploration into the implantable interfaces, the technologies that support the design of these interfaces, and the social acceptance of the proposed interfaces.

8.2.1 Implantable Interfaces

The implantable devices that are embedded in the body will not only change the wearable devices in functionality, but will also cause profound changes to the way users perceive and recognize the world. Implantable technology and development is seen mainly in the health industry. Currently, the development of medical implants that are used for birth control, heart monitoring, defibrillation, as well as tiny healing chips and smart tattoos [22], is becoming more common. From these generic applications, we can see that in addition to monitoring, implantable technology is capable of mediating and altering the body conditions of the user. For instance, defibrillators are used to deliver electrical power to the heart, to manage unusually fast heart rhythms. In the future, use of implantable devices will be extended to many other domains and even change our natural body functions by adding new sensing and actuating capabilities to the body.

Interaction designers, would like to explore the future of implantable interfaces, along with the applications innovated by the future implantable technology. Future implantable devices could be embedded within the body which keep collecting data from every aspect of the user's life. The devices in the body could implicitly track the objects the user is touching, the food they eating, the sports they are playing, the environments that they are living within, and much more. Wireless communicating components of implantable devices can feed the collected data into an intelligent processor, which sends instructions to provide assistance information with either visual or haptic display. Eventually, these devices might even predict the intentions of the user to provide better digital services.

Technology often outpaces imagination and what is considered normal and acceptable in society. When exploring possible applications and scenarios of the future, technology can help us better foresee what life in the future might be like. It is clear that the future will not be realized without the exploration of and investment in technology.

8.2.2 Implantable Technology

This thesis discusses the technology which could support the design of the implantable interfaces. This section follows the discussion of technologies which are worthy of investigation.

Miniature Actuator

As mentioned in Chapter Six and Chapter Seven, one critical challenge of implementing haptic interfaces on miniature devices (either wearable or implantable), is the relatively bulky size of the actuators and required structures. Chapter Six discussed adding mechanical structures to apply force feedback based on user input. To provide the desired forces, a DC motor was used and attached to the device. Although mechanical structures could be refined and further decreased in size, the size of the motor becomes a bottleneck. Chapter Seven discussed a hydraulic approach, which enabled vibrotactile and temperature feedback in a small form factor to emulate skin-like haptic display. This, however, still required two peristaltic pumps on the side of the end effector to actuate the system, making it impractical to use in the field.

To solve these challenges, miniature actuators need to be developed. Micro-Electro-Mechanical System (MEMS) technology are micro fabrication techniques that construct mechanical and electro-mechanical devices or structures [129]. There is considerable effort dedicated to the development of MEMS based actuators such as magnetic actuators [12] and piezoelectric actuators [77]. Future work could look into how to design haptic interfaces with the MEMS actuators. Besides MEMS, the development of microfluidics systems has made a profound impact on the the field of molecular biology, providing tools to biologists to control the complete cellular environment, leading to new questions and discoveries. Microfluidics are systems that precisely control fluids in a small scale that are geometrically constrained [89]. Microfluidics can be actuated with micropumps and microvalves. Future work could look into the applications of microfluidics in designing and developing hapitc interfaces on skin.

Skin as Interface

As discussed in the thesis, skin will become more and more important as an interface to communicate with users. Skin can be used for user touch input [93] and also for visual [120] and haptic display, as presented in Chapter Six and Chapter Seven. Skin interfaces with the environment and serves multiple functions such as protecting the body against pathogens and excessive water loss. Other functions of skin include temperature regulation and thermal insulation. Skin has rich sensing capabilities to detect environment changes and is able to self regulate to protect the body. These capabilities can be leveraged to design skin-based interfaces that embody information. Such information channels can be perceived by users implicitly without the need

for intervention. Additionally, the body can be augmented with new sensing and displaying capabilities via artificial skin. This potential stands to improve the skin's sensitivity to the environment and enable new functions, such as changing colour or thickness.

Intelligent Processors

Developing implantable interfaces is not only about sensors and actuators. Implantable interfaces provide opportunities to obtain data from every aspect of human life. For instances, such an interface may sense the colour, material, or temperature of an object when held. It may also sense the class and nutrition of food consumed. Such data shall be fed into processors that help the system to better understand the user. As these systems become intelligent, richer information could be provided to enrich the ambient experiences provided by the implantable interfaces. First, implantables will improve in analyzing the context, environment, and users' ongoing tasks, resulting in the ability to predict the intention of the users. In this way, services that better predict and meet user needs will be provided without users having to intervene. Second, these systems will be able to better understand human language of symbols, words, and gestures, which are likely the most common methods users will employ to interact with these devices. This understanding will help establish more reliable and flexible interfaces between users and the devices.

8.2.3 Understanding Users' Mental and Physical Workload in the Interactions

The work presented in this thesis focuses on sketching an interface design space through the transitions from wearable to implantable devices, along with the solutions required to tackle the input and output challenges. Although the ideas, design considerations, and benefits of the proposed interactions have been discussed in the thesis, it would be valuable to investigate how interaction would affect users' mental and physical workload.

It could be noticed that the input and output solutions proposed in the thesis were designed upon users' existing experiences, e.g., the book page flipping gestures, the hand gestures that produce audible sounds, and the force feedback that are triggered with users' actions. The interactions were designed in this way to leverages users' pre-established mental models. This method of design helps users in understanding and memorizing the interactions and specific gestures that are used. It is thus important to determine how users link their own life experiences to an interaction. Users often need to adapt their existing mental models to new contexts for interaction. Chapter Three raises these considerations. While flipping book pages is common and familiar to most users, using this gesture in menu selection tasks is new, requiring users to adapt their existing mental models to a task.

Derived from real life experiences, interaction design aims to define a set of gestures that are easy to perform and feedback that is easy to perceive. The objective is to reduce physical effort required from the user while performing the interactions. Normally, evaluating physical effort in an interaction involves measurements of user fatigue levels. Mid-air arm gestures, for example, normally require more physical effort. Existing hand activities that are short and easy are beneficial to consider in the design process, as they could potentially ease the burden on a user.

8.3 Final Words

The era of wearable and implantable computing is promising. The future world and technology prospects represent potential and excitement, which are likely to change every aspect of daily life. There is substantial motivation to envision the future and think deeply about the possibilities it holds. Designing for interactions while considering the evolution of technology, in both a historical and potential sense, is challenging and requires long-term effort and exploration. This thesis presents an interface design space that outlines the possible transitions in the input and output metaphors. The methodology employed aims to glimpse ripples of the future by looking at the changing waves. Accordingly, the ripples will become more pronounced as work in the field of implantable devices continues to progress. Technological advancements will always outpace our imagination in many ways, while challenging current social norms. This will bring higher requirements for interface designers and researchers, to understand the forthcoming implantable revolution and obtain the skills needed to operate in the space. Perhaps this thesis can inspire more research in the field to refine the design space and find answers to many interesting and important questions.

Bibliography

[1] Apple Developer. Human Interface Guidelines. Retrieved September 14, 2017 from https://developer.apple.com/ios/human-interface-guidelines/views/pages/

[2] Apple Watch. Last retrieved on Nov. 18th, 2018, from https://www.apple.com/ca/watch/

[3] Daniel Ashbrook. 2010. Enabling Mobile MicroInteractions. Thesis. Georgia Institute of Technology.

[4] Daniel Ashbrook, Kent Lyons, and Thad Starner. 2008. An investigation into round touchscreen wristwatch interaction. In *Proceedings of the 10th international conference on Human computer interaction with mobile devices and services* (MobileHCI '08). ACM, New York, NY, USA, 311-314. http://dx.doi.org/10.1145/1409240.1409276

[5] Daniel Ashbrook, Patrick Baudisch, and Sean White. 2011. Nenya: subtle and eyes-free mobile input with a magnetically-tracked finger ring. In *Proceedings of the SIGCHI Conference on Human Factors in Computing Systems* (CHI '11). ACM, New York, NY, USA, 2043-2046. https://doi-org.uml.idm.oclc.org/10.1145/1978942.1979238

[6] Hrvoje Benko, Andrew D. Wilson, and Patrick Baudisch. 2006. Precise selection techniques for multi-touch screens. In *Proceedings of the SIGCHI Conference on Human Factors in Computing Systems* (CHI '06), Rebecca Grinter, Thomas Rodden, Paul Aoki, Ed Cutrell, Robin Jeffries, and Gary Olson (Eds.). ACM, New York, NY, USA, 1263-1272. http://dx.doi.org/10.1145/1124772.1124963

[7] Hrvoje Benko, Christian Holz, Mike Sinclair, and Eyal Ofek. 2016. Normaltouch and texturetouch: High-fidelity 3d haptic shape rendering on handheld virtual reality controllers. Proceedings of the 29th Annual Symposium on User Interface Software and Technology, ACM, 717–728.

[8] Carlos Bermejo and Pan Hui. 2017. A survey on haptic technologies for mobile augmented reality. arXiv:1709.00698 [cs]. Retrieved December 12, 2017 from http://arxiv.org/abs/1709.00698

[9] Gábor Blaskó, Steven Feiner. 2006. Evaluation of an Eyes-Free Cursorless Numeric Entry System for Wearable Computers. *10th IEEE International Symposium on Wearable Computers* (ISWC 2006), Montreux, Switzerland. pp.21-28. doi: 10.1109/ISWC.2006.286338

[10] Matteo Bianchi, Edoardo Battaglia, Mattia Poggiani, Simone Ciotti, and Antonio Bicchi. 2016. A wearable fabric-based display for haptic multi-cue delivery. Haptics Symposium (HAPTICS), 2016 IEEE, IEEE, 277–283.

[11] Alex Butler, Shahram Izadi, and Steve Hodges. 2008. SideSight: multi-"touch" interaction around small devices. In *Proceedings of the 21st annual ACM symposium on User interface software and technology* (UIST '08). ACM, New York, NY, USA, 201-204. http://dx.doi.org.uml.idm.oclc.org/10.1145/1449715.1449746

[12] Cedrat Technologies. *Magnetic actuators*. Last retrieved on Jan 28th, 2018 from https://www.cedrat-technologies.com/en/products/magnetic-actuators.html

[13] Liwei Chan, Yi-Ling Chen, Chi-Hao Hsieh, Rong-Hao Liang, and Bing-Yu Chen. 2015. CyclopsRing: Enabling Whole-Hand and Context-Aware Interactions Through a Fisheye Ring. In *Proceedings of the 28th Annual ACM Symposium on User Interface Software & Technology* (UIST '15). ACM, New York, NY, USA, 549-556. http://dx.doi.org/10.1145/2807442.2807450

[14] Chen, Lisa Y., Tee, Benjamin C. -K., Chortos, Alex L., Schwartz, Gregor, Tse, Victor, J. Lipomi, Darren, Wong, H. -S. Philip, McConnell, Michael V., Bao, Zhenan. Continuous wireless pressure monitoring and mapping with ultra-small passive sensors for health monitoring and critical care. Nature Communications. 2014/10/06/online. https://doi.org/10.1038/ncomms6028

[15] Chih-Chung Chang and Chih-Jen Lin. 2011. LIBSVM: A library for support vector machines. *ACM Trans. Intell. Syst. Technol.* 2, 3, Article 27 (May 2011), 27 pages. DOI=http://dx.doi.org/10.1145/1961189.1961199

[16] Ke-Yu Chen, Kent Lyons, Sean White, and Shwetak Patel. 2013. uTrack: 3D input using two magnetic sensors. In *Proceedings of the 26th annual ACM symposium on User interface software and technology* (UIST '13). ACM, New York, NY, USA, 237-244. http://dx.doi.org.uml.idm.oclc.org/10.1145/2501988.2502035

[17] Xiang Anthony Chen, Tovi Grossman, and George Fitzmaurice. 2014. Swipeboard: a text entry technique for ultra-small interfaces that supports novice to expert transitions. In *Proceedings of the 27th*

annual ACM symposium on User interface software and technology (UIST '14). ACM, New York, NY, USA, 615-620. https://doi-org/10.1145/2642918.2647354

[18] Francesco Chinello, Monica Malvezzi, Claudio Pacchierotti, and Domenico Prattichizzo. 2015. Design and development of a 3RRS wearable fingertip cutaneous device. Advanced Intelligent Mechatronics (AIM), 2015 IEEE International Conference on, IEEE, 293–298

[19] Inrak Choi, Elliot W. Hawkes, David L. Christensen, Christopher J. Ploch, and Sean Follmer. 2016. Wolverine: A wearable haptic interface for grasping in virtual reality. Intelligent Robots and Systems (IROS), 2016 IEEE/RSJ International Conference on, IEEE, 986–993.

[20] Inrak Choi, Heather Culbertson, Mark R. Miller, Alex Olwal, and Sean Follmer. 2017. Grabity: A Wearable Haptic Interface for Simulating Weight and Grasping in Virtual Reality. Proceedings of the 30th Annual ACM Symposium on User Interface Software and Technology, ACM, 119–130.

[21] Yongsoon Choi, Jordan Tewell, Yukihiro Morisawa, Gilang A. Pradana, and Adrian David Cheok. 2014. Ring*U: a wearable system for intimate communication using tactile lighting expressions. In *Proceedings of the 11th Conference on Advances in Computer Entertainment Technology* (ACE '14). ACM, New York, NY, USA, Article 63, 4 pages. https://doi-org.uml.idm.oclc.org/10.1145/2663806.2663814

[22] Dr. Hempel Digital Heath Network. The future of wearables is implanted. last retrieved on Oct. 29th, from https://www.dr-hempel-network.com/digital-health-technolgy/implantable-wearables-in-healthcare/

[23] Gareth Edwards. 2016. Rogue One: A Star Wars Story. Retrieved April 4, 2018 from http://www.imdb.com/title/tt3748528/

[24] Flipboard. Retrieved September 14, 2017 from https://flipboard.com/

[25] FitBit. Last retrieved on Nov 18th, 2018, from https://www.fitbit.com/en-ca/home

[26] Jonathan Follett. Designing for Emerging Technologies. O'Reilly Media. Originally published in 2014.

[27] Ford Pilots New Exoskeleton Technology to Help Lessen Chance of Worker Fatigue, Injury — Ford Media Center. Retrieved April 4, 2018 from https://media.ford.com/content/fordmedia/fna/us/en/news/2017/11/09/ford-exoskeleton-technology-pilot.htm

[28] Euan Freeman, Stephen Brewster, and Vuokko Lantz. 2014. Tactile Feedback for Above-Device Gesture Interfaces: Adding Touch to Touchless Interactions. In *Proceedings of the 16th International*

Conference on Multimodal Interaction (ICMI '14). ACM, New York, NY, USA, 419-426. https://doi-org/10.1145/2663204.2663280

[29] Antonio Frisoli, Massimiliano Solazzi, Fabio Salsedo, and Massimo Bergamasco. 2008. A fingertip haptic display for improving curvature discrimination. Presence: Teleoperators and Virtual Environments 17, 6: 550–561.

[30] Antonio Frisoli, Massimiliano Solazzi, Fabio Salsedo, and Massimo Bergamasco. 2008. A fingertip haptic display for improving curvature discrimination. Presence: Teleoperators and Virtual Environments 17, 6: 550–561

[31] Bruno Fruchard, Eric Lecolinet, and Olivier Chapuis. 2017. MarkPad: Augmenting Touchpads for Command Selection. In *Proceedings of the 2017 CHI Conference on Human Factors in Computing Systems* (CHI '17). ACM, New York, NY, USA, 5630-5642. https://doi-org/10.1145/3025453.3025486

[32] Brittany Garcia, Sharon Lynn Chu, Beth Nam, and Colin Banigan. 2018. Wearables for Learning: Examining the Smartwatch as a Tool for Situated Science Reflection. In *Proceedings of the 2018 CHI Conference on Human Factors in Computing Systems* (CHI '18). ACM, New York, NY, USA, Paper 256, 13 pages. DOI: https://doi.org/10.1145/3173574.3173830

[33] Global Smart Rings Market 2017-2021, http://www.researchandmarkets.com/research/xqhhnz/global-smart. Accessed March 2017.

[34] Grace Colledge Online. *Rapid Growth: The Past, Present and Future of Wearable Technology.* Last retrieved on Sep 8th, 2018, from https://online.grace.edu/news/business/the-past-present-future-of-wearable-technology/

[35] Mathieu Le Goc, Stuart Taylor, Shahram Izadi, and Cem Keskin. 2014. A low-cost transparent electric field sensor for 3d interaction on mobile devices. In *Proceedings of the SIGCHI Conference on Human Factors in Computing Systems* (CHI '14). ACM, New York, NY, USA, 3167-3170. http://dx.doi.org/10.1145/2556288.2557331

[36] Jun Gong, Da-Yuan Huang, Teddy Seyed, Te Lin, Tao Hou, Xin Liu, Molin Yang, Boyu Yang, Yuhan Zhang, and Xing-Dong Yang. 2018. Jetto: Using Lateral Force Feedback for Smartwatch Interactions. In *Proceedings of the 2018 CHI Conference on Human Factors in Computing Systems* (CHI '18). ACM.

[37] Google Glass. Last retrieved on Nov. 18th, 2018, from https://www.x.company/glass/

[38] Brian T. Gleeson, Scott K. Horschel, and William R. Provancher. 2010. Design of a fingertip-mounted tactile display with tangential skin displacement feedback. IEEE Transactions on Haptics 3, 4: 297–301.

[39] Joseph Greenspun and Kristofer SJ Pister. 2013. Ring GINA: a wearable computer interaction device. In *International Conference on Mobile Computing, Applications, and Services*, Springer, 98-103.

[40] François Guimbretiére and Terry Winograd. 2000. FlowMenu: combining command, text, and data entry. In Proceedings of the 13th annual ACM symposium on User interface software and technology (UIST '00). ACM, New York, NY, USA, 213-216. http://dx.doi.org/10.1145/354401.354778

[41] Aakar Gupta, Antony Albert Raj Irudayaraj, and Ravin Balakrishnan. 2017. HapticClench: Investigating Squeeze Sensations using Memory Alloys. In *Proceedings of the 30th Annual ACM Symposium on User Interface Software and Technology.*(UIST '17). ACM, New York, NY, USA, 109-117. https://doi.org/10.1145/3126594.3126598

[42] Sean Gustafson, Daniel Bierwirth, and Patrick Baudisch. 2010. Imaginary interfaces: spatial interaction with empty hands and without visual feedback. In *Proceedings of the 23nd annual ACM symposium on User interface software and technology.*(UIST '10). ACM, New York, NY, USA, 3-12. DOI=http://dx.doi.org/10.1145/1866029.1866033

[43] Carl Gutwin, Andy Cockburn, Joey Scarr, Sylvain Malacria, and Scott C. Olson. 2014. Faster command selection on tablets with FastTap. In *Proceedings of the SIGCHI Conference on Human Factors in Computing Systems* (CHI '14). ACM, New York, NY, USA, 2617-2626. http://dx.doi.org/10.1145/2556288.2557136

[44] Sungdo Ha, Laehyun Kim, Sehyung Park, Cha-soo Jun and H Rho. 2009. Virtual prototyping enhanced by a haptic interface. *CIRP annals-manufacturing technology*, 58 (1). 135-138

[45] Chris Harrison and Scott E. Hudson. 2008. Scratch input: creating large, inexpensive, unpowered and mobile finger input surfaces. In *Proceedings of the 21st annual ACM symposium on User interface software and technology* (UIST '08). ACM, New York, NY, USA, 205-208. http://dx.doi.org/10.1145/1449715.1449747

[46] Chris Harrison and Scott E. Hudson. 2009. Abracadabra: wireless, high-precision, and unpowered finger input for very small mobile devices. In *Proceedings of the 22nd annual ACM symposium on User interface software and technology* (UIST '09). ACM, New York, NY, USA, 121-124. http://dx.doi.org/10.1145/1622176.1622199

[47] Chris Harrison, Julia Schwarz, and Scott E. Hudson. 2011. TapSense: enhancing finger interaction on touch surfaces. In *Proceedings of the 24th annual ACM symposium on User interface software and technology* (UIST '11). ACM, New York, NY, USA, 627-636. https://doi-org/10.1145/2047196.2047279

[48] Chris Harrison, Robert Xiao, and Scott Hudson. 2012. Acoustic barcodes: passive, durable and inexpensive notched identification tags. In *Proceedings of the 25th annual ACM symposium on User interface software and technology* (UIST '12). ACM, New York, NY, USA, 563-568. http://dx.doi.org/10.1145/2380116.2380187

[49] Chris Harrison, Desney Tan, and Dan Morris. 2010. Skinput: appropriating the body as an input surface. In *Proceedings of the SIGCHI Conference on Human Factors in Computing Systems* (CHI '10). ACM, New York, NY, USA, 453-462. http://dx.doi.org/10.1145/1753326.1753394

[50] Morton A. Heller. 2013. The psychology of touch. Psychology Press

[51] Steven J. Henderson and Steven K. Feiner. 2002. Augmented Reality for Maintenance and Repair (ARMAR). DTIC Document. Retrieved December 4, 2012 from http://oai.dtic.mil/oai/oai

[52] Seongkook Heo and Geehyuk Lee. 2012. ForceDrag: using pressure as a touch input modifier. In *Proceedings of the 24th Australian Computer-Human Interaction Conference* (OzCHI '12), Vivienne Farrell, Graham Farrell, Caslon Chua, Weidong Huang, Raj Vasa, and Clinton Woodward (Eds.). ACM, New York, NY, USA, 204-207. http://dx.doi.org/10.1145/2414536.2414572

[53] Ken Hinckley, Seongkook Heo, Michel Pahud, Christian Holz, Hrvoje Benko, Abigail Sellen, Richard Banks, Kenton O'Hara, Gavin Smyth, and William Buxton. 2016. Pre-Touch Sensing for Mobile Interaction. In *Proceedings of the 2016 CHI Conference on Human Factors in Computing Systems* (CHI '16). ACM, New York, NY, USA, 2869-2881. http://dx.doi.org/10.1145/2858036.2858095

[54] Christian Holz, Tovi Grossman, George Fitzmaurice, and Anne Agur. 2012. Implanted user interfaces. In Proceedings of the SIGCHI Conference on Human Factors in Computing Systems (CHI '12). ACM, New York, NY, USA, 503-512. DOI: https://doi.org/10.1145/2207676.2207745

[55] Tom Horak, Sriram Karthik Badam, Niklas Elmqvist, and Raimund Dachselt. 2018. When David Meets Goliath: Combining Smartwatches with a Large Vertical Display for Visual Data Exploration. In *Proceedings of the 2018 CHI Conference on Human Factors in Computing Systems* (CHI '18). ACM, New York, NY, USA, Paper 19, 13 pages. DOI: https://doi.org/10.1145/3173574.3173593

[56] Da-Yuan Huang, Ruizhen Guo, Jun Gong, Jingxian Wang, John Graham, De-Nian Yang, and Xing-Dong Yang. 2017. RetroShape: Leveraging Rear-Surface Shape Displays for 2.5D Interaction on Smartwatches.

In Proceedings of the 30th Annual ACM Symposium on User Interface Software and Technology (UIST '17). ACM, New York, NY, USA, 539-551. https://doi.org/10.1145/3126594.3126610

[57] Alexandra Ion, Edward Jay Wang, and Patrick Baudisch. 2015. Skin Drag Displays: Dragging a Physical Tactor across the User's Skin Produces a Stronger Tactile Stimulus than Vibrotactile. In *Proceedings of the 33rd Annual ACM Conference on Human Factors in Computing Systems* (CHI '15). ACM, New York, NY, USA, 2501-2504. https://doi.org/10.1145/2702123.2702459

[58] Seungwoo Je, Brendan Rooney, Liwei Chan, and Andrea Bianchi. 2017. tactoRing: A Skin-Drag Discrete Display. In *Proceedings of the 2017 CHI Conference on Human Factors in Computing Systems* (CHI '17). ACM, New York, NY, USA, 3106-3114. https://doi-org/10.1145/3025453.3025703

[59] Seungwoo Je, Minkyeong Lee, Yoonji Kim, Liwei Chan, Xing-Dong Yang, and Andrea Bianchi. 2018. PokeRing: Notifications by Poking Around the Finger. In *Proceedings of the 2018 CHI Conference on Human Factors in Computing Systems* (CHI '18). ACM, New York, NY, USA, Paper 542, 10 pages. DOI: https://doi.org/10.1145/3173574.3174116

[60] Lei Jing, Yinghui Zhou, Zixue Cheng and Tongjun Huang. 2012. Magic ring: A finger-worn device for multiple appliances control using static finger gestures. *Sensors*, 12 (5). 5775-5790

[61] Hamed Ketabdar, Peyman Moghadam and Mehran Roshandel. 2012. Pingu: A new miniature wearable device for ubiquitous computing environments. in *Complex, Intelligent and Software Intensive Systems* (CISIS), 2012 Sixth International Conference on, IEEE, 502-506.

[62] David Kim, Otmar Hilliges, Shahram Izadi, Alex D. Butler, Jiawen Chen, Iason Oikonomidis, and Patrick Olivier. 2012. Digits: freehand 3D interactions anywhere using a wrist-worn gloveless sensor. In *Proceedings of the 25th annual ACM symposium on User interface software and technology* (UIST '12). ACM, New York, NY, USA, 167-176. https://doi.org/10.1145/2380116.2380139

[63] Hwan Kim, Minhwan Kim, and Woohun Lee. 2016. Hapthimble: A wearable haptic device towards usable virtual touch screen. Proceedings of the 2016 CHI Conference on Human Factors in Computing Systems, ACM, 3694–3705

[64] Sangtae Kim, Jaejeung Kim, and Soobin Lee. 2013. Bezel-flipper: design of a light-weight flipping interface for e-books. In *CHI 13 Extended Abstracts on Human Factors in Computing Systems* (CHI EA '13). ACM, New York, NY, USA, 1719-1724. https://doi-org/10.1145/2468356.2468664

[65] Kenrich Kin, Björn Hartmann, and Maneesh Agrawala. 2011. Two-handed marking menus for multitouch devices. ACM Trans. Comput.-Hum. Interact. 18, 3, Article 16 (August 2011), 23 pages. https://doi-org/10.1145/1993060.1993066

[66] Sven Kratz and Michael Rohs. 2009. Hoverflow: exploring around-device interaction with IR distance sensors. In *Proceedings of the 11th International Conference on Human-Computer Interaction with Mobile Devices and Services* (MobileHCI '09). ACM, New York, NY, USA, Article 42, 4 pages. http://dx.doi.org.uml.idm.oclc.org/10.1145/1613858.1613912

[67] Sven Kratz, Patrick Chiu, and Maribeth Back. 2013. PointPose: finger pose estimation for touch input on mobile devices using a depth sensor. In *Proceedings of the 2013 ACM international conference on Interactive tabletops and surfaces* (ITS '13). ACM, New York, NY, USA, 223-230. http://dx.doi.org/10.1145/2512349.2512824

[68] Yuki Kubo, Buntarou Shizuki, and Jiro Tanaka. 2016. B2B-Swipe: Swipe Gesture for Rectangular Smartwatches from a Bezel to a Bezel. In Proceedings of the 2016 CHI Conference on Human Factors in Computing Systems (CHI '16). ACM, New York, NY, USA, 3852-3856. https://doi-org/10.1145/2858036.2858216

[69] Gordon Kurtenbatch. 1993. The Design and Evaluation of Marking Menus. Thesis. University of Toronto.

[70] Michel Beaudouin-Lafon. 2001. Novel interaction techniques for overlapping windows. In *Proceedings of the 14th annual ACM symposium on User interface software and technology* (UIST '01). ACM, New York, NY, USA, 153-154. http://dx.doi.org/10.1145/502348.502371

[71] Benjamin Lafreniere et al., 2016. Crowdsourced Fabrication. In *Proceedings of the 29th Annual Symposium on User Interface Software and Technology* (UIST '16). ACM, New York, NY, USA, 15-28. DOI: https://doi.org/10.1145/2984511.2984553

[72] Benjamin Lafreniere, Carl Gutwin, Andy Cockburn, and Tovi Grossman. 2016. Faster Command Selection on Touchscreen Watches. In *Proceedings of the 2016 CHI Conference on Human Factors in Computing Systems* (CHI '16). ACM, New York, NY, USA, 4663-4674. https://doi-org/10.1145/2858036.2858166

[73] Susan J. Lederman, Georgie Thorne, and Bill Jones. 1986. Perception of texture by vision and touch: Multidimensionality and intersensory integration. Journal of Experimental Psychology: Human Perception and Performance 12, 2: 169.

[74] Jaeyeon Lee and Geehyuk Lee. 2016. Designing a Non-contact Wearable Tactile Display Using Airflows. In *Proceedings of the 29th Annual Symposium on User Interface Software and Technology* (UIST '16). ACM, New York, NY, USA, 183-194. https://doi.org/10.1145/2984511.2984583

[75] G. Julian Lepinski, Tovi Grossman, and George Fitzmaurice. 2010. The design and evaluation of multitouch marking menus. In *Proceedings of the SIGCHI Conference on Human Factors in Computing Systems* (CHI '10). ACM, New York, NY, USA, 2233-2242. https://doi.org/10.1145/1753326.1753663

[76] Robert W. Lindeman, Yasuyuki Yanagida, Haruo Noma, and Kenichi Hosaka. 2006. Wearable vibrotactile systems for virtual contact and information display. Virtual Reality 9, 2–3: 203–213

[77] Linear Motions. *What are piezo actuators?*. Last retrieved on Jan 28th, 2018 from https://www.linearmotiontips.com/what-are-piezo-actuators/

[78] Yuexing Luo and Daniel Vogel. 2014. Crossing-based selection with direct touch input. In *Proceedings of the SIGCHI Conference on Human Factors in Computing Systems* (CHI '14). ACM, New York, NY, USA, 2627-2636. http://dx.doi.org/10.1145/2556288.2557397

[79] Yuexing Luo and Daniel Vogel. 2015. Pin-and-Cross: A Unimanual Multitouch Technique Combining Static Touches with Crossing Selection. In *Proceedings of the 28th Annual ACM Symposium on User Interface Software & Technology* (UIST '15). ACM, New York, NY, USA, 323-332. https://doi-org/10.1145/2807442.2807444

[80] Stefan Marti and Chris Schmandt. 2005. Giving the caller the finger: collaborative responsibility for cellphone interruptions. In *CHI 05 Extended Abstracts on Human Factors in Computing Systems* (CHI EA '05). ACM, New York, NY, USA, 1633-1636. http://dx.doi.org./10.1145/1056808.1056984

[81] D. McCoul, W. Hu, M. Gao, V.Mehta, Q. Pei, "Recent Advances in Stretchable and Transparent Electronic Materials", Adv Elect. Mater. DOI: 10.1002/aelm.201500407 (2016).

[82] William McGrath and Yang Li. 2014. Detecting tapping motion on the side of mobile devices by probabilistically combining hand postures. In *Proceedings of the 27th annual ACM symposium on User interface software and technology* (UIST '14). ACM, New York, NY, USA, 215-219. DOI: https://doi.org/10.1145/2642918.2647363

[83] Michael McGuffin, Nicolas Burtnyk, and Gord Kurtenbach. 2002. FaST Sliders: Integrating Marking Menus and the Adjustment of Continuous Values. In GI 2002 Conference proceedings: Graphics Interface Conference. pp. 35-42

[84] Kouta Minamizawa, Souichiro Fukamachi, Hiroyuki Kajimoto, Naoki Kawakami, and Susumu Tachi. 2007. Gravity grabber: wearable haptic display to present virtual mass sensation. ACM SIGGRAPH 2007 emerging technologies, ACM, 8.

[85] Cameron S. Miner, Denise M. Chan, and Christopher Campbell. 2001. Digital jewelry: wearable technology for everyday life. In *CHI 01 Extended Abstracts on Human Factors in Computing Systems* (CHI EA '01). ACM, New York, NY, USA, 45-46. http://dx.doi.org.uml.idm.oclc.org/10.1145/634067.634098

[86] Ditte Mortensen, *Natural User Interfaces – What are they and how do you design user interfaces that feel natural* Last retrieved on Sep 8th, 2018, from https://www.interaction-design.org/literature/article/natural-user-interfaces-what-are-they-and-how-do-you-design-user-interfaces-that-feel-natural

[87] Takaki Murakami, Tanner Person, Charith Lasantha Fernando, and Kouta Minamizawa. 2017. Altered touch: miniature haptic display with force, thermal and tactile feedback for augmented haptics. ACM SIGGRAPH 2017 Posters, ACM, 53.

[88] Keisuke Nakamura, Kazuhiro Nakadai, Futoshi Asano, Yuji Hasegawa, and Hiroshi Tsujino. 2009. Intelligent sound source localization for dynamic environments. *IEEE/RSJ International Conference on Intelligent Robots and Systems*, St. Louis, MO, pp. 664-669. doi: 10.1109/IROS.2009.5354419

[89] Nam-Trung Nguyen and Steven T. Wereley. 2002. Fundamentals and applications of microfluidics. Artech house.

[90] Jakob Nielsen. 1995. *10 Usability Heuristics for User Interface Design.* Last retrieved on Sep 8th, 2018, from https://www.nngroup.com/articles/ten-usability-heuristics/

[91] Nike+ FuelBand. Last retrieved on Nov 18th, 2018, from https://en.wikipedia.org/wiki/Nike

[92] Shahriar Nirjon, Jeremy Gummeson, Dan Gelb, and Kyu-Han Kim. 2015. TypingRing: A Wearable Ring Platform for Text Input. In *Proceedings of the 13th Annual International Conference on Mobile Systems, Applications, and Services* (MobiSys '15). ACM, New York, NY, USA, 227-239. http://dx.doi.org.uml.idm.oclc.org/10.1145/2742647.2742665

[93] Aditya Shekhar Nittala, Anusha Withana, Narjes Pourjafarian, and Jürgen Steimle. 2018. Multi-Touch Skin: A Thin and Flexible Multi-Touch Sensor for On-Skin Input. In Proceedings of the 2018 CHI Conference on Human Factors in Computing Systems (CHI '18). ACM, New York, NY, USA, Paper 33, 12 pages. DOI: https://doi.org/10.1145/3173574.3173607

[94] Nonald A. Norman and Jakob Nielsen. 2010. Gestural interfaces: a step backward in usability. interactions 17, 5 (September 2010), 46-49. https://doi.org/10.1145/1836216.1836228

[95] Ian Oakley, DoYoung Lee, MD. Rasel Islam, and Augusto Esteves. 2015. Beats: Tapping Gestures for Smart Watches. In Proceedings of the 33rd Annual ACM Conference on Human Factors in Computing Systems (CHI '15). ACM, New York, NY, USA, 1237-1246. https://doi-org/10.1145/2702123.2702226

[96] Masa Ogata, Yuta Sugiura, Hirotaka Osawa, and Michita Imai. 2012. iRing: intelligent ring using infrared reflection. In *Proceedings of the 25th annual ACM symposium on User interface software and technology* (UIST '12). ACM, New York, NY, USA, 131-136.

[97] Stephen Oney, Chris Harrison, Amy Ogan, and Jason Wiese. 2013. ZoomBoard: a diminutive qwerty soft keyboard using iterative zooming for ultra-small devices. In *Proceedings of the SIGCHI Conference on Human Factors in Computing Systems* (CHI '13). ACM, New York, NY, USA, 2799-2802. DOI: https://doi-org/10.1145/2470654.2481387

[98] Makoto Ono, Buntarou Shizuki, and Jiro Tanaka. 2013. Touch & activate: adding interactivity to existing objects using active acoustic sensing. In *Proceedings of the 26th annual ACM symposium on User interface software and technology.* (UIST '13). ACM, New York, NY, USA, 31-40. http://dx.doi.org/10.1145/2501988.2501989

[99] Claudio Pacchierotti, Stephen Sinclair, Massimiliano Solazzi, Antonio Frisoli, Vincent Hayward, and Domenico Prattichizzo. 2017. Wearable haptic systems for the fingertip and the hand: Taxonomy, review, and perspectives. IEEE transactions on haptics 10, 4: 580–600

[100] Henning Pohl, Peter Brandes, Hung Ngo Quang, and Michael Rohs. 2017. Squeezeback: Pneumatic Compression for Notifications. In *Proceedings of the 2017 CHI Conference on Human Factors in Computing Systems* (CHI '17). ACM, New York, NY, USA, 5318-5330. https://doi.org/10.1145/3025453.3025526

[101] Ronen Polsky, Roger J. Narayan, Phil Miller. 2016. Microneedle-Based Sensors for Medical Diagnosis. Journal of Material Chemistry B.

[102] Stuart Pook, Eric Lecolinet, Guy Vaysseix, and Emmanuel Barillot. 2000. Control menus: excecution and control in a single interactor. In CHI '00 Extended Abstracts on Human Factors in Computing Systems (CHI EA '00). ACM, New York, NY, USA, 263-264. http://dx.doi.org/10.1145/633292.633446

[103] Gilang Andi Pradana, Adrian David Cheok, Masahiko Inami, Jordan Tewell, and Yongsoon Choi. 2014. Emotional priming of mobile text messages with ring-shaped wearable device using color lighting

and tactile expressions. In *Proceedings of the 5th Augmented Human International Conference* (AH '14). ACM, New York, NY, USA, , Article 14 , 8 pages. http://dx.doi.org/10.1145/2582051.2582065

[104] Project Soli. Last retrieved on Jan 28th, 2018, from https://atap.google.com/soli/

[105] Jun Rekimoto. 2001. GestureWrist and GesturePad: Unobstrusive Wearable Interaction Devices. In *Proceedings of the 5th IEEE International Symposium on Wearable Computers* (ISWC '01). IEEE Computer Society, Washington, DC, USA, 21-.

[106] Thijs Roumen, Simon T. Perrault, and Shengdong Zhao. 2015. NotiRing: A Comparative Study of Notification Channels for Wearable Interactive Rings. In *Proceedings of the 33rd Annual ACM Conference on Human Factors in Computing Systems* (CHI '15). ACM, New York, NY, USA, 2497-2500. https://doi-org/10.1145/2702123.2702350

[107] T. Scott Saponas, Desney S. Tan, Dan Morris, Ravin Balakrishnan, Jim Turner, and James A. Landay. 2009. Enabling always-available input with muscle-computer interfaces. In *Proceedings of the 22nd annual ACM symposium on User interface software and technology* (UIST '09). ACM, New York, NY, USA, 167-176. http://dx.doi.org/10.1145/1622176.1622208

[108] Valkyrie Savage, Andrew Head, Björn Hartmann, Dan B. Goldman, Gautham Mysore, and Wilmot Li. 2015. Lamello: Passive Acoustic Sensing for Tangible Input Components. In *Proceedings of the 33rd Annual ACM Conference on Human Factors in Computing Systems* (CHI '15). ACM, New York, NY, USA, 1277-1280. DOI: https://doi.org/10.1145/2702123.2702207

[109] R. Schmidt. 1986. Multiple emitter location and signal parameter estimation. In *IEEE Transactions on Antennas and Propagation*, vol. 34, no. 3, pp. 276-280. doi: 10.1109/TAP.1986.1143830

[110] Samuel B. Schorr and Allison M. Okamura. 2017. Fingertip tactile devices for virtual object manipulation and exploration. Proceedings of the 2017 CHI Conference on Human Factors in Computing Systems, ACM, 3115–3119.

[111] J Ridley Stroop. 1935. Studies of interference in serial verbal reactions. *Journal of experimental psychology*, 18 (6). 643.

[112] Scott S. Snibbe, Karon E. MacLean, Rob Shaw, Jayne Roderick, William L. Verplank, and Mark Scheeff. 2001. Haptic techniques for media control. In *Proceedings of the 14th annual ACM symposium on User interface software and technology* (UIST '01). ACM, New York, NY, USA, 199-208. //dx.doi.org/10.1145/502348.502387

[113] Colin Edward Swindells. 2007. Incorporating affect into the design of 1-D rotary physical controls, University of British Columbia.

[114] Taichi Tajika, Tomoko Yonezawa, and Noriaki Mitsunaga. 2008. Intuitive page-turning interface of e-books on flexible e-paper based on user studies. In *Proceedings of the 16th ACM international conference on Multimedia* (MM '08). ACM, New York, NY, USA, 793-796. https://doi.org/10.1145/1459359.1459489

[115] Dzmitry Tsetserukou, Shotaro Hosokawa, and Kazuhiko Terashima. 2014. LinkTouch: A wearable haptic device with five-bar linkage mechanism for presentation of two-DOF force feedback at the fingerpad. Haptics Symposium (HAPTICS), 2014 IEEE, IEEE, 307–312.

[116] B. D. Van Veen and K. M. Buckley. 1988. Beamforming: a versatile approach to spatial filtering. In *IEEE ASSP Magazine*, vol. 5, no. 2, pp. 4-24. doi: 10.1109/53.665

[117] Wouter Van Vlaenderen, Jens Brulmans, Jo Vermeulen, and Johannes Schöning. 2015. WatchMe: A Novel Input Method Combining a Smartwatch and Bimanual Interaction. In *Proceedings of the 33rd Annual ACM Conference Extended Abstracts on Human Factors in Computing Systems* (CHI EA '15). ACM, New York, NY, USA, 2091-2095. http://dx.doi.org/10.1145/2702613.2732789

[118] Daniel Vogel and Géry Casiez. 2012. Hand occlusion on a multi-touch tabletop. In Proceedings of the SIGCHI Conference on Human Factors in Computing Systems (CHI '12). ACM, New York, NY, USA, 2307-2316. http://dx.doi.org/10.1145/2207676.2208390

[119] Saiwen Wang, Jie Song, Jaime Lien, Ivan Poupyrev, and Otmar Hilliges. 2016. Interacting with Soli: Exploring Fine-Grained Dynamic Gesture Recognition in the Radio-Frequency Spectrum. In *Proceedings of the 29th Annual Symposium on User Interface Software and Technology* (UIST '16). ACM, New York, NY, USA, 851-860. https://doi.org/10.1145/2984511.2984565

[120] Martin Weigel, Tong Lu, Gilles Bailly, Antti Oulasvirta, Carmel Majidi, and Jürgen Steimle. 2015. iSkin: Flexible, Stretchable and Visually Customizable On-Body Touch Sensors for Mobile Computing. In Proceedings of the 33rd Annual ACM Conference on Human Factors in Computing Systems (CHI '15). ACM, New York, NY, USA, 2991-3000. DOI: https://doi.org/10.1145/2702123.2702391

[121] Martin Weigel, Vikram Mehta, and Jürgen Steimle. 2014. More than touch: understanding how people use skin as an input surface for mobile computing. In Proceedings of the SIGCHI Conference on Human Factors in Computing Systems (CHI '14). ACM, New York, NY, USA, 179-188. DOI: https://doi.org/10.1145/2556288.2557239

[122] Hongyi Wen, Julian Ramos Rojas, and Anind K. Dey. 2016. Serendipity: Finger Gesture Recognition using an Off-the-Shelf Smartwatch. In *Proceedings of the 2016 CHI Conference on Human Factors in Computing Systems* (CHI '16). ACM, New York, NY, USA, 3847-3851. http://dx.doi.org/10.1145/2858036.2858466

[123] Julia Werner, Reto Wettach, and Eva Hornecker. 2008. United-pulse: feeling your partner's pulse. In *Proceedings of the 10th international conference on Human computer interaction with mobile devices and services* (MobileHCI '08). ACM, New York, NY, USA, 535-538. http://dx.doi.org/10.1145/1409240.1409338

[124] George M. Whitesides. 2006. The origins and the future of microfluidics. Nature 442, 7101: 368

[125] Anusha Withana, Daniel Groeger, and Jürgen Steimle. 2018. Tacttoo: A Thin and Feel-Through Tattoo for On-Skin Tactile Output. In Proceedings of the 31st Annual ACM Symposium on User Interface Software and Technology (UIST '18). ACM, New York, NY, USA, 365-378. DOI: https://doi.org/10.1145/3242587.3242645

[126] Wired. Why Flipping Through Paper-Like Pages Endures in The Digital World. 2012. Retrieved September 14, 2017 from https://www.wired.com/2012/05/why-flipping-through-paper-like-pages-endures-in-the-digital-world/

[127] Anusha Withana, Roshan Peiris, Nipuna Samarasekara, and Suranga Nanayakkara. 2015. zSense: Enabling Shallow Depth Gesture Recognition for Greater Input Expressivity on Smart Wearables. In *Proceedings of the 33rd Annual ACM Conference on Human Factors in Computing Systems* (CHI '15). ACM, New York, NY, USA, 3661-3670. http://dx.doi.org/10.1145/2702123.2702371

[128] Wikipedia.org. *Wearable technology.* Last retrieved on Jan 28th, 2018 from https://en.wikipedia.org/wiki/Wearable_technology

[129] Wikipedia.org. *Microelectromechanical systems.* Last retrieved on Jan 28th, 2018 from https://en.wikipedia.org/wiki/Microelectromechanical-systems

[130] Robert Xiao, Gierad Laput, and Chris Harrison. 2014. Expanding the input expressivity of smartwatches with mechanical pan, twist, tilt and click. In *Proceedings of the SIGCHI Conference on Human Factors in Computing Systems* (CHI '14). ACM, New York, NY, USA, 193-196. https://doi.org/10.1145/2556288.2557017

[131] Xing-Dong Yang, Khalad Hasan, Neil Bruce, and Pourang Irani. 2013. Surround-see: enabling peripheral vision on smartphones during active use. In *Proceedings of the 26th annual ACM symposium on User interface software and technology* (UIST '13). ACM, New York, NY, USA, 291-300. http://dx.doi.org/10.1145/2501988.2502049

[132] Hui-Shyong Yeo, Juyoung Lee, Andrea Bianchi, and Aaron Quigley. 2016. Sidetap & Slingshot Gestures on Unmodified Smartwatches. In *Proceedings of the 29th Annual Symposium on User Interface Software and Technology* (UIST 16 Adjunct). ACM, New York, NY, USA, 189-190. https://doi.org/10.1145/2984751.2984763

[133] Kiwon Yeom, Jounghuem Kwon, JooHyun Maeng and Bum-Jae You. 2015. [POSTER] Haptic Ring Interface Enabling Air-Writing in Virtual Reality Environment. in *Mixed and Augmented Reality* (ISMAR), 2015 IEEE International Symposium on, IEEE, 124-127.

[134] Xin Yi, Chun Yu, Weijie Xu, Xiaojun Bi, and Yuanchun Shi. 2017. COMPASS: Rotational Keyboard on Non-Touch Smartwatches. In *Proceedings of the 2017 CHI Conference on Human Factors in Computing Systems* (CHI '17). ACM, New York, NY, USA, 705-715. https://doi.org/10.1145/3025453.3025454

[135] Tomoyuki Yokota, Peter Zalar, Martin Kaltenbrunner, Hiroaki Jinno, Naoji Matsuhisa, Hiroki Kitanosako, Yutaro Tachibana, Wakako Yukita, Mari Koizumi, and Takao Someya, "Ultraflexible Organic Photonic Skin", Science Advances, vol. 2, No.4, pp.e1501856, DOI: 10.1126/sciadv.1501856.

[136] Sang Ho Yoon, Yunbo Zhang, Ke Huo, and Karthik Ramani. 2016. TRing: Instant and Customizable Interactions with Objects Using an Embedded Magnet and a Finger-Worn Device. In *Proceedings of the 29th Annual Symposium on User Interface Software and Technology* (UIST '16). ACM, New York, NY, USA, 169-181. https://doi-org.uml.idm.oclc.org/10.1145/2984511.2984529

[137] Koichi Yoshino, Koichi Obata, and Satoru Tokuhisa. 2017. FLIPPIN': Exploring a Paper-based Book UI Design in a Public Space. In *Proceedings of the 2017 CHI Conference on Human Factors in Computing Systems* (CHI '17). ACM, New York, NY, USA, 1508-1517. https://doi.org/10.1145/3025453.3025981e

[138] Boning Zhang, Yiqiang Chen, Yueliang Qian, and Xiangdong Wang. 2011. A ring-shaped interactive device for large remote display and mobile device control. In *Proceedings of the 13th international conference on Ubiquitous computing* (UbiComp '11). ACM, New York, NY, USA, 473-474. https://doi-org.uml.idm.oclc.org/10.1145/2030112.2030177

[139] Yang Zhang and Chris Harrison. 2015. Tomo: Wearable, Low-Cost Electrical Impedance Tomography for Hand Gesture Recognition. In *Proceedings of the 28th Annual ACM Symposium*

on User Interface Software & Technology (UIST '15). ACM, New York, NY, USA, 167-173. http://dx.doi.org.uml.idm.oclc.org/10.1145/2807442.2807480

[140] Yang Zhang, Junhan Zhou, Gierad Laput, and Chris Harrison. 2016. SkinTrack: Using the Body as an Electrical Waveguide for Continuous Finger Tracking on the Skin. In *Proceedings of the 2016 CHI Conference on Human Factors in Computing Systems* (CHI '16). ACM, New York, NY, USA, 1491-1503. http://dx.doi.org.uml.idm.oclc.org/10.1145/2858036.2858082

[141] Shengdong Zhao and Ravin Balakrishnan. 2004. Simple vs. compound mark hierarchical marking menus. In Proceedings of the 17th annual ACM symposium on User interface software and technology (UIST '04). ACM, New York, NY, USA, 33-42. http://dx.doi.org/10.1145/1029632.1029639